NATIONAL AERONAUTICS AND SPACE ADMINISTRATION

Technical Report No. 32-255

An Experimental Correlation of the Nonreactive Properties of Injection Schemes and Combustion Effects in a Liquid-Propellant Rocket Engine

Part I. The Application of Nonreactive-Spray Properties to Rocket-Motor Injector Design

Jack H. Rupe

N 65 - 33 129

(ACCESSION NUMBER)   (THRU)

60 _____   */* _____

(PAGES)   (CODE)

CR 64635   *28*

(NASA CR OR TMX OR AD NUMBER)   (CATEGORY)

JET PROPULSION LABORATORY
CALIFORNIA INSTITUTE OF TECHNOLOGY
PASADENA, CALIFORNIA

July 15, 1965

NATIONAL AERONAUTICS AND SPACE ADMINISTRATION

Technical Report No. 32-255

An Experimental Correlation of the Nonreactive Properties of Injection Schemes and Combustion Effects in a Liquid-Propellant Rocket Engine

Part I. The Application of Nonreactive-Spray Properties to Rocket-Motor Injector Design

Jack H. Rupe

DR Bartz

D. R. Bartz, Manager
Propulsion Research Section

JET PROPULSION LABORATORY
CALIFORNIA INSTITUTE OF TECHNOLOGY
PASADENA, CALIFORNIA

July 15, 1965

CONTENTS

TABLES

FIGURES

FIGURES (Cont'd)

FIGURES (Cont'd)

ABSTRACT

33129

The properties of the sprays produced by a pair of unlike imping-
ing streams of nonreactive fluids were utilized as the design basis for
a series of eight injectors having distinctively different specifications.
Particular emphasis was placed on the use of available information
and the development of new techniques, where required, to permit
quantitative description of the mass and mixture-ratio distributions
produced by each injection scheme. Methods of describing the mass-
distribution model of an element are presented in detail, together with
the properties of injector orifices, the jets they produce, and the com-
bined flows provided by each injector. This information is being uti-
lized as a basis for correlating injection schemes with combustion
phenomena.

I. INTRODUCTION

The design of injection systems for liquid-propellant
rocket engines has historically been an artful process
based on experience and intuition. Although this pro-
cedure has succeeded in satisfying the requirements of
current propulsion systems, it has leaned heavily on the
compromise of performance characteristics and on long
and expensive development efforts. Since the space age
is in its infancy, many additional systems and hence
injection schemes will be required as this effort grows.
It is clear, therefore, that a sound, logical basis for the
design of injection systems would be invaluable.

When stripped to its bare essentials, the usual problem
facing the rocket injector and/or engine designer con-
sists simply of specifying a piece of hardware that will,
in a very efficient manner, convert the chemical energy

stored in a liquid propellant (or propellants) into the
thermal energy of the reaction products. It is also usual
to require that the conversion process be achieved in a
minimum volume, that it be easily controlled, and that it
be extremely reliable and reproducible. It is therefore
obvious that the accomplishment of these objectives is
dependent on the designer's having at his disposal suf-
ficient quantitative information to allow him to control,
through injector design details, those parameters that in-
fluence the combustion phenomena.

Thus, if it is determined that an efficient reaction is
dependent on the mixture ratio at which the reaction
proceeds, the designer must be able to predetermine and
control the *local* mixture ratio. Obviously, control of the
overall or gross mixture ratio is insufficient in itself, since

the reaction requires mixing to a relatively small scale—ultimately, to the molecular level. Similarly, if it is determined that the efficiency of the reaction is dependent on the mean particle size of the injected propellant, the designer must be able to predetermine the required particle size and then to specify the particular injector configuration that will produce that particle size. This procedure must be continued until all the significant parameters are considered.

The one singular fact that evolves from this assessment of the problem is that the only parameters available to the designer are of a geometrical nature and are contained within the physical configuration of the injector and chamber. It therefore follows that the designer must utilize these parameters to control, not the combustion process, but only the prereaction situation achieved before combustion actually takes place. Since neither injector nor chamber (i.e., their geometrical properties) enters into the combustion process, and since it is assumed that combustion will proceed in identically the same fashion, regardless of the scheme used to achieve particular prereaction conditions, then it must be concluded that there is no unique correlation between injector geometry and combustion, and that an intermediate correlation with the prereaction conditions is essential to a logical design procedure. Thus, although it is clear that the ultimate objective is to achieve efficient combustion, the relative success of an injector design is more dependent on the designer's ability to correlate, first, the geometric parameters at his disposal with those parameters that are significant to the prereaction situation and, subsequently, this prereaction situation with combustion phenomena.

A. Significant Properties of the Prereaction Zone

A complete and general description of the combustion-chamber environment is probably impossible; but, if one concentrates on those prereaction properties that are directly relatable to the injection scheme, it is possible to limit the so-called significant parameters to the mass-flux distribution, the local composition as exemplified by the local mixture ratio, and (to the extent that multiphase components exist) the local droplet-size distributions. Further, if the characterization of the relatable chamber properties is restricted to the so-called prereaction volume (i.e., the volume whose properties are dominated by the geometry and hydrodynamics of the injection scheme), then the significance of these several terms can be summarized as indicated below.

1. Mass Distribution

The term *mass distribution* refers to the distribution of axial mass flow rate for a cylindrical chamber with one-dimensional flow. This parameter serves to define the relative concentrations and, on an absolute scale, should presumably define the maximum tolerable concentrations for any given propellant combination. Control and specification of this parameter provide a basis for achieving uniformity in local concentrations and, hence, in axial mass flux in a chamber. Also, when the injector is a composite of a number of essentially identical elements, the properties of the element can be used to construct the gross injection characteristics. This procedure can be utilized to obtain a prescribed injection pattern (i.e., mass distribution) since, in most cases, it is simpler to "organize" the mass distribution of a number of small elements to conform to a particular chamber geometry than it is to fabricate suitable chamber boundaries to suit the mass distribution of a small number of elements (i.e., one or two).

2. Mixture-Ratio Distribution

This parameter is simply a measure of the degree of mixing uniformity achieved by the injection processes. Presumably, the ideal situation from a chemical-combustion viewpoint is attained when a predetermined mixture ratio (i.e., peak performance or its equivalent) is achieved on a molecular scale in a minimum time and/or space. For most engine applications, however, it is probable that a scale of mixing substantially coarser than molecular is sufficiently small.

3. Particle-Size Distribution

This property of the propellant is important whenever heat transfer to the propellant surface is the dominant mechanism in elevating the propellant to an exothermic (self-sustaining) reaction temperature. Monopropellant systems are certainly contained in this category, whereas highly hypergolic systems, with reasonable mixing in the liquid phase, can achieve the required reaction temperature without relying on heat transfer from the reaction products and hence may be unaffected by changes in droplet-size distributions.

B. The Hypothesis

Although it is reasonable to expect that combustion will affect all spray properties to some degree, the fact remains that such effects are simply additional variables

and serve only to modify the detailed properties of the prereaction environment. Thus, injection into a combustion environment does not alter the possibility that the overall characteristics of the prereaction region may be deduced from the properties of the injected sprays. Further, at least for those systems utilizing relatively non-hypergolic propellants, or single-component sprays, where combustion effects can be considered negligible (insofar as the initial propellant distributions are concerned), the characteristics of the injection scheme can be determined directly from sprays produced by similar element configurations used with nonreactive fluids. Thus, one is led to the hypothesis that it is possible to utilize readily attainable nonreactive-spray information as a logical basis for injector design.

In an effort to provide a portion of the information required as a basis for this design concept, this author has studied experimentally the properties of sprays produced by a pair of unlike impinging jets of nonreactive liquids. The single pair of unlike impinging streams was the configuration chosen for these studies because (1) it is widely used as an elemental injector component (hence, the so-called injector element); (2) it has the potential of substantially enhancing the mixing of unlike fluids; and (3) it is the simplest of a large family of impinging-stream elements (such as the coplanar-symmetrical-triplet, the symmetrical-quadruplet, etc.). The results of these studies, summarized from time to time in the bimonthly JPL publications, were presented in detail in Refs. 1 and 2. In addition, one of the earliest attempts to apply mass-distribution data to the combustion problem was reported in Ref. 3. Thus, a substantial amount of information on the simulated nonreactive properties of propellant sprays was available, but the hypothesis stating that these properties were relevant to conditions in a combustion chamber had not been tested. Before continuing efforts to describe the prereaction zone in a combustion chamber in this manner, it was essential that the applicability of the hypothesis be demonstrated.

It should be clear that, if such a hypothesis could be verified, its real significance would lie in the ability to predict a priori a prereaction environment that would be controlled by the specified geometrical and hydraulic properties of the injection scheme. Although the approach should be applicable to any required specification, it seemed that its worthiness could be best demonstrated by attempting to achieve near-optimum performance with an arbitrarily chosen propellant system at a reasonable thrust level. Since, in rocket engines, maximum relative performance also implies a chamber-volume limitation,

it was presumed from strictly intuitive arguments that a uniform mixture-ratio distribution, as well as a uniform mass-flux distribution should be achieved within a minimum axial length. Hence, the injectors designed to these specifications became known as *Uniform Mass and Mixture-Ratio Distribution* (UMMR) injectors. It was intended that the performance characteristics of such injectors would be compared with schemes which did not achieve these objectives, and also with those for which one or more of the significant variables were degraded to a measurable extent. In order to minimize the complexity of these experiments, hypergolic propellant systems were used throughout, so that droplet-size distribution was not included as an injection parameter.

C. Program Scope

To accomplish the objectives outlined above, an experimental program was initiated at this Laboratory early in 1955. The interim results of this effort were reported at the JANAF Meeting in New Orleans in 1959 (Ref. 4). Substantial portions of that initial publication have been reproduced here, in some cases verbatim, so that the pertinent arguments and essential background information would be assembled in a single volume. This is particularly true with respect to the description of the nonreactive properties of injection schemes and their relation to the combustion process. The objectives of that initial program were, however, broadened considerably to include (1) extension of the demonstration to a number of different propellant combinations; (2) application of the concepts to the design of large-scale elements; (3) a cursory investigation of combustion instability; and (4) an attempt to correlate the injection scheme with boundary phenomena in the chamber. This effort ultimately resulted in the design and evaluation of eight injectors, in addition to the so-called *Corporal*[1] injector, which was used as a datum reference (Section III). The properties of these injectors, as determined with nonreactive fluids, are presented here. The evaluation of the combustion phenomena associated with these injectors is covered in Parts II to VIII of this Report (Refs. 5 to 11), which present, respectively, discussions of the experimental techniques and instrumentation, the gross performance characteristics, the relation of the injection pattern to chamber heat transfer, the combustion-stability

[1]The designation *Corporal* refers to a ballistic missile developed by JPL for the Army Ordnance Corps under contract DA-04-495-Ord-18. *Corporal* propellants are mixtures of nitric acid and nitric oxide as oxidizer, and analine, furfuryl alcohol, and hydrazine as fuel. See Section III.

correlations, the starting-transient effects, the performance achieved by high-flow-rate elements, and the performance attained with the pentaborane–hydrazine propellant combination.

D. Literature Review

A search of the literature on injection schemes applicable to rocket engines reveals almost immediately that, in contrast to the hypothesis outlined above, the prime effort has been expended on obtaining a direct correlation between injector geometry (usually a word description of the element type, number, and placement) and gross combustion effects (i.e., c^* and I_s); only rarely is any consideration given to the hydrodynamic properties of the injector elements and the prereaction configuration resulting therefrom. In particular, it is clear from Refs. 1 and 12 to 15 (for example) that the short sharp-edge orifices fed by extremely complex flows, as incorporated in nearly all injection schemes described in the literature, will produce jets whose properties are unpredictable, unknown, and uncontrolled, and therefore can be expected to have only a superficial relation to the geometrical properties of the orifice. It follows, therefore, that the really significant prereaction parameters, such as mass distribution, mixture-ratio distribution, and drop-size distribution, will be only superficially related to injector geometry. "Misalignment," for example, as deduced from measurements of the hole centerlines, is apt to be a meaningless parameter insofar as the real jets are concerned. Also, as a consequence of a distorted momentum profile, the "effective" misalignment may be many times the value determined for the centerlines.

In this author's view, these observations are pertinent to nearly all the attempts to achieve correlations between injection schemes and combustion that have to date appeared in the literature. Admittedly, recognition of the significance of jet properties will not in itself provide the desired correlations, but will certainly assist in promoting the controlled experiment essential to defining a correlation.

In those instances where the investigator does concern himself with the hydraulic properties of the injector, the interest usually stems from the system viewpoint, rather than from a desire to control conditions in the combustion chamber. Typical of this effort are the studies reported by Wright (Ref. 16), who investigated the flow characteristics (i.e., the discharge coefficients) of short sharp-edged entry orifices obtained by drilling a hole in a flat plate. This geometry is very popular for rocket injectors because of the apparent simplicity of manufacture. Although it is true that such data can produce information suitable for specifying time-averaged flow rates, and that this information is essential for correlating engine system characteristics, it is extremely doubtful that it can be used to provide the injector-design correlations that are required.

Noteworthy exceptions to the situation outlined above are the contributions of Heidman, et al. (Ref. 17), who used relatively long glass tubes[2] for orifices in studies of the fluctuations in sprays formed by a pair of impinging water jets and, later (Refs. 18 and 19), employed long metal tubes in studies of drop-size distributions and spatial characteristics of impinging-stream sprays. However, these investigators were not concerned with unlike streams and, hence, with mixture-ratio distributions in such sprays. Ryan (Ref. 20) evaluated the mixture ratio of individual drops formed by such sprays (finding them "essentially equal" to the gross mixture ratio throughout the range of his determinations, which included sizes as small as 75μ), but did not attempt to identify spatial properties of the spray. Also, he utilized a pair of sharp-edged orifices which, as indicated in Ref. 14, have several desirable features, but produce jets which are extremely susceptible to upstream disturbances.

In a somewhat different approach to the problem, Ingebo (Refs. 21 to 24) has adopted the viewpoint that correlation of the prereaction environment with combustion phenomena does not necessarily depend on the geometrical properties of the injection system if the significant parameters can be determined directly in a combustion chamber. Although it would appear, even in this case, that the achievement of a truly "steady" injection process might be extremely helpful, conceptually at least, this does not appear to be necessary if the experimental techniques are sufficiently sophisticated. As indicated in Refs. 21 to 24, Ingebo has evaluated drop-size distributions, evaporation rates, and heat-transfer rates to drops (rather than mass and mixture-ratio distributions) under actual combustion conditions. This, of course, is an exceptionally difficult experimental approach and, from the design viewpoint, must eventually provide a correlation between the observed spray properties and injector geometry. As indicated above, the latter step may be extremely difficult if jet properties and orifice geometry are not uniquely related.

---

[2]Precision-bore glass tubing, 2 in. long, with inside diameters of 0.025, 0.040, and 0.057 in.

This very brief review of the literature includes only a few of the published reports considered most pertinent to the present investigations, and is certainly not complete. More comprehensive bibliographies are given by DeJuhaz in Ref. 25 and by Marshall in Ref. 26. In summary, it can be stated that the greater part of the available information relating injector configuration to combustion performance has proved to be unsuitable for injector-design purposes because the hydrodynamic properties of the injection scheme were inadequately controlled and/or specified. This situation excludes any possibility of correlating such schemes with the prereaction situation and, in many instances, completely invalidates attempts to correlate injection and combustion. Thus, one of the prime objectives of the effort reported here was to incorporate in the injector designs the features necessary to control jet characteristics and the dominating spray properties: i.e., the local mixture-ratio distribution and the local axial-mass-flow-rate distribution. If this could be accomplished, the application of such a design concept would be assured. To this end, the information found in Refs. 1, 2, and 14 was used almost exclusively as a basis for specifying and evaluating these parameters. These studies are briefly reviewed to acquaint the reader with the underlying ideas and concepts, and to provide a basis for the extension of these concepts as presented here.

II. DETERMINATION OF SPRAY PROPERTIES WITH NONREACTIVE FLUIDS

The significant properties of sprays can best be visualized by referring to Fig. 1, which incorporates several pertinent photographs, together with an artist's conception of six of the more basic injector elements. These sketches are intended to show that, despite certain obvious differences, the prime objective in every case is to achieve some degree of controlled mixing with a particular mass distribution; and, further, that in every case the element depends on the hydrodynamic properties of free-liquid sheets or jets to accomplish this objective. The control of these properties is prerequisite to the control of mass and mixture-ratio distributions. It should also be noted at this point that, once the required properties of an injection scheme have been defined, any or all such elements could be utilized to achieve those requirements. It is only because the properties of sprays formed with *unlike impinging streams* have been evaluated in some detail that this element was utilized in these investigations.

Figure 1(b) shows two views of a spray produced by impingement of a pair of nearly identical water jets. It is seen that the bulk of the spray is concentrated about a "resultant momentum line" and has (at least in this case of identical jets with equal momenta) a nearly elliptical cross section. Now, if a collector of the type shown in

Fig. 1(c) is exposed to such a spray for a reasonable time interval, a series of samples such as those shown in Fig. 1(d) can be obtained. In this case, the vertical height of the sample in each tube is proportional to the local mass flow rate at a different position within the spray and is, therefore, a direct evaluation of the mass distribution produced by the spray. In addition, if the injected fluids are immiscible, they will separate after the sample is obtained (as indicated in the photographs). It is thus possible to determine the relative flow rates at a particular point in the spray and hence to obtain the local mixture ratio which, together with additional samples, obviously yields the mixture-ratio distribution.

A great deal of this kind of information was obtained with the carbon tetrachloride–water system, in order to simulate the density ratio of *Corporal* propellants. These data have been utilized to produce a correlation of a quantity η_m, known as the *mixing factor*, with the gross dynamic properties of the two jets (Refs. 1 and 2). The mixing factor is expressed by

$$\eta_m \equiv 100 \left\{ 1 - \left[\sum_0^n \frac{K\dot{w}_s (\phi_0 - \phi)}{(\Sigma K\dot{w}_s)\,\phi_0} + \sum_0^{\bar{n}} \frac{K\dot{w}_s (\phi_0 - \bar{\phi})}{(\Sigma K\dot{w}_s)(\phi_0 - 1)} \right] \right\}$$

(a) TYPICAL ROCKET-INJECTOR ELEMENTS

SHOWER HEAD

LIKE-ON-LIKE IMPINGING JET

UNLIKE-ON-UNLIKE IMPINGING JET

2-ON-1 IMPINGING JET SYMMETRICAL COPLANAR TRIPLET

SPLASH PLATE IMPINGING JET

IMPINGING SPRAYS

(b) SPRAY FROM A PAIR OF IMPINGING JETS

(c) SPRAY-SAMPLING COLLECTOR

DISASSEMBLED FOR PHOTOGRAPHING   ASSEMBLED FOR SAMPLING

$\theta = 0°$ $\theta = 15°$ $\theta = 30°$

$\theta = 45°$ $\theta = 60°$ $\theta = 75°$

(d) TYPICAL SERIES OF SPRAY SAMPLES
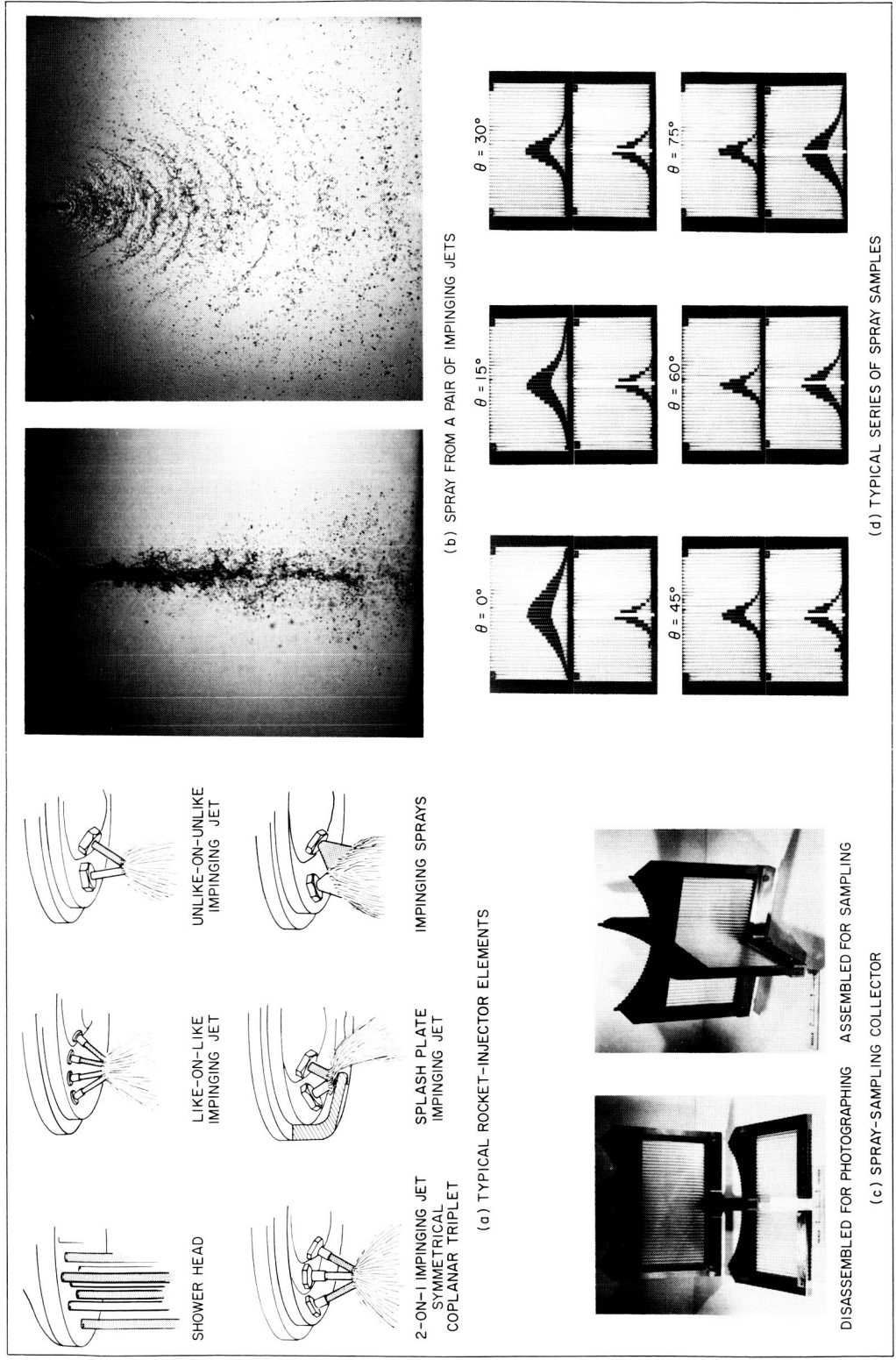
Fig. 1. Montage of nonreactive-spray experiments

where

K = area correction factor = A_s/A_0

A_s = local area represented by sample, in.^{2}

A_0 = tube area = 0.0227 in.^{2}

$\dot{w}_s$ = total local flow rate of spray
$= (\dot{w}_{1s} + \dot{w}_{2s})_{\theta,R}$, lb/sec

ϕ = local mass-fraction ratio of spray
$= \dot{w}_{2s}/(\dot{w}_{1s} + \dot{w}_{2s})_{\theta,R}$

ϕ_0 = nominal mass-fraction ratio of spray
$= \dot{w}_{2el}/(\dot{w}_{1el} + \dot{w}_{2el})$

n = number of samples in which $\phi < \phi_0$

$\bar{n}$ = number of samples in which
ϕ is designated as $\bar{\phi}$ because
$\phi > \phi_0$

Thus, the mixing factor is essentially a summation of the mass-weighted value of the difference between the local mass-fraction ratio and the nominal mass-fraction ratio, which has been modified to yield limiting values of 0 and 100. In at least one sense, it can be imagined to represent the percentage of the total spray that has achieved the intended mixture ratio.

Figure 2 (taken from Ref. 2) shows the correlation resulting from this effort, which has been used as the basis for the conclusion that (within the limitations of the experiments) the most uniform mixture-ratio distribution is achieved in the spray produced by a pair of impinging streams when the products of fluid density, velocity squared, and jet diameter are equal for both streams, or when

$$\frac{\delta_1 V_1^2 d_1}{\delta_2 V_2^2 d_2} = 1.0$$

This quantity has become known as the *uniformity criterion*, although it should more appropriately be termed the *mixture-ratio* or *mixing-uniformity criterion* to distinguish it from mass-flux uniformity.

If, in addition to the usual mixture-ratio specifications, it is required that the element satisfy this mixing-uniformity criterion, then the orifice diameter ratio and the jet velocity ratio for any given propellant system are defined, respectively, by Eqs. (c) and (d) of Fig. 2. If it is further assumed that the total flow rate for the element $\dot{w}_{el}$ is determined from other considerations, then Eq. (e) of Fig. 2 must also be satisfied. Obviously, then, the additional arbitrary choice of one velocity or one diameter
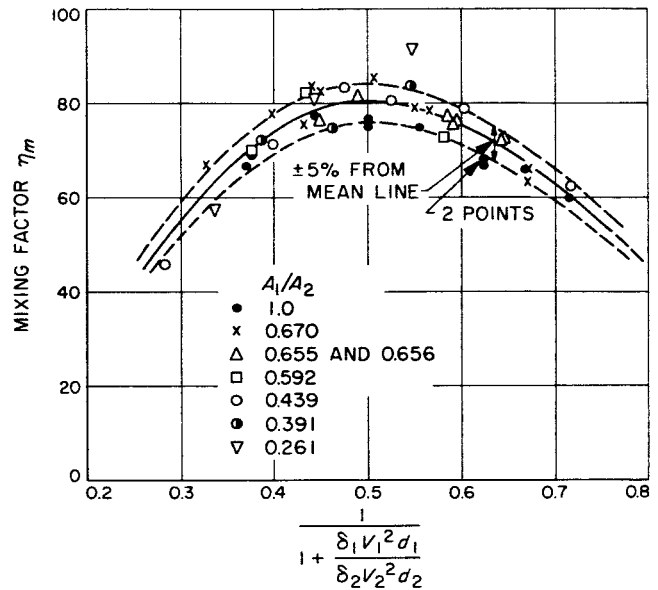
For the maximum value of η_m (i.e., near–uniform r distribution), the uniformity criterion is expressed by

$$\frac{\delta_1 V_1^2 d_1}{\delta_2 V_2^2 d_2} = 1.0 \qquad (a)$$

and, by definition,

$$r = \frac{\delta_2 V_2}{\delta_1 V_1}\left(\frac{d_2}{d_1}\right)^2 \qquad (b)$$

Therefore, combining Eqs. (a) and (b) gives

$$\frac{d_1}{d_2} = \left(\frac{\delta_2}{\delta_1}\right)^{1/3}\left(\frac{1}{r}\right)^{2/3} \qquad (c)$$

and

$$\frac{V_1}{V_2} = \left(\frac{\delta_2}{\delta_1}\,r\right)^{1/3} \qquad (d)$$

For a particular flow rate,

$$V_1 = \frac{576\,\dot{w}_{el}}{\pi\delta_1\,d_1^2\,(1+r)} \qquad (e)$$

Note also that, for design conditions where r, δ_1, δ_2, and d_1/d_2 satisfy the uniformity criterion,

$$\frac{P_1}{P_2} = \frac{d_1}{d_2}$$

where P is momentum per second. Thus, for any given injector, the value of r which satisfies the uniformity criterion is expressed by

$$r_{unif} = \left[\frac{\delta_2}{\delta_1}\left(\frac{d_2}{d_1}\right)^3\right]^{1/2}$$

Fig. 2. A correlation of mixing factor and uniformity criterion and derivation of pertinent equations

will determine all other values. In any event, when Eqs. (c) and (d) are satisfied, the element will produce a spray having a near-uniform mixture-ratio distribution, so that at least that aspect of the design can be delineated.

It has been shown that similar correlations are possible for the coplanar-triplet element and certain other element geometries (Refs. 27 and 28), but, experimentally at least, the mixing-uniformity criterion tends toward the same relative level: i.e., $\eta_{m_{max}} = 85$ to 90. Thus, any advantages to be derived from the use of these relatively complex elements must stem from some other consideration.

Unfortunately, no simple way of characterizing the *mass distribution* of the spray produced by an element has been devised. This problem is particularly difficult, since such distributions tend to be strong functions of the relative geometry and dynamic properties of the jets, even when they satisfy the mixing-uniformity criterion, as well as the included angle between the jet centerlines, (impingement angle), which has a relatively small effect on *mixing* uniformity (Ref. 1). Thus, in designing a composite injector, it has been necessary to specify the impingement angle on a nearly arbitrary basis and then to utilize experimental information obtained with an actual injector element similar to the proposed design. This procedure is permissible, since the geometrical properties of the sprays produced by a pair of jets having similar impingement angles, orifice diameter ratios, and jet velocity ratios tend to be insensitive to scale and absolute levels of mass flow rates (Ref. 1). It is possible, therefore, to approximate the mass distributions of a proposed element from other data that may be available (e.g., from the experimental data used to determine the mixing correlation).

It can now be seen, at least for the case without combustion, that such data provide (1) a means of obtaining a near-uniform mixture-ratio distribution of the injected propellants, and (2) a means of predicting and controlling the axial-mass-flow-rate distributions in a chamber of arbitrary cross section. Therefore, if it could be shown that these parameters unquestionably characterize the "early-combustion" region of an actual combustion chamber, then the hypothesis would be verified, and the parameters could be utilized as a logical basis for injector design.

III. EXPERIMENT TO TEST THE HYPOTHESIS

The validity of using these parameters to characterize the prereaction configuration of an actual combustion chamber was determined by the design and evaluation of a series of injectors incorporating the pertinent nonreactive-spray characteristics to varying degrees. Since it was expected that the injectors would exhibit different performance characteristics (if, in reality, the truly significant parameters had been chosen for evaluation), it was essential that the combustion experiments have a sound datum plane for comparison. These reference data could have been produced as part of this program; however, a rather extensive development program, conducted by JPL on the *Corporal* propulsion system, had failed to realize the full potential of the propellant system. Thus, it seemed reasonable to adopt the design criteria established for the *Corporal* engine, but to require in addition that the injection scheme produce near-uniform mixture-ratio and axial-mass-flux distributions as inferred from the properties of nonreactive sprays. If such a design should produce near-optimum performance, it could then be argued that the hypothesis had been verified. The achievement of appreciable performance improvement would be particularly significant in view of the considerable development effort already expended in attempts to achieve that objective. On the other hand, failure to achieve performance improvement would be inconclusive, since the assumption that high performance is uniquely related to uniformity of mass and mixture-ratio distributions might not be valid. Similar demonstrations with other design objectives would be essential to a more general proof of the hypothesis.

The final development version of the injector for the *Corporal* engine (Fig. 3) incorporated 52 pairs of unlike impinging jets, arranged to produce two concentric rows of impingement points tending to concentrate the injected
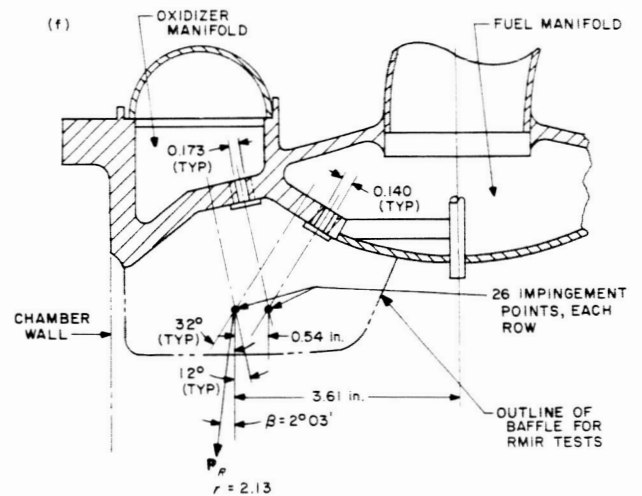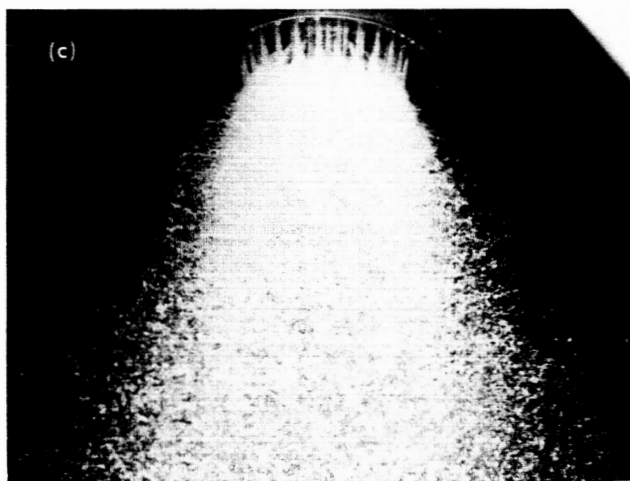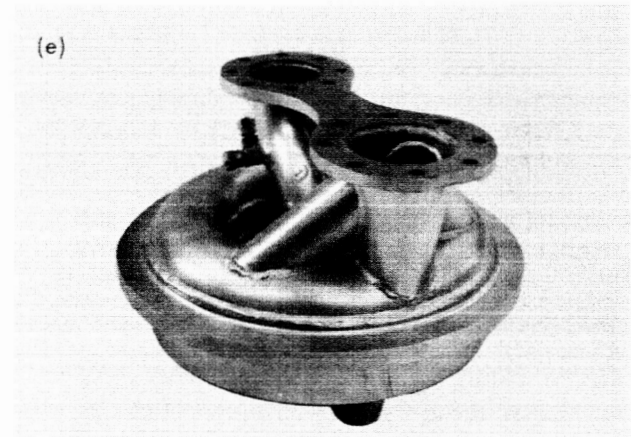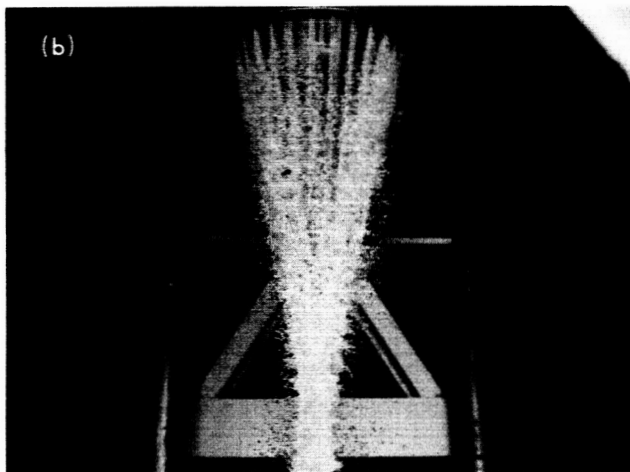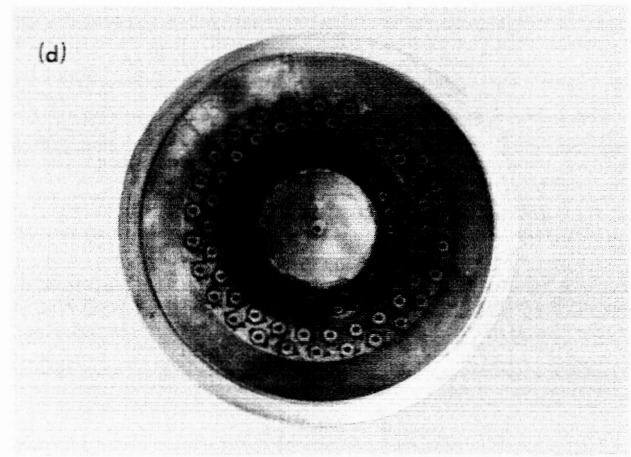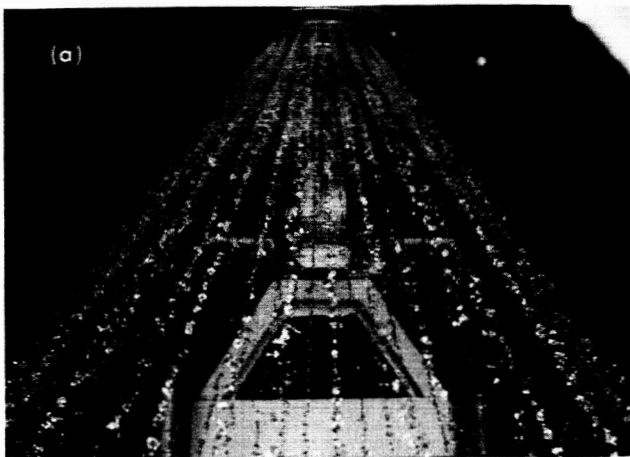
Fig. 3. Hydraulic and geometric characteristics of *Corporal* Injector, Type 1. (a) Fuel jets. (b) Oxidizer jets.
(c) Combined flow. (d) Injector face. (e) Side view of injector, showing manifold.
(f) Element and manifold geometry

fluids in an annular section of the combustion chamber. The mass distribution achieved by this injection scheme was highly nonuniform and, hence, was admirably suited to a comparison with the so-called uniform axial-mass-flux distribution. Also, for the peak-performance mixture ratio (i.e., 2.13), the orifice diameters were such that the value of the mixing-uniformity criterion was considerably less than 1.0. It was clear that substantial changes in both the mixing effectiveness and the uniformity of mass distribution could be achieved while retaining all the gross operating conditions for the engine, and that a reasonable demonstration of the hypothesis should be possible.

A number of other considerations influenced this choice of a reference system: (1) a large number of reference data, as well as a substantial amount of suitable hardware, were already available; (2) the propellants were hypergolic, so that the influence of droplet-size distribution was minimized (Section I-A-3); (3) the injector element incorporated a pair of unlike impinging jets for which many nonreactive-spray data were already available (Section II). Also, the choice of a particular injector configuration permitted specification of a number of otherwise variable parameters: for example, the number of injector elements, the impingement angle (and therefore a particular mass distribution for the element), the propellants, and, by retention of the motor and nozzle geometry of the uncooled version of the *Corporal* system, the thrust level.

Since some changes in the details of the orifices would be required for conformance with the uniformity criterion (at reasonable mixture ratios), it was decided on a strictly arbitrary basis to retain, insofar as possible, the oxidizer orifice diameter used in the *Corporal* injector and hence the same oxidizer jet velocity. Thus, the major modification of the element would be in the fuel-jet properties (i.e., velocity and diameter) and ultimately in the placement and scale of the elements.

A prime objective of the investigation was a direct comparison of the performance characteristics of the *Corporal* system with an injector intended to produce near-uniform mass and mixture-ratio distribution. It was also pertinent, however, to obtain a comparison with several intermediate injector modifications in order to determine, if possible, the relative significance of mass distribution, mixture-ratio distribution, and the contribution (if any) of controlled injector hydraulics. Also, since the *Corporal* injector had achieved peak performance at a mixture ratio of 2.13, which is substantially different

from the mixture ratio for peak theoretical performance (i.e., 2.80), it was essential that the mixture-ratio effect be determined.

To this end, four injectors having an element geometry and orientation similar to those of the *Corporal* injector were designed, evaluated, and compared with a fifth model intended to produce near-uniform mass and mixture-ratio distributions in the same chamber configuration with the same propellant combination. These four "*Corporal*-like" injectors included designs intended to duplicate the centerline geometry of the *Corporal* orifices, but using modified orifice geometry and manifolding so as to obtain stable jets with symmetrical and similar velocity profiles.

For two of these injectors, the fuel orifice diameters were decreased to satisfy the mixing-uniformity criterion at mixture ratios of 2.13 and 2.80. One consequence of this modification was a substantial change in the β-angle (the true angle between the resultant momentum line for the spray and a perpendicular to a plane normal to the chamber axis). Since variations in the β-angle had been associated with significant changes in performance during the *Corporal* development effort, it was also necessary to distinguish any effects due to changes in the β-angle per se. Therefore, the other two injectors were made geometrically similar to those described above, except that the element was "rotated" about its impingement point so that the resultant β was identical with that of the original *Corporal* design. A two-point check would thus be obtained on the influence of changes in mass distribution resulting from changes in β with no change in mixture-ratio distribution, and the performance characteristics of these injectors could be compared with the so-called UMMR injection scheme.

In an effort to determine, in a preliminary way, the extent to which the "scale" of the element (i.e., the thrust level per element) would influence the gross performance characteristics of an engine, a sixth injector configuration was also proposed in which the scale was increased by approximately one order of magnitude. As will be seen, the ultimate design incorporated six elements rather than five, in order to provide a more nearly uniform axial-mass-flux distribution. To verify the demonstration with a significantly different propellant system ($N_2O_4 + N_2H_4$), two additional designs were subsequently created (one injector for each scale) in an effort to achieve near-uniform mass and mixture-ratio distribution with elements having

approximately the same thrust as those designed for the *Corporal* propellants.

Thus, eight different injector designs, intended to optimize conditions for two different propellant combinations at two element scales and to evaluate the significance of the β-angle for a particular injector geometry, were completed and subsequently tested. As noted above, only the nonreactive mass and mixture-ratio distributions of these several injectors, as inferred from similar properties

of an individual element together with certain dynamic characteristics of individual jets, are discussed here; their performance characteristics and an updated performance evaluation of an actual *Corporal* injector are presented in Refs. 5 to 11. The pertinent dimensional details of the uncooled *Corporal* engine, together with a photograph of a typical thrust-stand installation, are shown in Fig. 4. Additional test-stand and instrumentation details may be obtained from Ref. 5, and the performance characteristics of the several engine configurations from Refs. 6 and 10.

ENGINE CONSTANTS

$A_t = 47.15$ in.^{2}

$\epsilon_e = 4.578$

$\epsilon_c = 2.030$

$C_{F_{exp}} = 1.410$ λ $C_d = 1.362$

ASSUMPTIONS:

$\gamma = 1.25$

$p_c = 300$ psia

$p_0 = 13.5$ psia

$\lambda = 0.984$ (15 deg)

$C_d = 0.985$

$F = 19,300$ lb

$L^* \simeq 40$ in.

CHAMBER DIAMETER = 11.06 in.
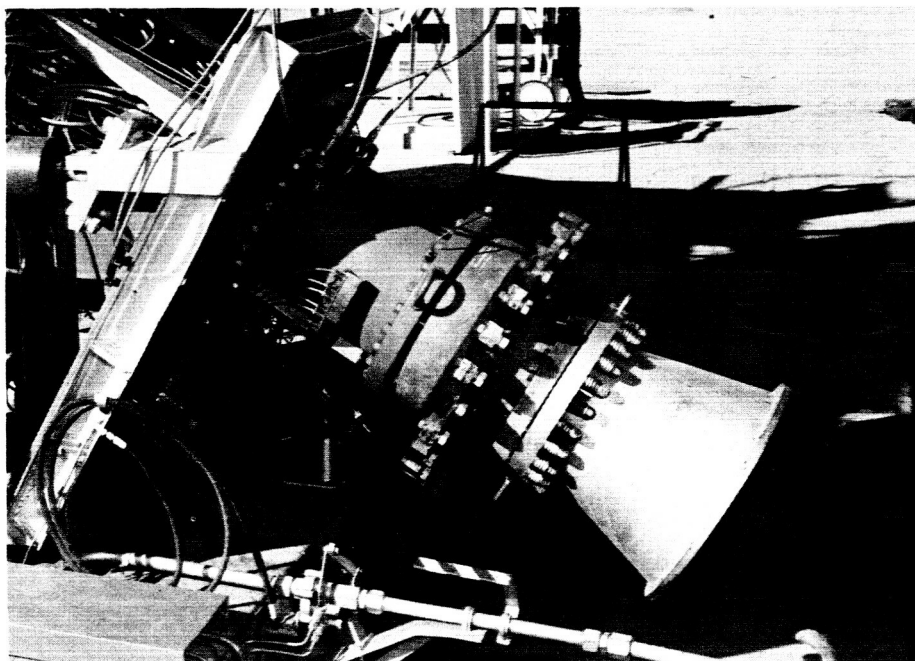
Fig. 4. Typical test-stand installation for uncooled *Corporal* engine

IV. INJECTOR DESIGN PROCEDURES

A. Specifications

The design specifications for the *Corporal* injector and the eight experimental models utilized in these studies are summarized below, and the pertinent geometrical constants are presented in Table 1. The various experimental designs are designated as RMIR Injectors 1 to 8, referring to *Rocket Motor Injection Research*, the title of the experimental project under which the effort was funded.

Corporal Injector (Type 1). Figure 3 presents a sketch of the significant geometrical details of this injector, together with several photographs of the actual injector and high-speed-flash photographs of the jets and sprays that it produces. This design was characterized by an annular array of 52 unlike-impinging-stream elements incorporating relatively short orifices combined with relatively long free-jet lengths. Considerable attention was given to minimizing manifold volumes. As noted above, the "design" mixture ratio r (i.e., the mixture ratio that

Table 1. Design specifications for RMIR Injectors

Design conditions[a]	Corporal Injector (Type 1) J-360	RMIR Injectors							
		Injector 1 J-373, J-371	Injector 2 J-375	Injector 3 J-374	Injector 4 J-376	Injector 5	Injector 6	Injector 7	Injector 8
Propellants									
Oxidizer	SFNA[b]	SFNA	SFNA	SFNA	SFNA	SFNA	SFNA	N_2O_4	N_2O_4
Fuel	Corporal fuel[c]	Corporal fuel	Corporal fuel	Corporal fuel	Corporal fuel	Corporal fuel	Corporal fuel	N_2H_4	N_2H_4
Specific gravity									
Oxidizer $\left(\dfrac{20°}{4}\right)$	1.550	1.550	1.550	1.550	1.550	1.550	1.550	1.450	1.450
Fuel $\left(\dfrac{20°}{4}\right)$	1.073	1.073	1.073	1.073	1.073	1.073	1.073	1.010	1.010
Mixture ratio	2.13	2.13	2.13	2.80	2.80	2.80	2.80	1.20	1.20
Number of elements	52	52[d]	52	52	52	52	6	47	6
$\dot{w}$ per element, lb/sec	1.95[e]	1.95[e]	1.95[e]	1.85[f]	1.85[f]	1.85[f]	16.53[f]	1.74[g]	13.6[g]
Mixing factor η_m	N.A.	76.3	76.3	85.0	85.0	85.0	85.0	73.6	70.6
Element geometry									
Impingement angle α, deg	44	44	44	44	44	44	44	45	80
Oxidizer orifice diameter, in.	0.173	0.173	0.173	0.173	0.173	0.173	0.509	0.173	0.402
Fuel orifice diameter, in.	0.140	0.118	0.118	0.0986	0.0986	0.0986	0.289	0.173	0.402
Oxidizer free-jet length, in.	1.770	0.692	0.692	0.692	0.692	0.692	2.036	0.692	1.608
Fuel free-jet length, in.	1.478	0.472	0.472	0.394	0.394	0.394	1.156	0.692	1.608
Oxidizer jet velocity, fps	84.2	84.2	84.2	86.5	86.5	86.5	89.3	64.2	93.2
Fuel jet velocity, fps	100.8	148.0	148.0	137.6	137.6	137.6	141.8	73.5	108.3
Element orientation	Two annular rows of impingement points, with plane of orifice centerlines on radii (see Fig. 16)					Oriented to achieve near-uniform mass-distribution at the model plane (see Figs. 17 to 20)			
β angle	2°03′	5°40′	2°05′	3°38′	2°03′	0°0′	0°0′	0°0′	0°0′
ζ angle	−7°57′	−4°20′	−4°20′	−6°22′	−6°22′	−6°18′	−6°18′	0°0′	0°0′
P_1/P_2[h]	0.4864	0.6844	0.6844	0.5677	0.5677	0.5677	0.5677	1.00	1.00
Chamber geometry[i]									
Distance from station 0 to impingement point, in.	2.461 to outer row, 2.479 to inner row	2.461 to outer row, 2.479 to inner row	2.461 to outer row, 2.479 to inner row	2.461 to outer row, 2.479 to inner row	2.461 to outer row, 2.479 to inner row	0.767	2.767	1.142	1.079
Distance from impingement point to model plane, in.	Not evaluated[j]	Not evaluated[j]	Not evaluated[j]	1.98	1.98	1.98	5.83	2.13	3.37
Distance from station 0 to injector face, in.	Contoured face[l]	Contoured face[l]	Contoured face[l]	Contoured face[l]	Contoured face[l]	0.017	0.267	0.142	−0.688
G_{max} at nozzle entrance,[k] lb/sec-in.^{2}	Not evaluated[j]	Not evaluated[j]	Not evaluated[j]	0.0786	0.0786	0.0627	0.738	0.090	0.223

[a]Total thrust $\simeq$ 20,000 lb; $p_c = 300$ psia; $p_o = 13.5$ psia.
[b]SFNA: 83.5% HNO_3 + 13% NO_2 + 3% H_2O + 0.5% HF (by weight).
[c]Corporal fuel: 46.55% $C_5H_6O_2$ + 44.54% $C_6H_5 \cdot NH_2$ + 7.13% N_2H_4 + 1.78% H_2O (by weight).
[d]Also run with 49 elements (see Ref. 8).
[e]Based on $c^*/c^*_{th} = 0.92$.
[f]Based on $c^*/c^*_{th} = 0.95$.
[g]Based on $(I_s)_{exp} = 245$ sec.
[h]Relative to resultant momentum line.
[i]Station 0 is upstream end of chamber.
[j]Similar to RMIR Injectors 3, 4, and 5
[k]Nozzle entrance at station 16.45 in.
[l]Volume-average station = 1.107 in.

produced maximum experimental performance) was 2.13, while the mixture ratio for peak theoretical performance, based on equilibrium characteristic exhaust velocity c^* with *Corporal* propellants, was approximately 2.80. (Theoretical performance data for the *Corporal* propellant system were taken from Ref. 29.) It should also be noted that the relatively poor control of the dynamic characteristics of the *Corporal* injector jets does not allow a meaningful inference regarding its mass or mixture-ratio distribution.

RMIR Injector 1. This design was geometrically similar to the *Corporal* injector, but was modified to (1) produce fully developed turbulent jets, which were hence stable, similar, and reproducible (Section 1-B); (2) provide a free-jet length of 4 diameters;[3] (3) satisfy the mixing-uniformity criterion at $r = 2.13$; and (4) maintain an oxidizer-jet mean flow rate identical with the value for the *Corporal*. As noted above, these changes resulted in a different β-angle from that produced by the *Corporal*.

RMIR Injector 2. This model was geometrically similar to Injector 1, above, except that the resultant momentum angle β of the element was made identical with that of the *Corporal* by "rotating" the element about its impingement point in the plane of the stream centerlines.

RMIR Injector 3. This model was geometrically similar to Injector 1, except for modification of the fuel-orifice diameters to satisfy the mixing-uniformity criterion at $r = 2.80$.

RMIR Injector 4. This injector was geometrically similar to Injector 3, except that the resultant momentum angle β was made identical with that of the *Corporal* by "rotating" the element about its impingement point in the plane of its centerlines.

RMIR Injector 5. This design also had 52 elements and the same element geometry (i.e., impingement angles, orifice diameters, etc.) as Injectors 3 and 4. It therefore satisfied the uniformity requirements for $r = 2.80$, but was modified by revision of the element location to achieve near-uniform axial mass flow rate (as well as uniform

---

[3]A free-jet length of 4 diameters was chosen as a "best compromise" for minimizing the free-jet length while assuring that the "standing wave" formed by impingement did not extend upstream as far as the orifice exit. The data of LeClerc (Ref. 30) indicate that an appreciable pressure associated with the wave is still apparent at distances of 2.5 diameters. Hence, a 4-diameter free-jet length should assure a negligible interaction.

mixture-ratio distribution), as inferred from nonreactive-spray properties.

RMIR Injector 6. This configuration was designed for the same element geometry (except the required change in orifice diameters), propellant combination, and total thrust level as those used in Injector 5, but was modified to reduce the number of elements by nearly an order of magnitude (i.e., to 6), while maintaining the oxidizer jet velocity constant.

RMIR Injector 7. This injector contained approximately the same number of elements and produced the same total thrust level as Injector 5, but had the element properties required to produce near-uniform axial-mass-flow-rate distribution and mixture-ratio distribution with the propellant combination N_2O_4–N_2H_4; the impingement angle and oxidizer jet diameter for Injector 5 were retained.

RMIR Injector 8. The geometry of this model was similar to that of Injector 7 except for α and the dimensional scale, since the number of elements was reduced by nearly an order of magnitude (i.e., to 6). The same oxidizer jet velocity was retained, but the impingement angle was modified to decrease the maximum value of the axial mass flux produced by the injector element, insofar as was possible within the other design constraints of a cylindrical chamber, the axial resultant momentum line, etc. (Section V-A and Ref. 10). It should be noted that this last requirement represented an effort to evaluate, in a very limited sense, the influence of the absolute level of local axial propellant flow rate on combustion.

B. Determination of Element Configuration

The procedure used in satisfying these specifications was really a three-step process. Once the propellant combination and mixture ratio were chosen, the first step was to use the correlation of Ref. 2 (see Fig. 2) to specify the orifice diameter ratios and velocity ratios. Since the oxidizer orifice diameter and jet velocity and the impingement angle were specified, it was a straightforward process to compute the fuel orifice diameters necessary to satisfy the mixing-uniformity criterion. This then assured (within the limits of the original correlation) that the mixture-ratio distribution would be as nearly uniform as it is possible to achieve with a single pair of impinging streams. For convenience, the following paragraphs summarize the calculations required for RMIR Injector 5. (The basic design procedures are presented in detail in Ref. 2.)

1. Specified Test Conditions for RMIR Injector 5

The propellants, element geometry, chamber geometry, and thrust level specified for tests of RMIR Injector 5 were as shown below. (See Nomenclature for mathematical notation.)

a. Propellants. The specified propellants were SFNA and *Corporal* fuel. For SFNA, designated in these calculations by the subscript 2, the specific gravity (Ref. 31) was

$$\frac{\delta_2}{\delta_w} = 1.550 \left(\frac{20°}{4} \right)$$

The nominal composition (Ref. 31) was $0.835\ HNO_3 + 0.13\ NO_2 + 0.03\ H_2O + 0.005\ HF = 1.0$ SFNA.

For the *Corporal* fuel, designated here by the subscript 1, the specific gravity[4] was

$$\frac{\delta_1}{\delta_w} = 1.073 \left(\frac{20°}{4} \right)$$

The nominal composition (Ref. 31) was $0.4655\ C_4H_3O \cdot CH_2OH + 0.4454\ C_6H_5 \cdot NH_2 + 0.0713\ N_2H_4 + 0.0178\ H_2O = 1.0$ *Corporal* fuel.

b. Element Geometry. In conformance with the specifications noted in Section II-A, the elements for Injector 5 were of the 1-on-1 impinging-jet design.

c. Chamber Geometry. Unless otherwise specified, the chamber geometry for tests of Injector 5 was as shown in JPL Dwg. 6-11818E.

d. Thrust Level. The nominal thrust level was set at 20,000 lb.

2. Assumed Gross Properties for RMIR Injector 5

To establish the flow rate per element $\dot{w}_{el}$, the following values were assumed:

$$c^* \simeq 95\% \text{ of } c_{th}^*$$

$$A_t = 47.5 \text{ in.}^2$$

$$p_{c_{eff}} = 300 \text{ psia}$$

---
[4]From unpublished JPL data, 1953.

Then

$$\dot{w}_{el} = \frac{(47.5)\,(300)\,(32.17)}{0.95\,N\,c_{th}^*}$$

where N is the number of elements.

Injector 5 required 52 elements (i.e., 52 pairs of unlike impinging jets). It was also specified that the oxidizer orifice diameter $d_2 = 0.173$ in., to conform with *Corporal* design; that $\beta = 0$ deg, hence being axial at the design value of r; and that $\alpha = 44$ deg.

It was necessary to choose a value for r that would maximize the characteristic exhaust velocity c^*. Hence, from the theoretical data of Ref. 29,

$$r = 2.80$$

$$c_{th}^* = 5025 \text{ ft/sec}$$

at that value of r.

The diameter ratio was then computed from Eq. (c), Fig. 2, as

$$\frac{d_1}{d_2} = \left(\frac{\delta_2}{\delta_1} \right)^{1/3} \left(\frac{1}{r} \right)^{2/3}$$

$$= \left(\frac{1.550}{1.073} \right)^{1/3} \left(\frac{1}{2.80} \right)^{2/3}$$

$$= 0.5677$$

Similarly, from Eq. (d), the mean-velocity ratio was determined as

$$\frac{V_1}{V_2} = \left(\frac{\delta_2}{\delta_1}\, r \right)^{1/3}$$

$$= \left(\frac{1.550}{1.073}\, 2.80 \right)^{1/3}$$

$$= 1.59$$

From the values given above,

$$d_1 = (0.173)\,(0.5677) = 0.0984 \text{ in.}$$

$$\dot{w}_{el} = \frac{482550}{(52)\,(5025)} = 1.847 \text{ lb/sec}$$

so that, with Eq. (e),

$$V_1 = \frac{576\, \dot{w}_{el}}{\pi\, d_1^2\, \delta_1\, (1 + r)}$$

$$= \frac{(4)\,(1.847)\,(144)}{\pi\,(0.0986)^2\,(1.073)\,(3.80)\,(62.3)}$$

$$= 136.5 \text{ ft/sec}$$

Hence,

$$V_2 = 86.0 \text{ ft/sec}$$

The element orientation was then determined for the momentum ratio as given by

$$\frac{P_1}{P_2} = \frac{d_1}{d_2} = 0.5677$$

for the geometry and r value satisfying the mixing-uniformity criterion, and for ζ as given by

$$\zeta = -\tan^{-1}\left[\frac{1 - \dfrac{P_1}{P_2}}{\cot\dfrac{\alpha}{2}\left(1 + \dfrac{P_1}{P_2}\right)} \right]$$

$$= -\tan^{-1}\left[\frac{1 - 0.5677}{(2.475)\,(1.5677)} \right]$$

$$= -\tan^{-1}(0.1097)$$

$$= -6°18'$$

Thus, the angle between the oxidizer-orifice centerline and the axis was determined as

$$\frac{\alpha}{2} + \zeta = 15°42'$$

and the angle between the fuel-orifice centerline and the axis was

$$\frac{\alpha}{2} - \zeta = 20°18'$$

The element configuration determined by these calculations is summarized graphically in Fig. 5. Similar calculations for the other injector designs and propellant combinations yielded the specifications listed in Table 1.
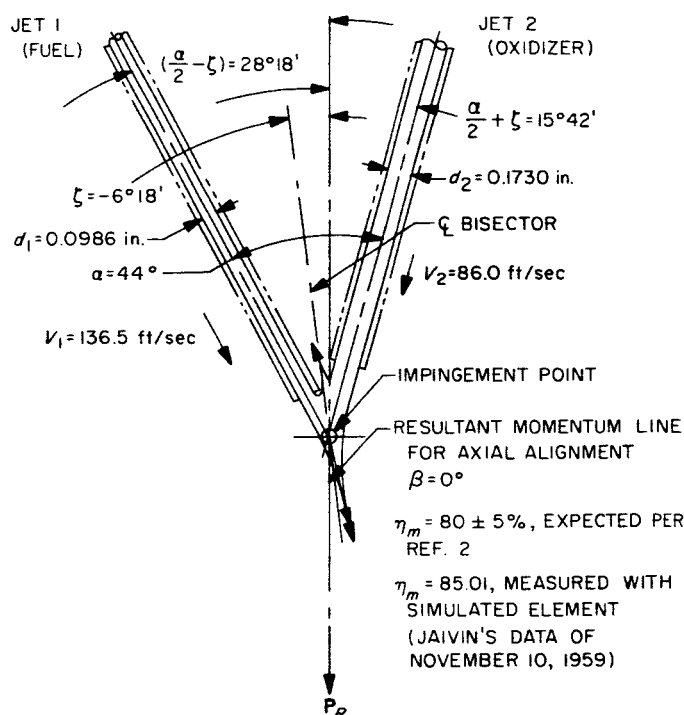

Fig. 5. Geometrical properties of element for RMIR Injector 5

C. Nonreactive-Spray Properties of Injector Elements

With the element geometry and flow rates established, the second step in the design was to determine the mass and mixture-ratio distributions produced by a particular element configuration, and the third step was to utilize them in devising the required injection scheme. As noted above, it was necessary to resort to actual experimental results for this determination. The design data used to predict the mass distributions for RMIR Injectors 1, 2, and 8 were based on results that had previously been evaluated in the course of the experimental studies reported in Refs. 1 and 2.[5] Since the absolute diameters of the orifices forming these elements were smaller than those used for the final designs, the mass-distribution analogs obtained for these injectors were based on an extrapolation for element scale. For Injectors 3, 4, 5, and 6 (i.e., optimum design for *Corporal* propellants), the mass and mixture-ratio distributions were reevaluated by sampling the spray from the intended element geometry for Injector 5 and using fluids simulating the densities of the *Corporal* propellants (Jaivin's data, presented here in Figs. 6 to 9). Even in this case, the available sampling

---

[5]These and similar data are available at JPL to any interested person.
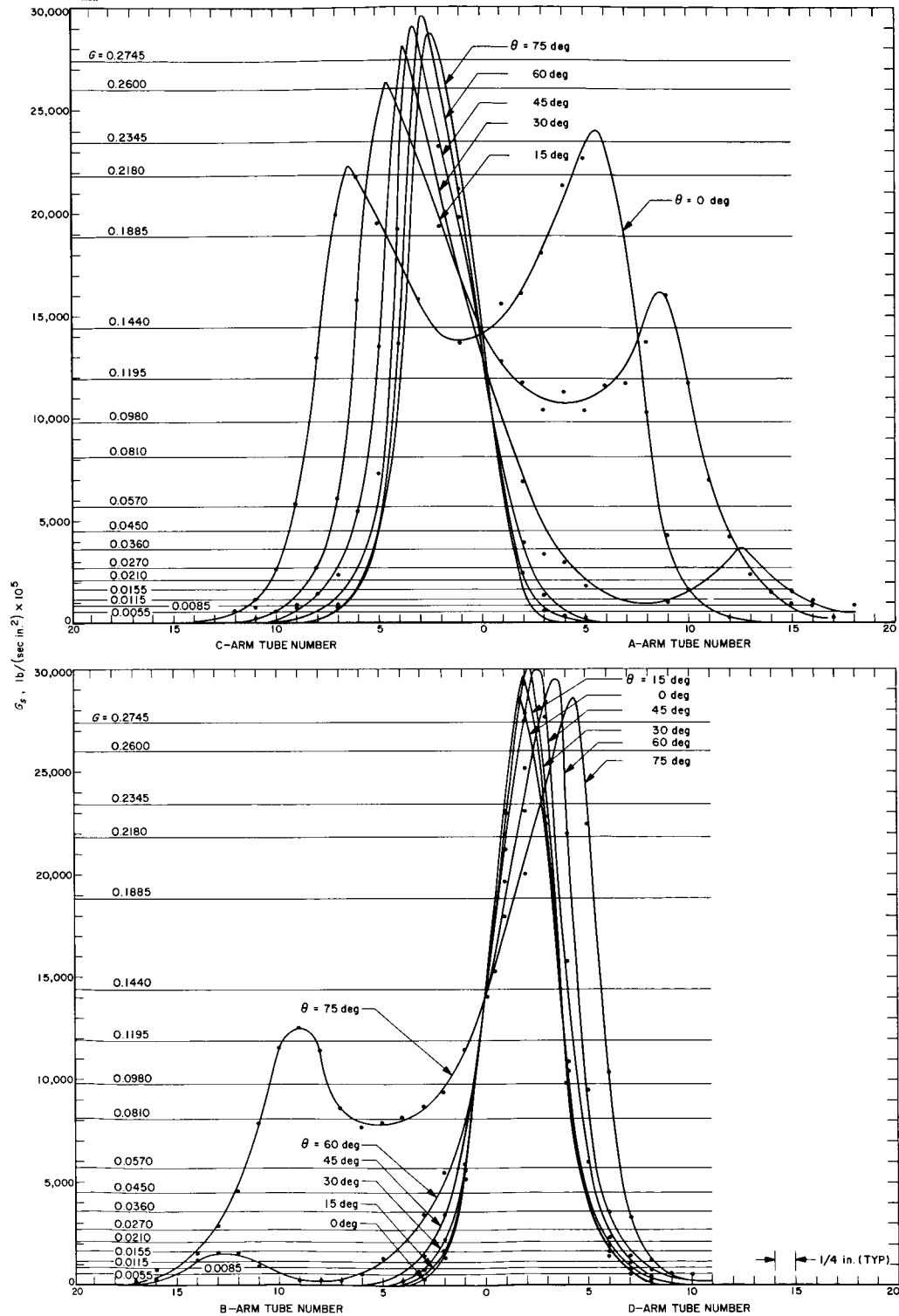
Fig. 6. Mass flux on a spherical surface at various angles of rotation about resultant momentum line for element of RMIR Injector 5

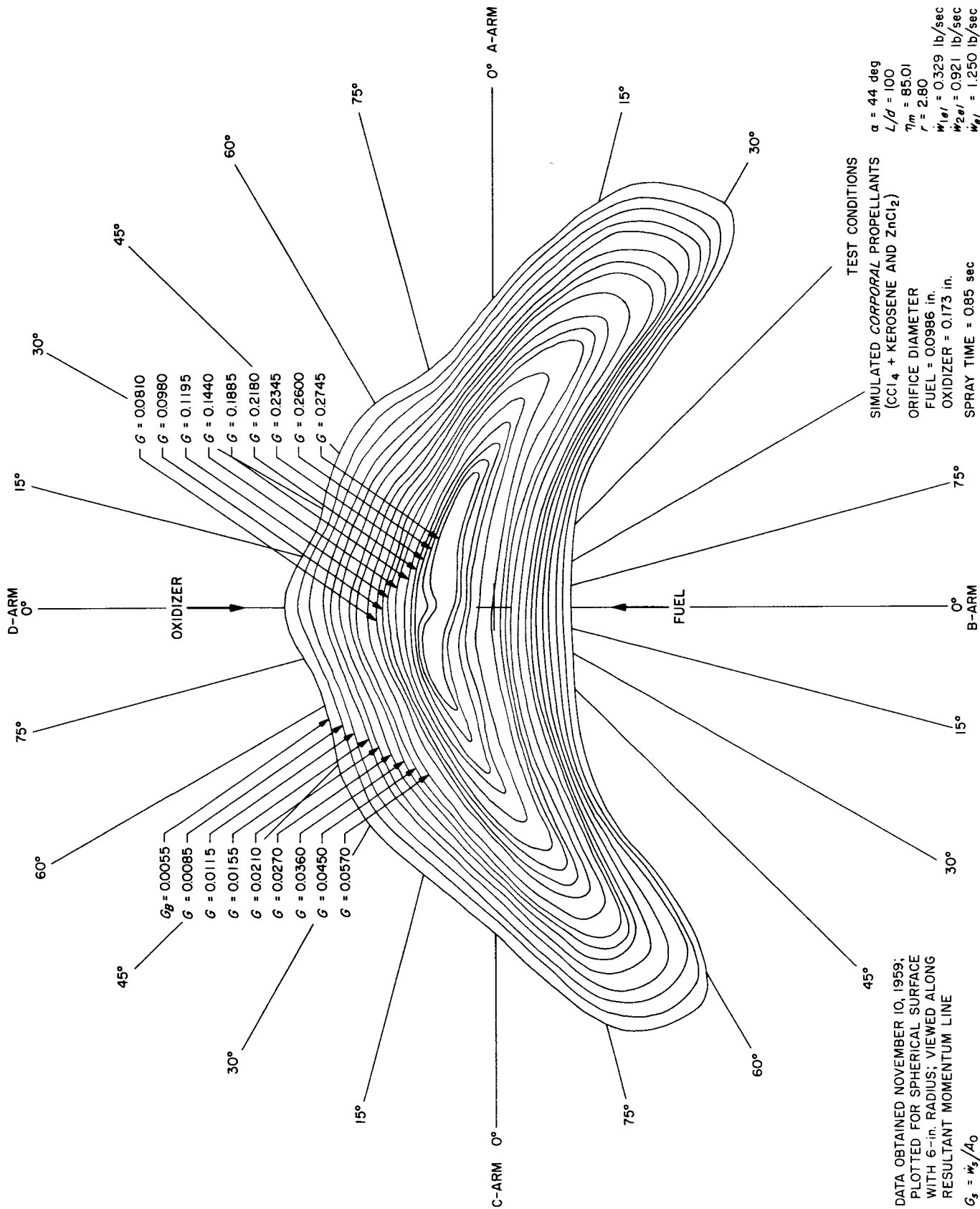**Fig. 7. Mass-flux distribution on a plane surface for element of RMIR Injector 5**

PLANE OF JET CENTER LINES

$d_2/d_1 = 1.755$

$\dot{w}_2/\dot{w}_1 = 2.80$

$\delta_2/\delta_1 = 1.445$

OXIDIZER

G_B

G_1

$G_2 \cdots G_{10}$

OXIDIZER

15° 42'

28° 18'

FUEL

FUEL

VIEWED ALONG
RESULTANT MOMENTUM
LINE

	MASS FLUX, $\dfrac{\text{lb/(in.}^2\text{sec)}}{(\text{lb/sec})_{el}}$	CUMULATIVE MASS FLUX CONTAINED WITHIN BOUNDARY, %
$G_B =$	585×10^{-5}	95.0
$G_1 =$	3,098	82.0
$G_2 =$	4,895	76.0
$G_3 =$	6,854	70.0
$G_4 =$	8,814	54.3
$G_5 =$	10,771	48.5
$G_6 =$	12,729	44.3
$G_7 =$	14,688	37.0
$G_8 =$	16,646	30.5
$G_9 =$	18,603	16.0
$G_{10} =$	$20,562 \times 10^{-5}$	9.0

MASS-FLÜX VALUES NORMALIZED TO $\dot{w}_{el} = 1.0$ lb/sec

DISTANCE FROM IMPINGEMENT POINT = 6.0 in.

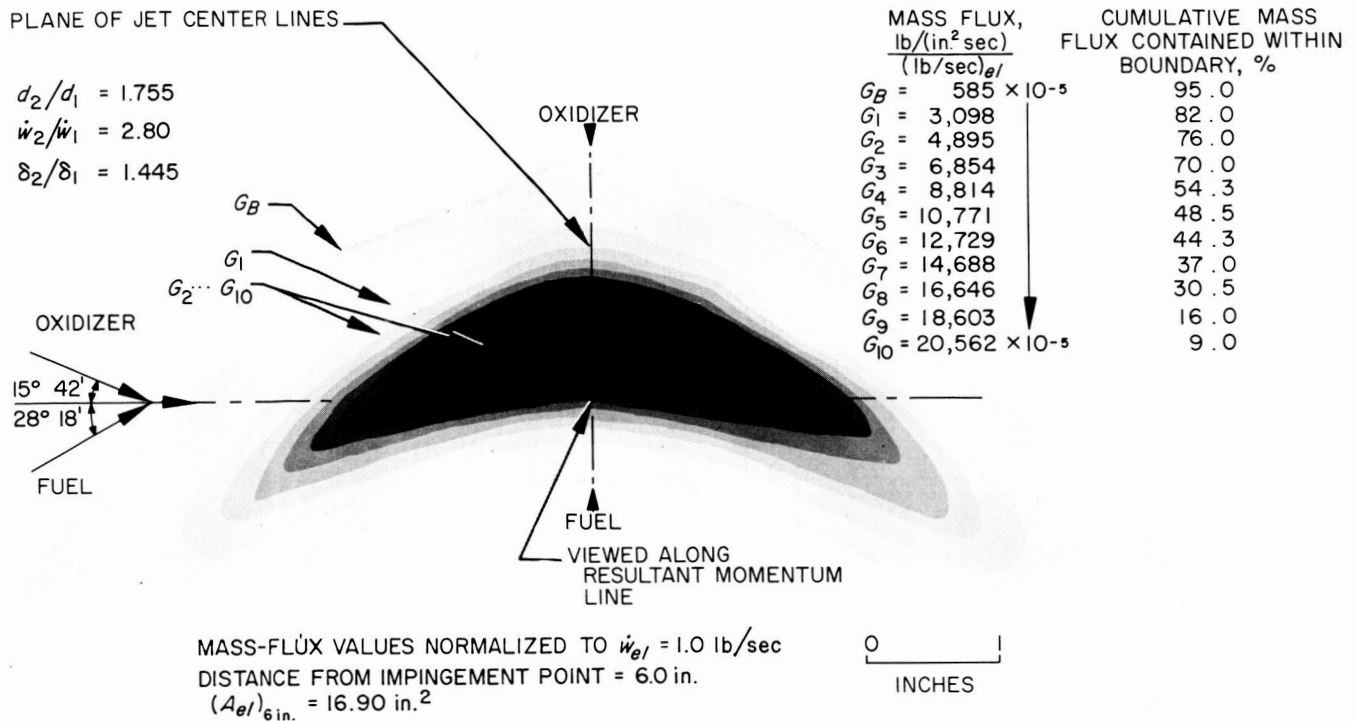$(A_{el})_{6\,\text{in.}} = 16.90$ in.^{2}

0   1

INCHES

Fig. 8. Three-dimensional analog of mass-flux distribution on a plane surface for RMIR Injector 5

scheme was flow-rate-limited, so that the nonreactive mass and mixture-ratio distributions were based on a flow rate representing approximately 70% of the design value for Injector 5 and only 7% for Injector 6. However, previous experiments had shown that flow rate alone (i.e., Δp or "kinetic energy," as discussed in Ref. 1) had a small effect on relative mass distributions (of the order of 1% for the extrapolation required for Injector 5), and it was assumed that this would also hold for extrapolation to the very-high-flow-rate elements used in Injectors 6 and 8. In a similar fashion, the mass and mixture-ratio distributions for the element configuration proposed for Injector 7 were evaluated (Gerbracht's data, presented here in Figs. 10 to 13) with fluids simulating the N_2O_4–N_2H_4 propellant combination. Here, too, the element flow rate was limited to approximately 63% of the design flow rate.

These two sets of data were used to produce the mass and mixture-ratio distributions for the single elements of Injectors 5 and 7, as portrayed in Figs. 6 to 13. The original values of mass flux vs position along a great circle of the sampling surface were first plotted as shown in

Figs. 6 and 10, where each set of values is represented by a faired curve giving a "best-fit" approximation to the experimental data. These curves were then used to locate lines of constant mass flux on the spherical surface for those great circles on which data had been obtained. A second curve fairing was required to generate the contours shown in Figs. 7 and 11 as orthographic projections along the resultant momentum line from the spherical surface to a plane. These contours, taken as representative of the mass distribution of the spray, were utilized in subsequent manipulations of the data where additional resolution of the mass distribution was required.

The contours shown in Figs. 9 and 13 represent the lines of constant local mass-fraction ratio (i.e., mixture ratio) and clearly indicate the variations in that parameter which existed in the spray. Note that the spatial properties of mixture-ratio distribution were obtained by extrapolating along radial lines from an impingement point to the x–y plane that is perpendicular to the resultant momentum line and located 6 in. from the impingement point. The spray boundary, as superimposed on the mixture-ratio curves in these Figures, is also located in that

Fig. 9. Mixture-ratio distribution on a plane surface for element of RMIR Injector 5

15°

30°

60°

75°

0° A-ARM

$r/(r+1) = 0.58940, r = 1.43$
$= 0.66310, r = 1.97$
$= 0.73680, r = 2.80$
$= 0.76310, r = 3.22$
$= 0.78940, r = 3.75$
$= 0.81570, r = 4.42$

TEST CONDITIONS

SIMULATED *CORPORAL* PROPELLANTS
(CCl$_4$ + KEROSENE AND ZnCl$_2$)

ORIFICE DIAMETER
FUEL = 0.0986 in.
OXIDIZER = 0.173 in.

$\alpha = 44$ deg
$L/\phi = 100$
$\eta_m = 85.01$
$r/(r+1) = 0.73680, r = 2.80$ (NOMINAL)

60°

45°

30°

15°

D-ARM
0°

OXIDIZER →

75°

60°

45°

30°

15°

C-ARM 0°

$G_B = 0.00058$
$G = 0.00309$
$G = 0.00881$
$G = 0.1468$
$G = 0.2056$

$r/(r+1) = 0.76310, r = 3.22$
$= 0.78940, r = 3.75$
$= 0.81570, r = 4.42$

75°

60°

← FUEL

0°
B-ARM

15°

30°

60°

75°

DATA OBTAINED NOVEMBER 10, 1959;
PLOTTED FOR PLANE SURFACE,
6 in. FROM IMPINGEMENT POINT;
VIEWED ALONG RESULTANT MOMENTUM LINE
VALUES OF G NORMALIZED TO
$\dot{w}_{o'} = 1.0$ lb/sec

19

TEST CONDITIONS

DATA OBTAINED MARCH 6, 1959;
PLOTTED FOR SPHERICAL SURFACE
WITH 6-in. RADIUS; VIEWED ALONG
RESULTANT MOMENTUM LINE

$G_s = \dot{w}_s/A_0$

$G_{max} = 37,835 \times 10^{-5}$

SIMULATED *CORPORAL* PROPELLANTS
$(CCl_4 + \text{KEROSENE AND } ZnCl_2)$

ORIFICE DIAMETER
FUEL = 0.173 in.
OXIDIZER = 0.173 in.
SPRAY TIME = 0.5 sec

$\alpha = 45$ deg
$L/d = 100$
$\eta_m = 73.64$
$r = 1.23$

$\dot{w}_{1o/} = 0.493$ lb/sec
$\dot{w}_{2o/} = 0.609$ lb/sec
$\dot{w}_{o/} = 1.102$ lb/sec

Fig. 10. Mass flux on a spherical surface at various angles of rotation about resultant momentum line for element of RMIR Injector 7

plane and indicates the iso-mass line that includes 95% of the total mass flow of the spray (Section V-A). In Fig. 9, which represents the element utilized in the design of Injectors 3, 4, 5, and 6, two regions of high local mixture ratio symmetrically located about the plane of the stream centerlines are significant features of this distribution. In Fig. 13, however, which represents the element for Injector 7, it is seen that, characteristically, the contours are parallel lines which are generally perpendicular to the plane of the stream centerlines. In both cases, the so-called penetration phenomenon (i.e., fuel-rich in the area of spray *across* the resultant momentum line from the fuel source) along that plane of symmetry is apparent.

The comparable distributions obtained for the elements of the other injectors were, of course, somewhat different. However, insofar as the application of the element geometry to the integrated design is concerned, these distributions were sufficiently similar to those discussed above that it was considered permissible to omit them from this presentation, except as they were characterized by the mixing factor (Table 1) and, in the case of mass distribution, as they were incorporated into the multi-element design for the injector.

Although the mass-flux distributions produced by these elements appeared to be adequately represented by the
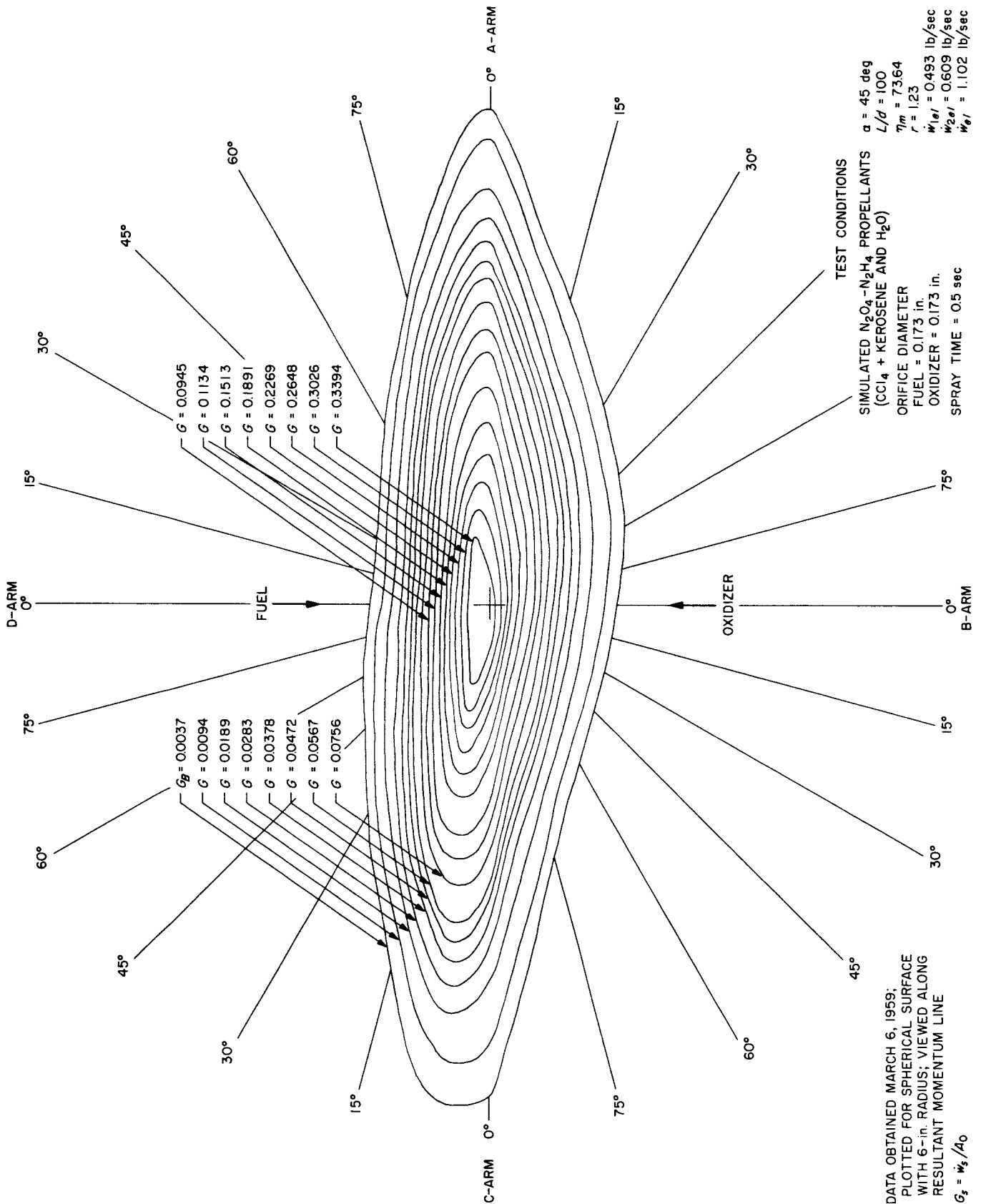
Fig. 11. Mass-flux distribution on a spherical surface for element of RMIR Injector 7
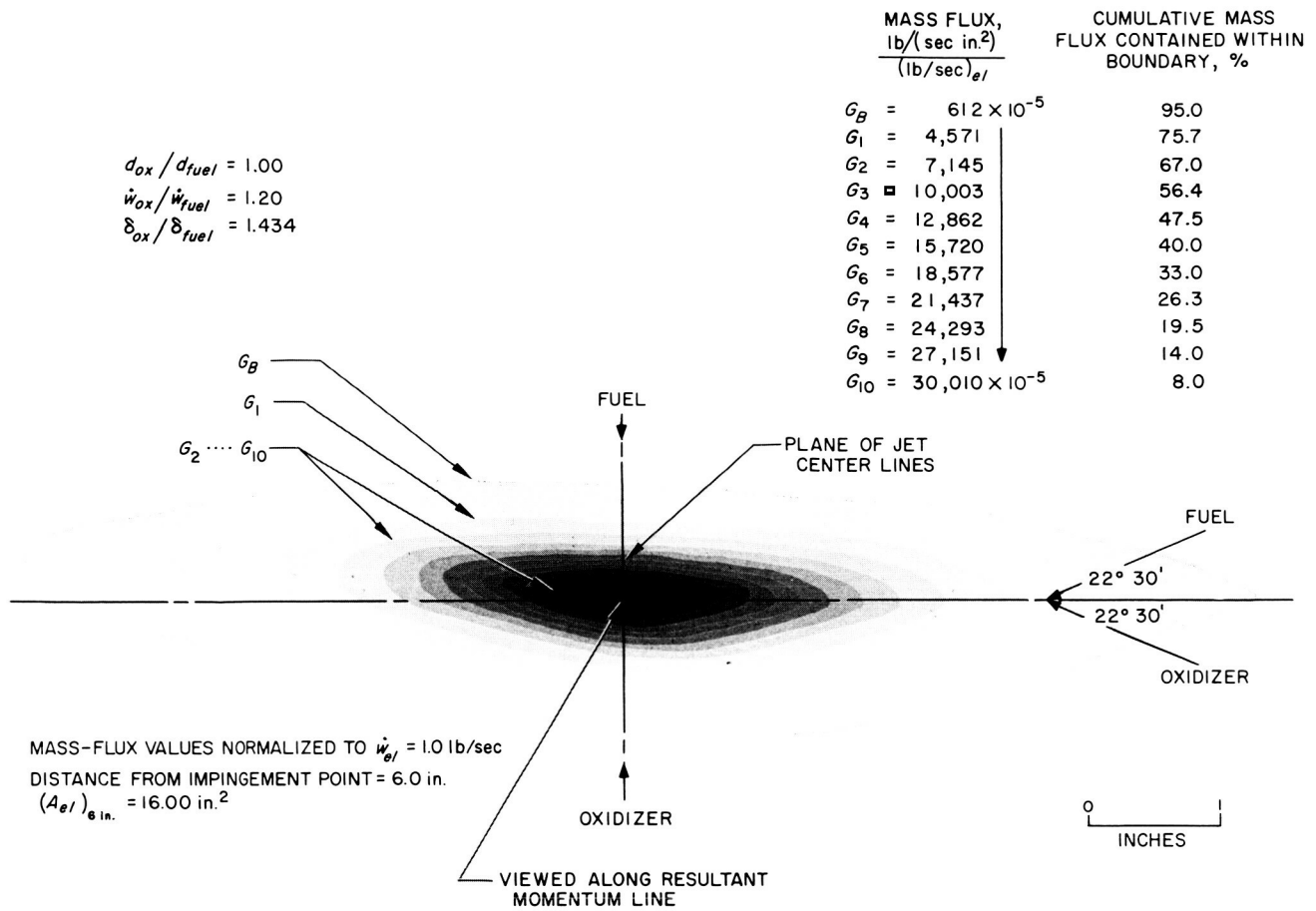
$d_{ox}/d_{fuel} = 1.00$

$\dot{w}_{ox}/\dot{w}_{fuel} = 1.20$

$\delta_{ox}/\delta_{fuel} = 1.434$

	MASS FLUX, $\dfrac{\text{lb}/(\text{sec in.}^2)}{(\text{lb}/\text{sec})_{el}}$	CUMULATIVE MASS FLUX CONTAINED WITHIN BOUNDARY, %
G_B =	612×10^{-5}	95.0
G_1 =	4,571	75.7
G_2 =	7,145	67.0
G_3 =	10,003	56.4
G_4 =	12,862	47.5
G_5 =	15,720	40.0
G_6 =	18,577	33.0
G_7 =	21,437	26.3
G_8 =	24,293	19.5
G_9 =	27,151	14.0
G_{10} =	$30,010 \times 10^{-5}$	8.0

MASS-FLUX VALUES NORMALIZED TO $\dot{w}_{el} = 1.0$ lb/sec
DISTANCE FROM IMPINGEMENT POINT = 6.0 in.
$(A_{el})_{6\,in.} = 16.00$ in.^{2}

FUEL

PLANE OF JET CENTER LINES

FUEL

22° 30'

22° 30'

OXIDIZER

OXIDIZER

VIEWED ALONG RESULTANT MOMENTUM LINE

0   1
INCHES

Fig. 12. Three-dimensional analog of mass-flux distribution on a plane surface for RMIR Injector 7

graphs of Figs. 7 and 11, a "three-dimensional model" of such distributions was also devised, wherein the photographic-transmission density of a negative is proportional to the axial mass flux. It was intended that this model would provide a quantitative description of the mass distribution achieved in a combustion chamber and, within limits, would be useful in representing local mass fluxes from the combined flows of several elements. The model was used extensively in characterizing the integrated mass-flux distribution of complete injectors, and also provided a guide to element placement for injector designs intended to produce near-uniform mass distributions.

Photographic reproductions of these analogs (i.e., as positives, rather than negatives) for the elements used in RMIR Injectors 5 and 7 are presented in Figs. 8 and 12. The techniques and procedures utilized in generating these models are summarized in the discussion which follows.

D. Preparation of the Mass-Distribution Model

As noted above, the local mass flux G_s on a spherical surface can be obtained directly from the experimental sampling of a spray when the fluid densities are known (Section V-C and Refs. 1 and 2). For our purposes, these faired data were then read at 5-deg intervals (or less when the increment of contour length between coordinate points appeared large) for each of some 20 contours for which values were chosen to give approximately equal "radial" spacing. A table of coordinates for each contour was prepared from these readings.

In order to extrapolate these data to a new spherical radius, it was assumed that the influences of gravity and aerodynamic drag on the spray were negligible, so that the spray particles would travel along radial lines emanating from the impingement point. The local mass flux at
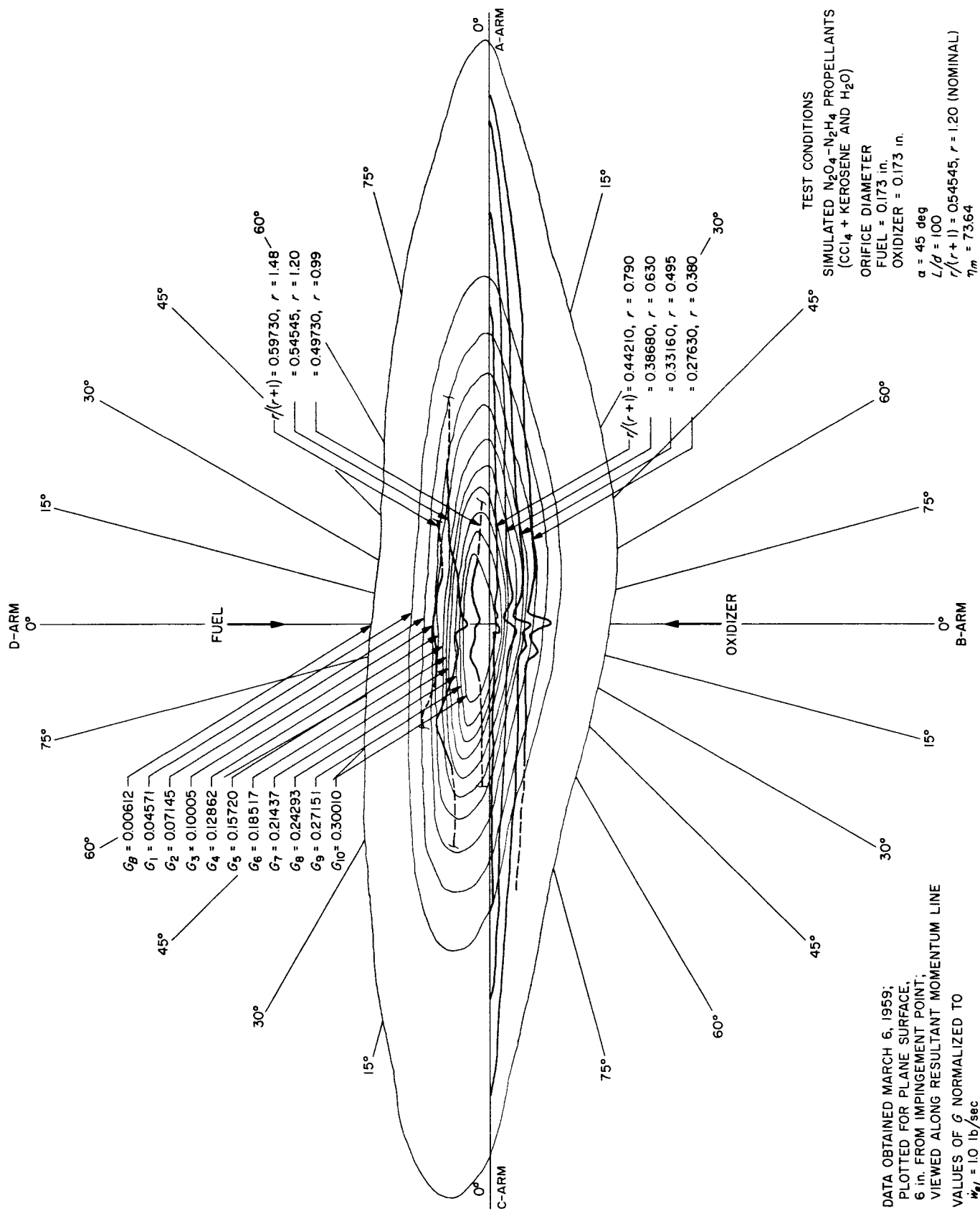
D-ARM 0°

FUEL

0° A-ARM

75°

60°

45°

30°

15°

15°

30°

45°

60°

75°

$r/(r+1) = 0.59730, r = 1.48$

$= 0.54545, r = 1.20$

$= 0.49730, r = 0.99$

$r/(r+1) = 0.44210, r = 0.790$

$= 0.38680, r = 0.630$

$= 0.33160, r = 0.495$

$= 0.27630, r = 0.380$

TEST CONDITIONS

SIMULATED N_2O_4–N_2H_4 PROPELLANTS
(CCl$_4$ + KEROSENE AND H_2O)

ORIFICE DIAMETER
FUEL = 0.173 in.
OXIDIZER = 0.173 in.

$a = 45$ deg
$L/d = 100$
$r/(r+1) = 0.54545, r = 1.20$ (NOMINAL)
$\eta_m = 73.64$

45°

60°

75°

OXIDIZER

0° B-ARM

15°

30°

45°

60°

75°

$G_B = 0.00612$
$G_1 = 0.04571$
$G_2 = 0.07145$
$G_3 = 0.10005$
$G_4 = 0.12862$
$G_5 = 0.15720$
$G_6 = 0.18517$
$G_7 = 0.21437$
$G_8 = 0.24293$
$G_9 = 0.27151$
$G_{10} = 0.30010$

60°

45°

30°

15°

0° C-ARM

DATA OBTAINED MARCH 6, 1959;
PLOTTED FOR PLANE SURFACE,
6 in. FROM IMPINGEMENT POINT;
VIEWED ALONG RESULTANT MOMENTUM LINE

VALUES OF G NORMALIZED TO
$\dot{w}_{el} = 1.0$ lb/sec

Fig. 13. Mixture-ratio distribution on a plane surface for element of RMIR Injector 7

some new distance L along any given line would then be given by

$$G_L = G_s \frac{36}{L^2}$$

where

G_L = mass flux at a distance L from the impingement point

G_s = mass flux at the distance sampled (6 in.)

It is noted that G_L, like G_s, is a point value (based on an average value determined by experiment) at the new distance, so that the mass flux in a new direction (for example, in a direction parallel to the resultant momentum line on a plane located at a distance L_{Rp} from the impingement point) is simply given by

$$G_p = G_s \frac{36}{L_{Rp}^2} \cos \sigma$$

where

G_p = mass flux on a plane perpendicular to the resultant momentum line, located 6 in. from the point

L_{Rp} = distance from the impingement point to the plane, along a line that includes the point from which G_s is obtained

σ = true angle between the resultant momentum line and the path of the particle

The geometry for this extrapolation is illustrated in Fig. 14. It is obvious from the Figure that this extrapolation of the original contours resulted in a set of contours that are variable in G_p; thus, it was again necessary to interpolate along radial lines (contained in the plane perpendicular to, and emanating from, the resultant momentum line) for the coordinates of particular values of G_p, in order to identify contours representing lines of constant mass flux in the plane. In this case, however, the values for the contours were chosen to give a number of desira-
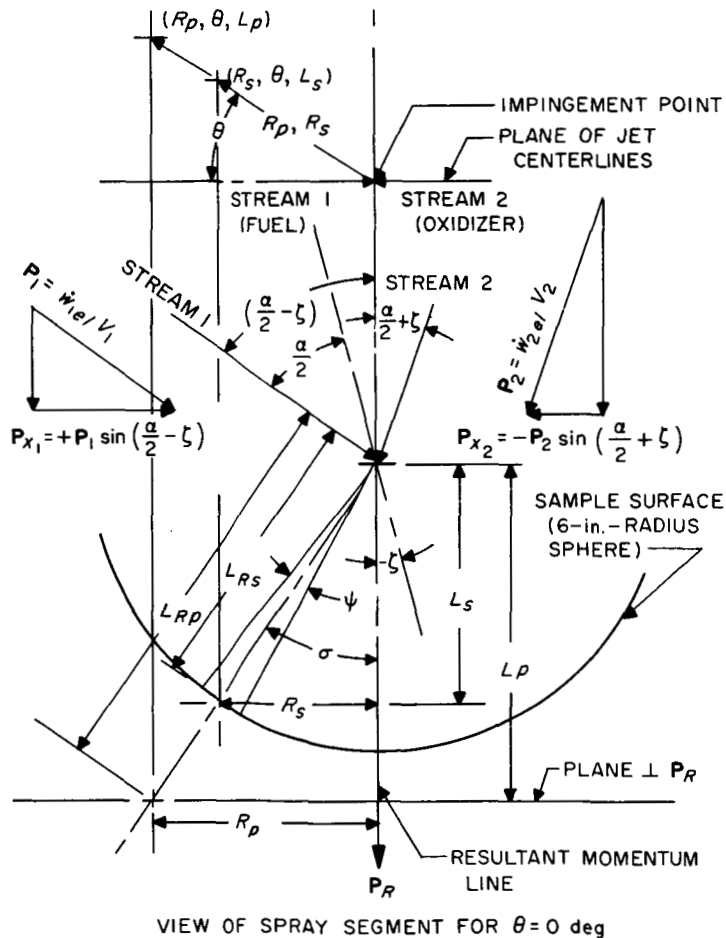
NOTE:

WITH STREAM I ON LEFT:

1. ζ IS POSITIVE FOR CLOCKWISE ROTATION OF BISECTOR RELATIVE TO P_R.
2. MOMENTUM IS TAKEN AS POSITIVE FOR DIRECTION OF x – COMPONENT OF STREAM I.

HENCE, IF $P_1 < P_2$, THEN Γ IS NEGATIVE, AND

$$\zeta = \tan^{-1} \left[\frac{\dfrac{P_1}{P_2} - 1}{\cot \dfrac{\alpha}{2} \left(\dfrac{P_1}{P_2} + 1 \right)} \right]$$

VIEW OF SPRAY SEGMENT FOR $\theta = 0$ deg

Fig. 14. Geometrical properties and nomenclature for a spray element

ble features to the mass-distribution model. To this end, the following arbitrary determinations were made:

1. It was reasonable to assume that the relative mass distribution would be independent of flow rate, so that the local mass flux could be normalized by dividing by the sample flow rate; hence, the contour identification would bear a simple relationship to any element flow rate.

2. The model would be a stepwise variation in the transmission of the film density, in which each step would represent an "average" value of local mass flux directly proportional to density.

3. The proportionality factor between optical density and mass flux would be established from an arbitrary value of G_p, taken as the arithmetic average of a "reference" value G_R and G_{max}. For this purpose, G_R was taken as the value of G_p that bounds 10% of the cumulative mass fraction of the spray, and G_{max} as the value of the axial mass flux on a plane obtained by extrapolating, along the radial line from the impingement point to the plane, the maximum value observed on the spherical surface. Thus, $G_{pD} = (G_R + G_{max})/2 \equiv$ the value of G_p that is proportional to D_{max}. Then, if D_{i-j} is the optical density of the increment bounded by the ith and jth contours, one may write

$$\frac{D_{i-j}}{D_{max}} = \frac{\dfrac{G_{i-j}}{G_R + G_{max}}}{2}$$

so that

$$G_{i-j} = D_{i-j}\frac{G_R + G_{max}}{2D_{max}}$$

4. The boundaries between mass-flux increments would be located at values of G_p representing an average of the two adjacent increments, so that

$$G_j = \frac{G_{i-j} + G_{j-k}}{2}$$

or

$$G_j = (D_{i-j} + D_{j-k})\frac{G_R + G_{max}}{4D_{max}}$$

5. A possible exception to assumption 3, above, would be the outermost boundary, which was always taken at the value of G_p which bounded 95% of the total mass flow for the element.

6. The outermost increment would be represented by the "minimum" density of which the film was capable.

7. Unless otherwise specified, the model would incorporate a total of 11 increments, so that

$$D_{j-k} - D_{i-j} \simeq D_{max}/11$$

Note, however, that any other method of assigning "density" (hence, average mass flux) to each increment would be equally suitable, and that conditions 3, 4, and 5 are consistent only when

$$D_{min}/D_{max} = 4G_B/(G_R + G_{max})$$

where G_B is the value of mass flux at the spray boundary (see condition 4 for the case where the density outside the boundary is taken as zero). Also, in general, G_{10} (the boundary of the maximum density increment) is not equal to G_R.

The normalized values of G_B and G_R were taken from a curve of the weighted cumulative percent of mass flow to the plane vs G_p, as shown in Fig. 15. This curve was obtained by considering that the point values of G_p, determined from the extrapolation of G_s to the plane, would then represent an area on the plane bounded by two radial lines (emanating from the resultant momentum line and equidistant from the two lines on which data were available) and two concentric circles having radii equidistant from the point in question and the two data points adjacent to it on the same radial line. Thus, multiplication of G_p by that area gave the total mass flow through that area, so that, by first collating the resulting mass flows in ascending sequence in G_p and then continuously summing, the data could be presented in the form shown. Once this curve was obtained, it was possible to choose the values of G_p (i.e., G_B and G_R) that included given fractions of the total mass flow of the spray; or, conversely, to relate any given G_p with a given mass fraction of the spray. As shown in Figs. 8 and 12, this value was then used to identify a given contour.

The basis having thus been specified for defining the increment boundaries that would yield the desirable features for the model, it was then necessary to devise a photographic-reproduction process that would achieve the density analog in the final transparency. A number of different schemes were tried, but only one was really successful: first, the boundaries were defined as noted above, and then each increment was "painted" with a
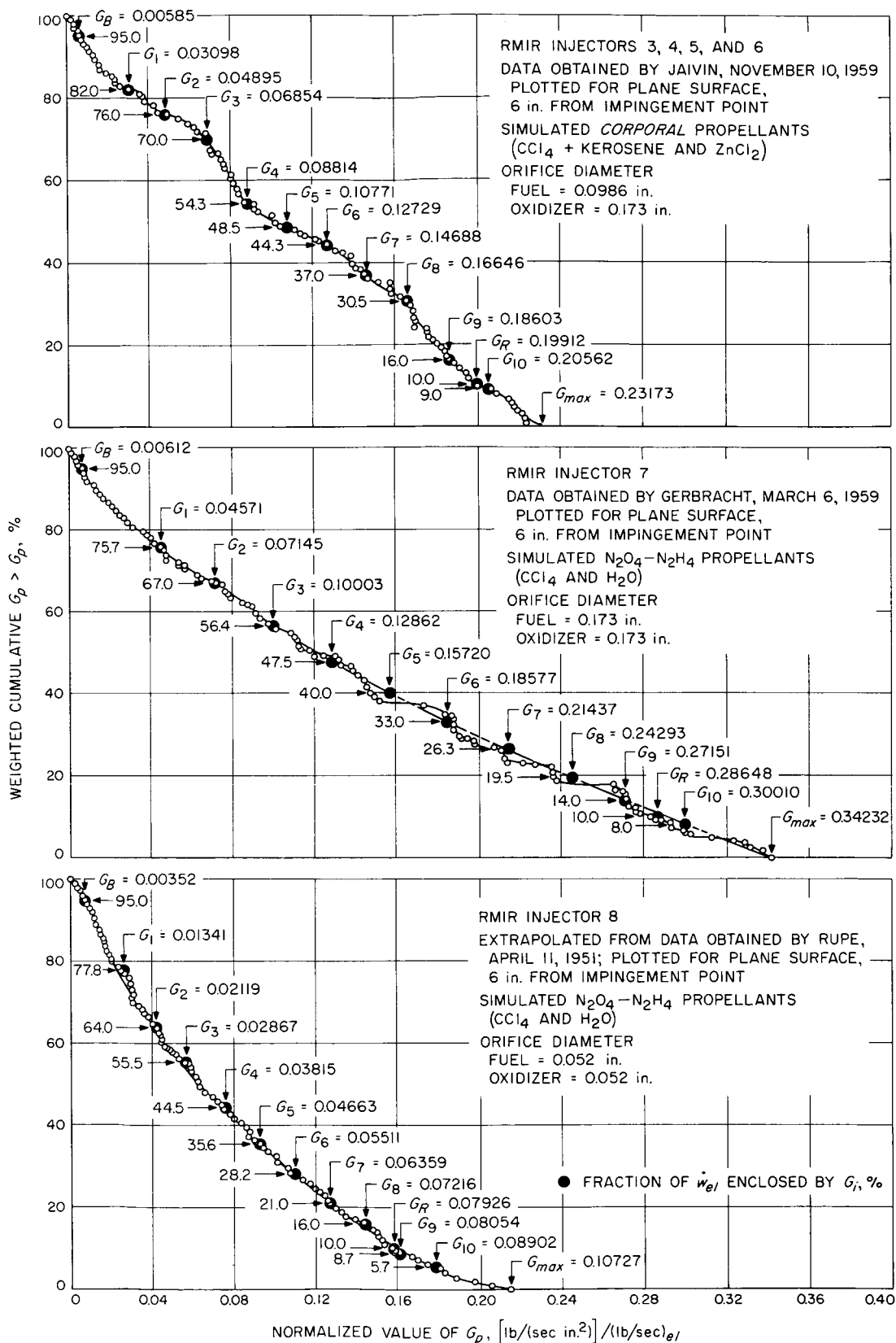
Fig. 15. Weighted cumulative percentage of mass flow to a plane vs local flow rate per unit area for elements of RMIR Injectors 3 to 8

"cartoon color"[6] that would provide the appropriate transmission density in the final transparency. This was the only technique found that could: (1) produce the *minimum* density of which the film was capable, thus limiting the outer increment of the model to a reasonable area; (2) provide, together with step (1), a reasonable value of film gamma, which is required if successive steps are to be differentiated (i.e., achievement of a high ratio of D_{max}/D_{min}); and (3) provide density increments that are reasonably equal.

This scheme also circumvented any linear density-exposure requirement for the emulsion, since variations could be compensated for in the model. It was found that adequate reproducibility in density (± 0.02) could be achieved with: (1) Eastman commercial film, exposed to blue light for 1.0 sec at f:22 with an intensity of 250 ft-c, and (2) development in "D-19" at 68°F for 5 min by a nitrogen-burst method.

It was also found that equal density increments were readily achieved by first evaluating transmission densities corresponding to a series of paint grades varying from black to white, and then mixing appropriate grades to produce the desired result, on the assumption that linear interpolation of composition was permissible.

Thus, using as an example the element for Injector 5 (after normalizing the element flow rate to 1.0 lb/sec),

$$G_{max} = 0.2317 \text{ lb/sec-in.}^2$$

and, from Fig. 15,

G_B = contour enclosing 95% of total mass flow

$$= 0.00585 \frac{\text{lb/(sec in.}^2)}{(\text{lb/sec})_{el}}$$

G_R = contour enclosing 10% of total mass flow

$$= 0.19912 \frac{\text{lb/(sec in.}^2)}{(\text{lb/sec})_{el}}$$

Then, with Eastman commercial film exposed as noted above,

$$D_{min} = 0.09$$

$$D_{max} = 0.85$$

so that

$$D_{j-k} - D_{i-j} = \frac{0.85}{11} = 0.0773$$

Computation of the appropriate values of G_p for each boundary and the average value for each increment from the equations and conditions noted above resulted in the values indicated in Fig. 15. These, of course, were the values used in the interpolation for the coordinates of G_p which ultimately yielded the contours and, hence, the mass-distribution analog presented in Figs. 8 and 12.

E. Mass Distributions for Multi-element Injection Schemes

It will be remembered that the model described above was constructed from the information provided by a single element, as determined on a plane located at a given distance from the impingement point in a given experiment, and the intent was that it be suitable for illustrating mass distributions for multi-element injection schemes. Thus, in order that the model be applicable to the final step in the design, it must be capable of representing different "scales" of both flow rate and area.

Experiments have shown that both mass and mixture-ratio distributions are relatively insensitive to flow rate and, in fact, that the local mass flux for a given element configuration is directly proportional to total flow rate for the element. It should be clear that this holds true only for elements with similar geometrical properties, as well as similar dynamic properties of the jets. Thus, as noted above, the local mass-flux distribution produced by similar elements can be normalized by dividing by total flow rate. Conversely, the absolute levels of G appropriate to some new flow rate can be obtained by multiplying the indicated values by the new flow rate per element. This would give the new mass flux *at the same distance from the impingement point.*

When it is desired to obtain the relative distribution at some new station along the resultant momentum line, it can be assumed that the particles travel radially from the impingement point. In that case, the local mass flux varies inversely as the square of the distance from the impingement point, whereas the area enclosed within the spray boundary varies directly with the square of the distance. Thus, once a set of mass-distribution data is available, a new distribution can be obtained from the relation

$$G_{mp} = G_s \frac{\dot{w}_{el}}{\dot{w}_s} \left(\frac{L_{Rs}}{L_{Rp}}\right)^2$$

---

[6]Paints of the type used for artwork of animated cartoons are available, for example, from Cartoon Color Company, 9398 Culver Blvd., Culver City, Calif.

where

G_{mp} = local mass flux at new station

G_s = local mass flux of sample

$\dot{w}_{el}$ = new mass flow of element

$\dot{w}_s$ = sample mass flow of element

L_{Rp} = distance from impingement point to location of G_{mp}

L_{Rs} = distance from impingement point to location of G_s

Note that both L_{Rs} and L_{Rp} are distances measured along a single line emanating from the impingement point, and that G_{mp} and G_s are, in general, located at different radial distances from the resultant momentum line. Thus,

$$G_s = f(\theta, R_s)$$

and

$$G_{mp} = f(\theta, R_{mp})$$

where $L_s/L_{mp} = R_s/R_{mp} = L_{Rs}/L_{Rmp}$; L_{mp} is the perpendicular distance from the impingement point to the plane perpendicular to the resultant momentum line that includes R_{mp}; and R_s and θ are, respectively, the distance and angular coordinates of G_s (see Fig. 14).

This latter characteristic of the spray was utilized to generate the analog of the mass-flux distribution at the so-called *model plane* of the injector. The model plane is defined as the axial station at which the boundary of the mass-distribution model for one element encloses an area equal to $1/N$ times the area of the chamber cross section, and is usually identified by its distance from the impingement point. In the ideal case, if the element areas could be fitted together like the pieces of a jig-saw puzzle bounded by the chamber wall, they would, at that station, just fill the chamber cross section. Further, if the axial-mass-flux distribution for each element were uniform, then the axial mass flux for the chamber (at that station) would also be uniform. Obviously, the location of the model plane for a given element configuration will vary with the number of elements in a given chamber, as well as with the chamber cross-sectional area. In addition, for a given chamber geometry, the magnitude of the local mass flux at that station will vary with total propellant flow rate.

As may be seen in Section V, the achievement of the above-mentioned ideal (i.e., uniform) mass distribution with a finite number of elements is next to impossible in a practical sense, because of the nonuniformity of mass distributions produced by real sprays and the difficulty of achieving a truly homogeneous injection scheme. However, at least for multiple-element injectors, "secondary" mixing always occurs as the spray continues to diverge from its point source, so that the distribution can be modified as the propellant proceeds down the chamber. As indicated in Ref. 10, the required "combustion length" can be related to this changing axial-mass-flow-rate distribution; although the data are sketchy, it appears that the attainment of uniform mass flow (and hence concentrations) is prerequisite to high performance in a minimum combustion volume.

In practice, the axial-mass-flux distribution for each injector is obtained at the model plane by proceeding in the following manner:

1. Determine the mass distribution produced by the required element spraying nonreactive fluids. Use actual scale and propellant densities, if possible.

2. Construct a three-dimensional analog of the axial mass flux for one element, as described in Section IV-D.

3. Prepare an appropriate number of these mass-distribution analogs at the scale appropriate to the model plane.

4. Assemble a composite model corresponding to the required number of elements, with the distributions oriented as specified by the injector geometry; e.g., Injectors 1 to 4.

5. Orient elements to achieve a particular mass distribution (that is, as nearly uniform as possible); e.g., Injectors 5 to 8.

6. Utilize the orientation of step 5 to define the required orifice and manifolding geometry.

It is evident that this procedure will produce a scheme which, when coupled with the uniformity criterion for controlling mixture-ratio distribution, can provide a quantitative description of the prereaction mass and mixture-ratio distributions within a combustion chamber.

V. NONREACTIVE-SPRAY PROPERTIES OF RMIR INJECTORS

A. Mass Distributions

The composite mass distributions for RMIR Injectors 4 to 8 are presented in Figs. 16 to 20. The distributions for Injectors 1 to 3 have not been reproduced here because of their marked similarity to that of Injector 4. Although real differences do exist, they are minor and would undoubtedly be masked by real effects associated with the
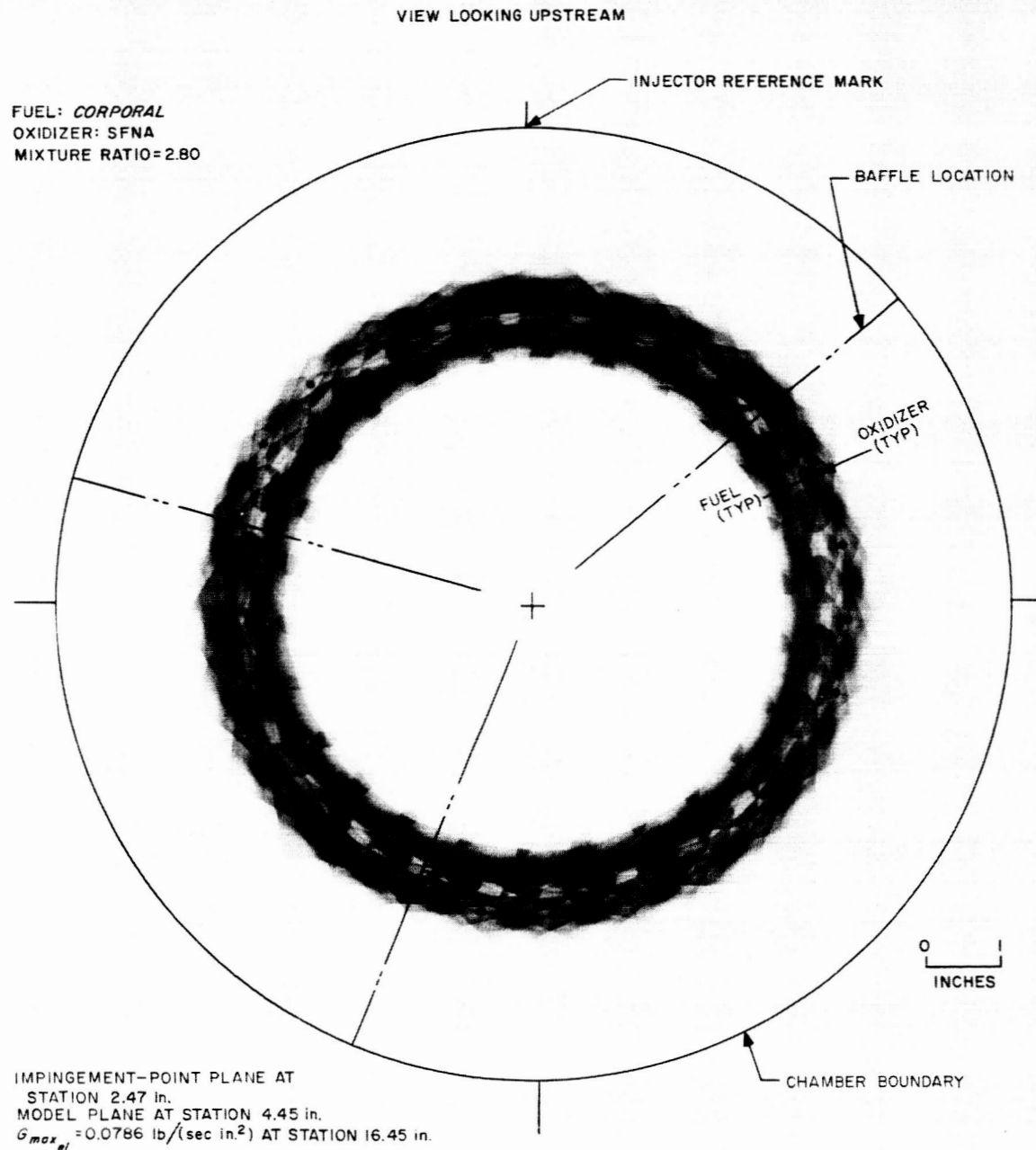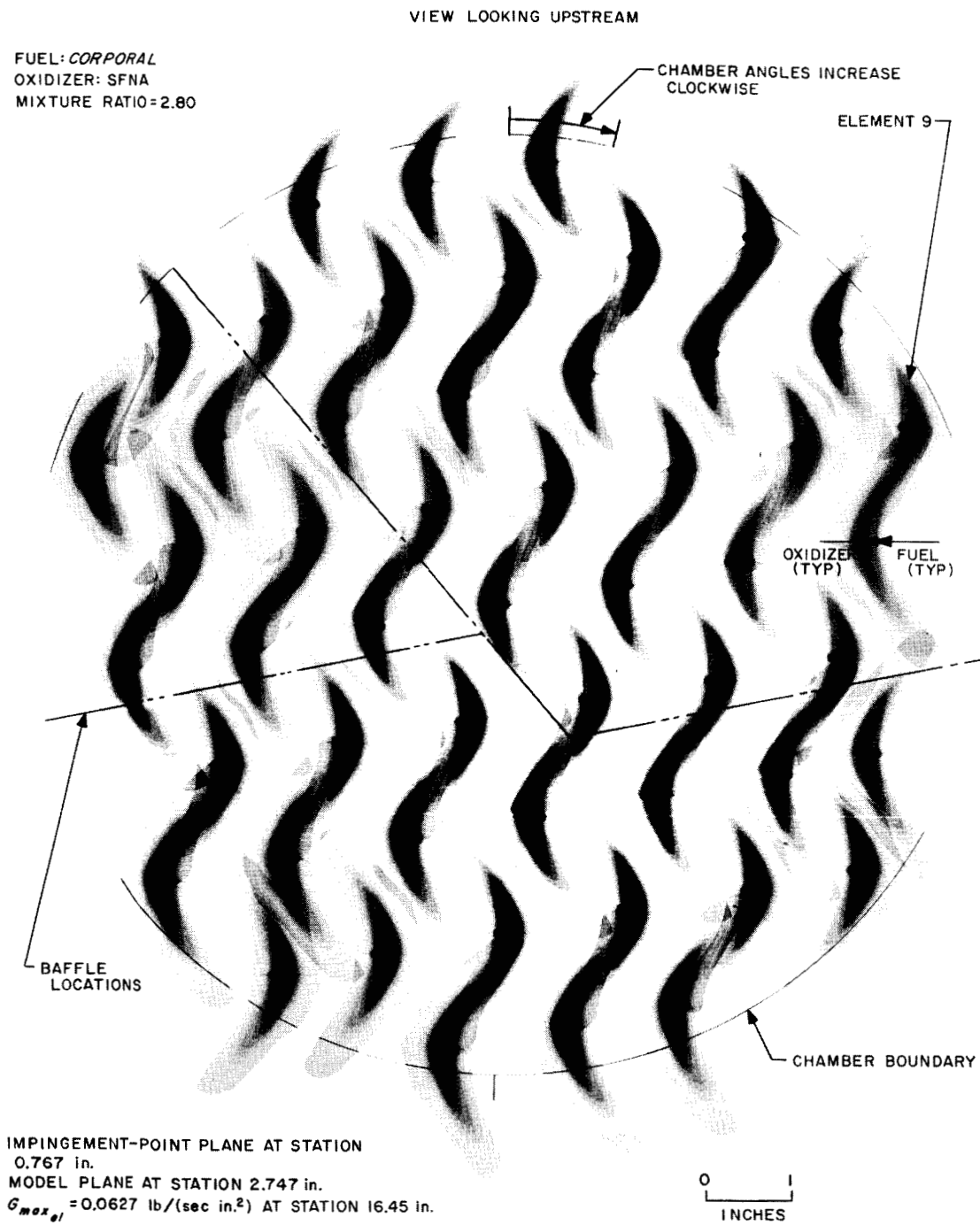

VIEW LOOKING UPSTREAM

FUEL: *CORPORAL*
OXIDIZER: SFNA
MIXTURE RATIO = 2.80

INJECTOR REFERENCE MARK

BAFFLE LOCATION

OXIDIZER (TYP)

FUEL (TYP)

CHAMBER BOUNDARY

IMPINGEMENT–POINT PLANE AT STATION 2.47 in.
MODEL PLANE AT STATION 4.45 in.
$G_{max_{el}} = 0.0786$ lb/(sec in.^{2}) AT STATION 16.45 in.

Fig. 16. Model of axial-mass-flux distribution for RMIR Injector 4

VIEW LOOKING UPSTREAM

FUEL: *CORPORAL*
OXIDIZER: SFNA
MIXTURE RATIO = 2.80

CHAMBER ANGLES INCREASE
CLOCKWISE

ELEMENT 9

OXIDIZER   FUEL
(TYP)   (TYP)

BAFFLE
LOCATIONS

CHAMBER BOUNDARY

IMPINGEMENT-POINT PLANE AT STATION
0.767 in.
MODEL PLANE AT STATION 2.747 in.
$G_{max_{el}}$ = 0.0627 lb/(sec in.^{2}) AT STATION 16.45 in.

0   1
INCHES

Fig. 17. Model of axial-mass-flux distribution for RMIR Injector 5

relatively large variations observed in jet properties (see Section V-B). Thus, for purposes of this presentation, it can be assumed that the mass distributions of these four *Corporal*-like injectors are characterized by Fig. 16.

The parameters achieved by each injection scheme at the model plane are indicated in the pertinent Figure.

Together with the concept that mass density is proportional to local flow rate, these data illustrate the substantial differences between the several composite designs. It will be remembered that these designs include: a modified *Corporal* injector (Fig. 16); a model in which an attempt was made to achieve uniform axial mass flux with the modified *Corporal* element (Fig. 17); a design

VIEW LOOKING UPSTREAM

INJECTOR REFERENCE
MARK

FUEL: *CORPORAL*
OXIDIZER: SFNA
MIXTURE RATIO = 2.80

FUEL
(TYP)

CHAMBER
BOUNDARY

IMPINGEMENT—POINT PLANE AT STATION 2.767 in.
MODEL PLANE AT STATION 8.597
$G_{max_{el}}$ = 0.738 lb/(sec in.^{2}) AT STATION 16.45 in.

0   1
INCHES
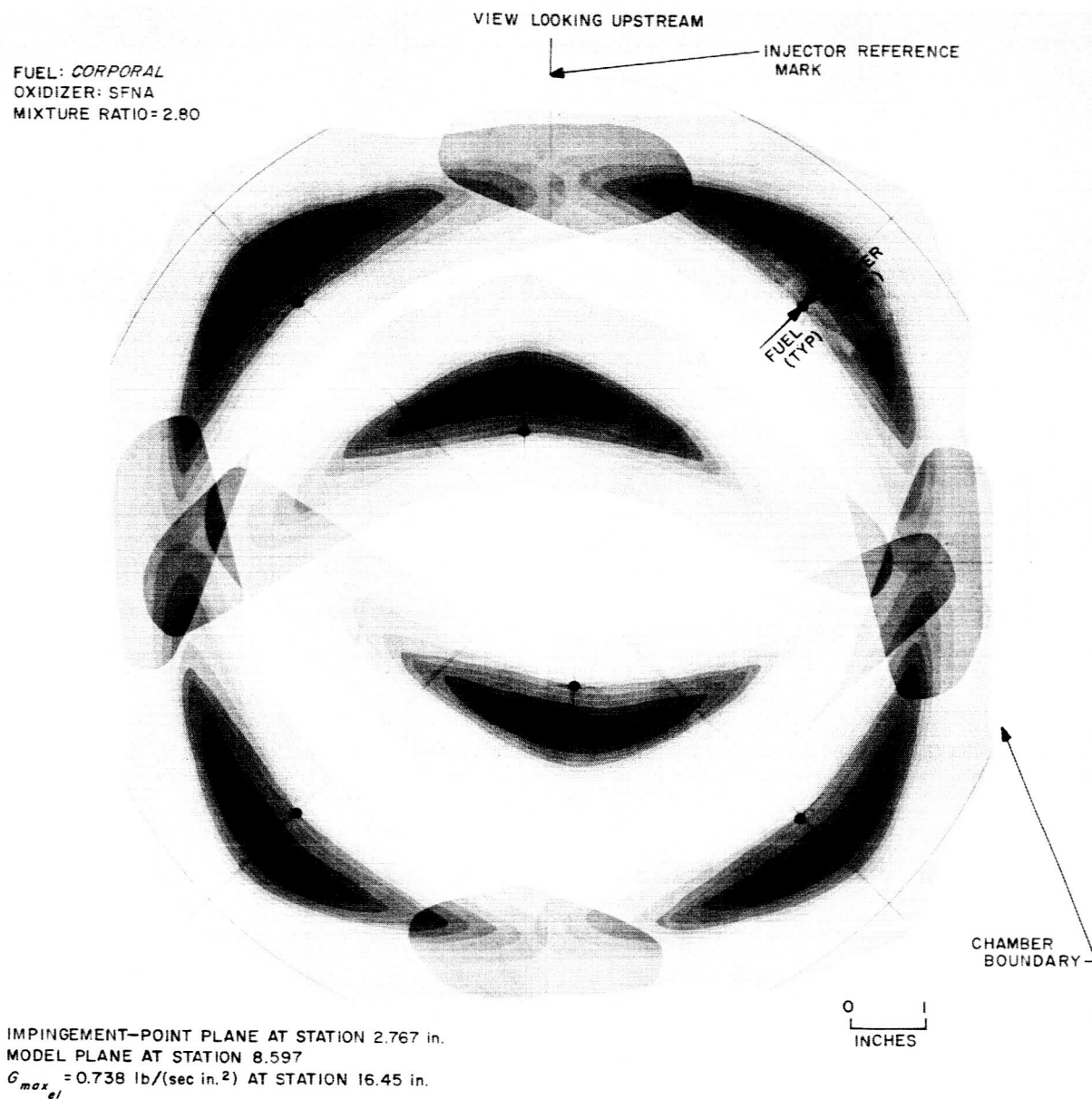
Fig. 18. Model of axial-mass-flux distribution for RMIR Injector 6

illustrating the attempt to increase element scale for an otherwise similar element using the *Corporal* propellant system (Fig. 18); and designs intended to achieve near-uniform axial mass flux at two element scales, comparable with those used in the *Corporal* propellant system, but designed for the N_2O_4–N_2H_4 propellant system (Figs. 19 and 20). In all other respects, the engine operating conditions were identical. Thus, chamber pressure, thrust level, thrust-chamber geometry, etc., were constants.

It should be pointed out that the mass-distribution model for Injector 4 (Fig. 16) misrepresents the actual distribution to the extent that the model for the element is the same as that used for Injector 5, so that the resultant momentum line is parallel to the chamber axis (i.e., $\beta = 0$), while the actual geometry for the injector predicts that $\beta = +2°05'$. This difference would not be discernible in the composite array, so it did not seem that construction of a different model for the element was warranted.

With regard to those designs intended to achieve uniformity, it is noted that these models predict a substantial interaction with the chamber wall, even at the model plane, which could presumably modify the gross combustion effects. However, in the preparation of the original

VIEW LOOKING UPSTREAM

FUEL: N_2H_4
OXIDIZER: N_2O_4
MIXTURE RATIO = 1.20

INJECTOR REFERENCE MARK

CHAMBER BOUNDARY

FUEL →

OXIDIZER ←

BAFFLE
LOCATIONS

0   1
INCHES

IMPINGEMENT-POINT PLANE AT STATION
1.142 in.
MODEL PLANE AT STATION 3.272 in.
$G_{max_{el}}$ = 0.0900 lb/(sec in.^{2}) AT STATION 16.45 in.
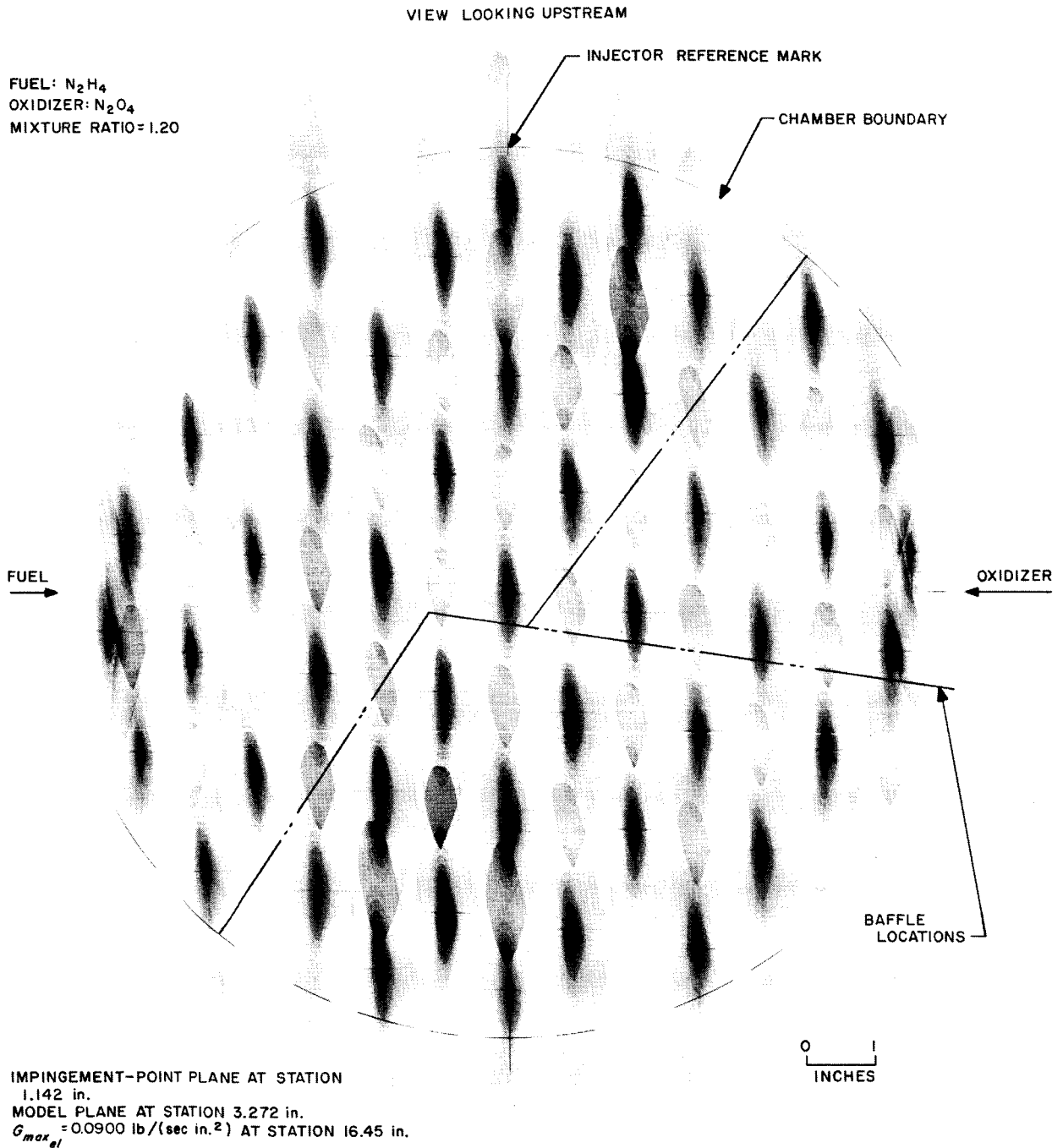
Fig. 19. Model of axial-mass-flux distribution for RMIR Injector 7

design, all attempts to obtain even a qualitative prediction of the effects that might be expected were fruitless. It was not even possible to ascertain whether impingement of the supposedly mixed and reacting fluids on the wall would produce a "hot spot" due to the reaction on the surface or, rather, a "cold spot" due to the quenching action of the wall. Therefore, prime consideration was given to retaining uniformity in element placement and orientation, with the intention of evaluating the consequences of wall impingement in supplementary investigations. A first

FUEL: N_2H_4
OXIDIZER: N_2O_4
MIXTURE RATIO = 1.20

VIEW LOOKING UPSTREAM

INJECTOR REFERENCE MARK

BAFFLE LOCATIONS

OXIDIZER (TYP)

FUEL (TYP)

CHAMBER BOUNDARY

IMPINGEMENT—POINT PLANE AT STATION 1.079 in.
MODEL PLANE AT STATION 4.449 in.
$G_{max_{el}}$ = 0.223 lb/(sec in.²) AT STATION 16.45 in.

0   1
INCHES
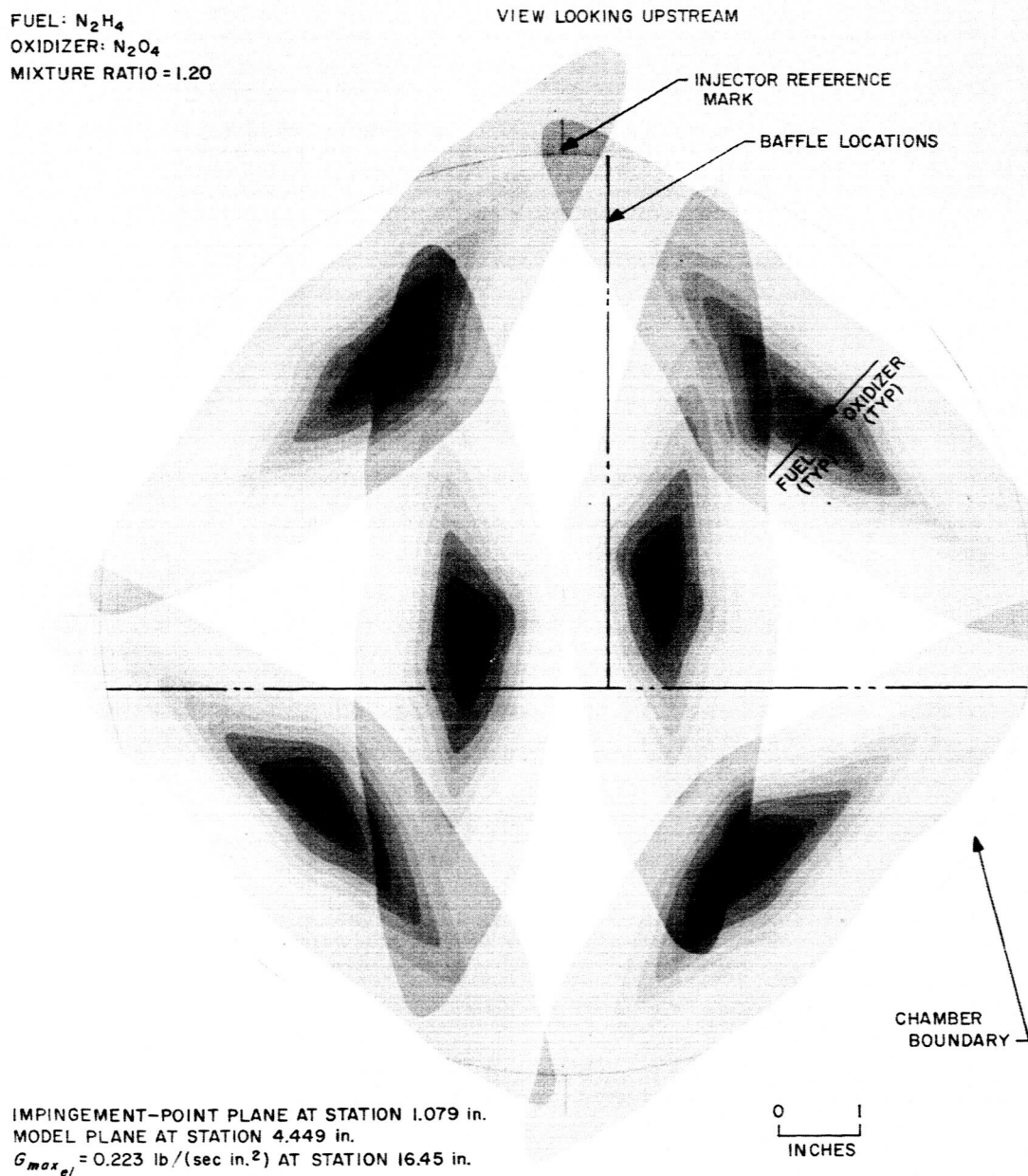
Fig. 20. Model of axial-mass-flux distribution for RMIR Injector 8

evaluation of these effects is included in the discussion of heat transfer in the chamber, as reported in Ref. 32.

It should also be noted that these models do not attempt to describe the effects introduced by the "baffles" that were added to all injectors, except model 6, to eliminate combustion instability (Ref. 8). It is certainly obvious that these surfaces modify the local mass distribution, an effect which may be particularly noticeable at the chamber wall. However, it was assumed that the fraction of
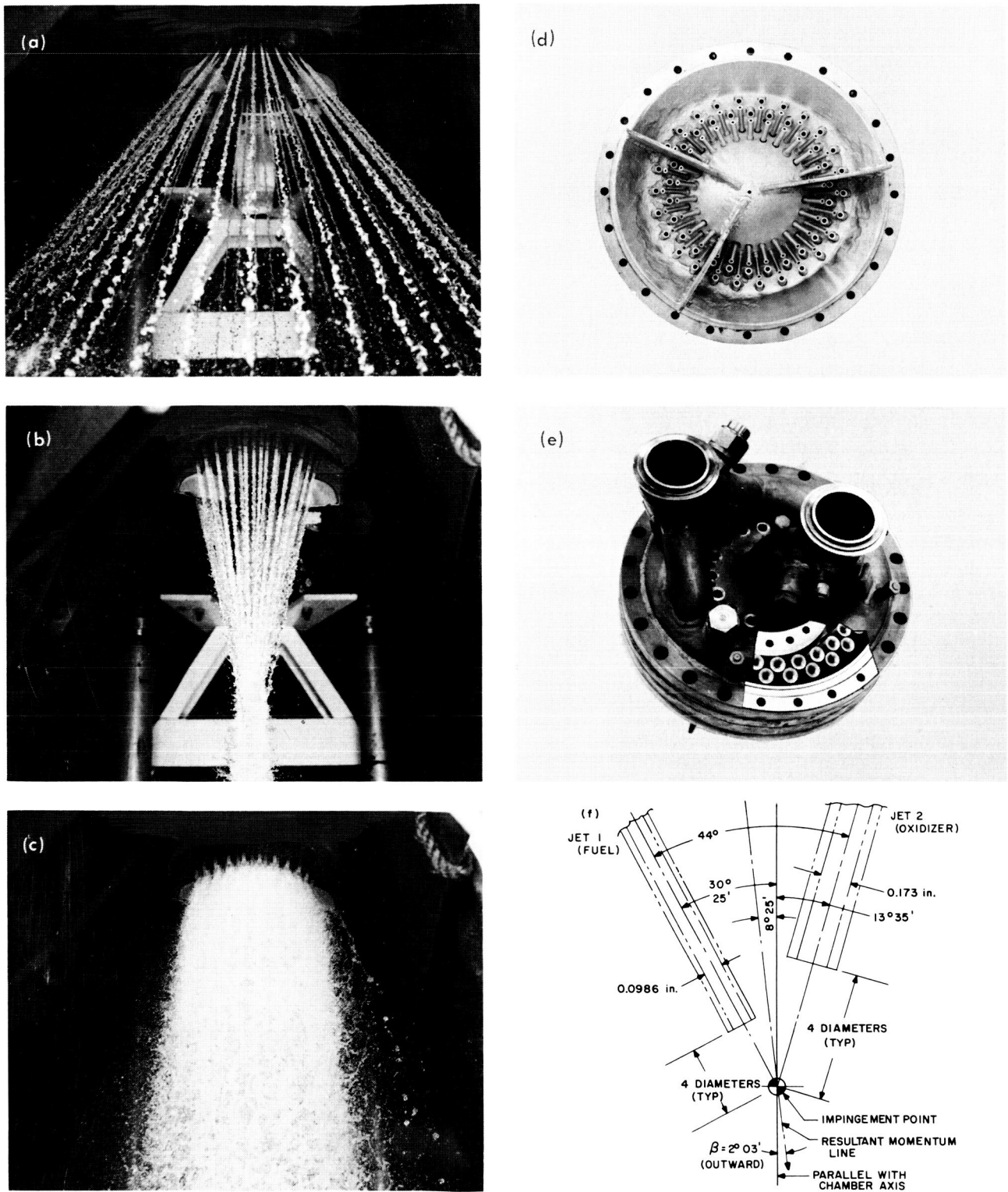
Fig. 21. Hydraulic and geometric characteristics of RMIR Injector 4. (a) Fuel jets. (b) Oxidizer jets.
(c) Combined flow. (d) Cutaway view of manifold, showing orifice inlets.
(e) Injector face. (f) Element geometry

propellant involved in this interaction was small, and that the consequent change in mass distribution would have a negligible effect on combustion. It was not possible to verify this assumption except in a very cursory way; a few isolated tests with Injector 5 (Tests B-871 through B-882 of Ref. 8) and with the *Corporal* Injector (Tests B-520 through B-522 of Ref. 8), where similar experiments were made with and without baffles, showed that the baffles did not influence the gross performance characteristics. In all cases, the baffles were planes parallel to the chamber axis. However, their orientation and length varied somewhat from injector to injector, as indicated by the dashed overlay on the mass-distribution models and in the photographs of the several injectors shown in Figs. 21 to 25.

Finally, it should be noted that the element for Injector 8 incorporates a substantial change in element geometry in an attempt to *decrease* G_{max} for the element while still *increasing* the flow-rate scale by nearly an order of magnitude. As discussed in Ref. 10, this was accomplished by increasing the impingement angle from 45 to 80 deg, and apparently had some merit from the standpoint of minimizing combustion length. Insofar as the nonreactive properties for the injector are concerned, this change is indicated by the change in absolute levels of mass flux, by a new model plane, and, to a lesser extent, by the spatial configuration of the element.

B. Jet Properties and Manifold Effects

As indicated above, and also in Ref. 1, prediction and control of the mass and mixture-ratio distributions of sprays produced by impinging streams are completely dependent on adequate control of jet characteristics. This is particularly true with respect to symmetry and similarity of the velocity profiles and similarity in jet flow rates, particularly when the jets are fed from a common manifold. Because the mass and mixture-ratio distributions of the elements were obtained under laboratory conditions utilizing fully developed pipe flow and/or relatively quiescent upstream conditions to assure stable jets having known dynamic properties, it was essential that the evaluated injector designs produce similar jets. Considerable effort was expended in monitoring flow rates and centerline stagnation pressures for individual jets, both before and after their assembly in an injector, and in attempting to develop manifolds that would not introduce serious defects in these same jet characteristics. Particular emphasis was placed on attempts to achieve fully developed turbulent flow at the orifice exit, since it had been shown in Ref. 14 that this was a preterable flow regime for rocket-engine applications. In all cases,

the jet characteristics were characterized by, or inferred from, measurements obtained with the flat-plate probe and the associated techniques described in Ref. 33.

The jet properties evaluated included (1) centerline-stagnation-pressure ratios,[7] (2) symmetry of the velocity profile in all cases, (3) flat-plate pressure distributions (Ref. 33) for "typical" fuel and oxidizer orifices from each injector, (4) the flow rate for each orifice under typical manifold conditions, and (5) superficial jet characteristics and stability, verified by high-speed-flash photographs of the exit jets.

In the case of Injectors 1 to 4, it was found that manifold effects influenced these measurements to a marked degree, even though a considerable modification of the orifice geometry (relative to the *Corporal*) had been incorporated in these designs. In fact, these orifices conformed to the geometry recommended by this author in Ref. 14 (i.e., a length of 20 diameters, with contoured entries and a turbulence-inducing wall for the first 5 diameters), but failed rather miserably in achieving the expected results in the initial modification of the *Corporal* manifold.

The jet-properties data for this first modification (i.e., RMIR Injector 1, Serial 1), which extended the manifold volume only enough to provide approximately the same clearance over the modified orifices as that available in the *Corporal* injector, are summarized in Fig. 26. These results can be compared with those shown in Fig. 27, which presents similar data for the same set of orifices individually fed from a relatively quiescent manifold. The latter data were obtained by removing the rear section of the manifold and supplying the orifices individually with a long approach section which formed a low-speed, stable, symmetrical velocity profile at the orifice entrance. Hence, any modifications of jet properties due to the installation process are incorporated in the measurements. A comparison of these data[8] shows that (1) there is a substantial change in jet properties due to the manifold effects; (2) the properties of the individually fed jets are quite similar; and (3) the gross geometrical properties

---

[7] The ratio of the centerline stagnation pressure produced by a free jet to the centerline stagnation pressure that would have been produced by a jet having the same flow rate but a *uniform* velocity profile. This ratio is expressed here as p_q/p_u.

[8] It should be noted that only variations in centerline stagnation pressure from orifice to orifice for constant manifold and/or upstream conditions are presented here; these do not compensate for variations in individual orifice flow rates, as is the case in subsequent Figures. Note also, however, that Fig. 27 implies very uniform flow rates, as well as similar velocity profiles for individual orifices, so that Fig. 26 truly represents a manifold effect.
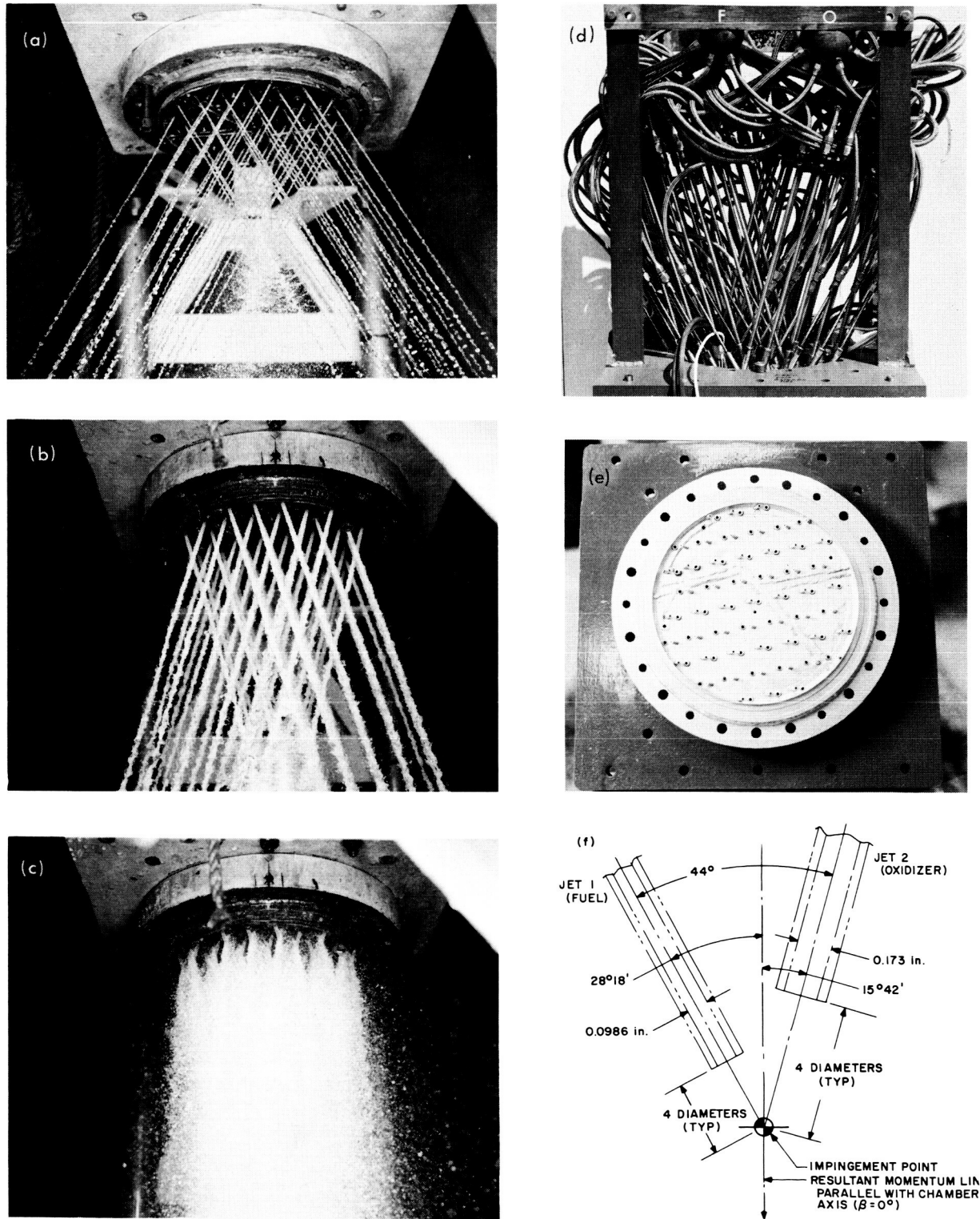
Fig. 22. Hydraulic and geometric characteristics of RMIR Injector 5. (a) Fuel jets. (b) Oxidizer jets. (c) Combined flow. (d) Manifold configuration. (e) Injector face. (f) Element geometry
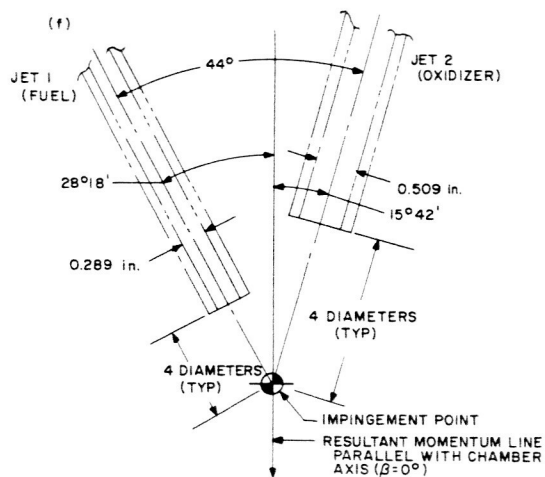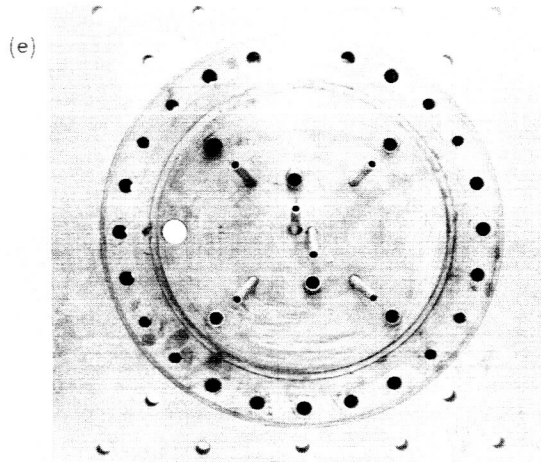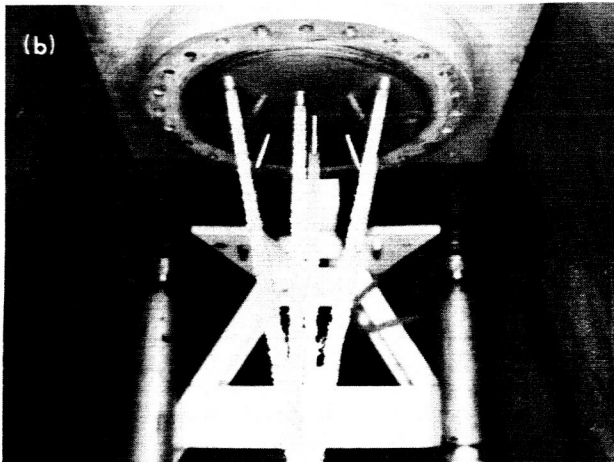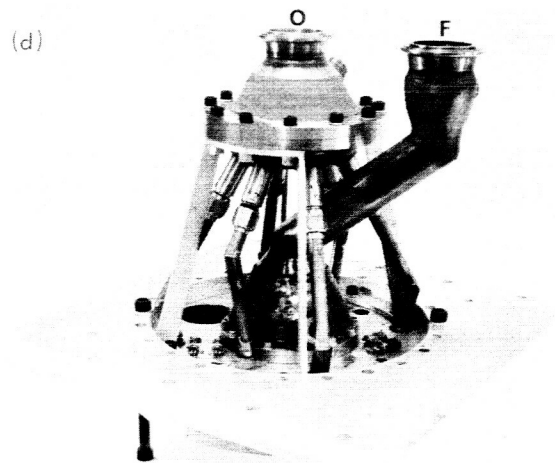
Fig. 23. Hydraulic and geometric characteristics of RMIR injector 6. (a) Fuel jets. (b) Oxidizer jets.
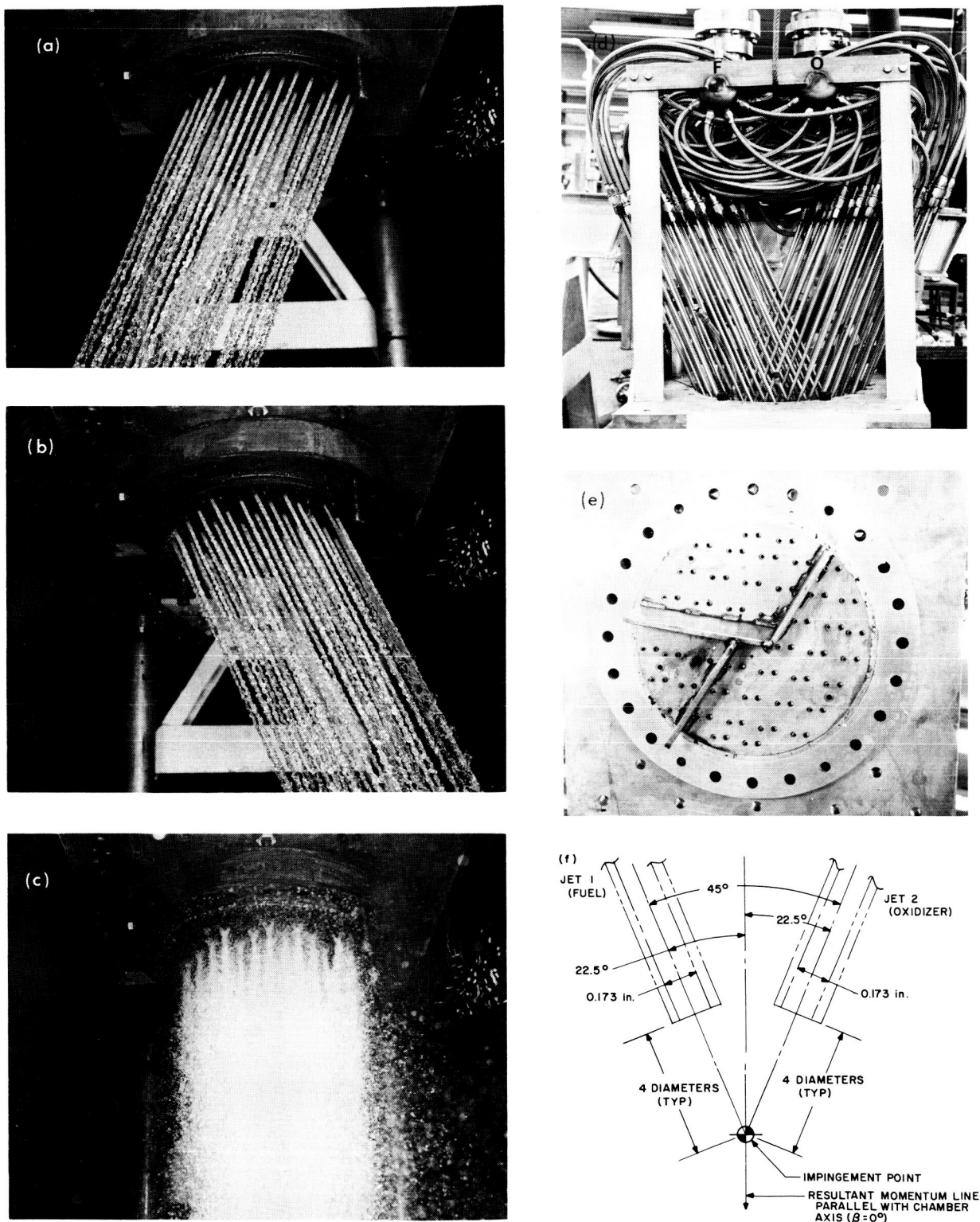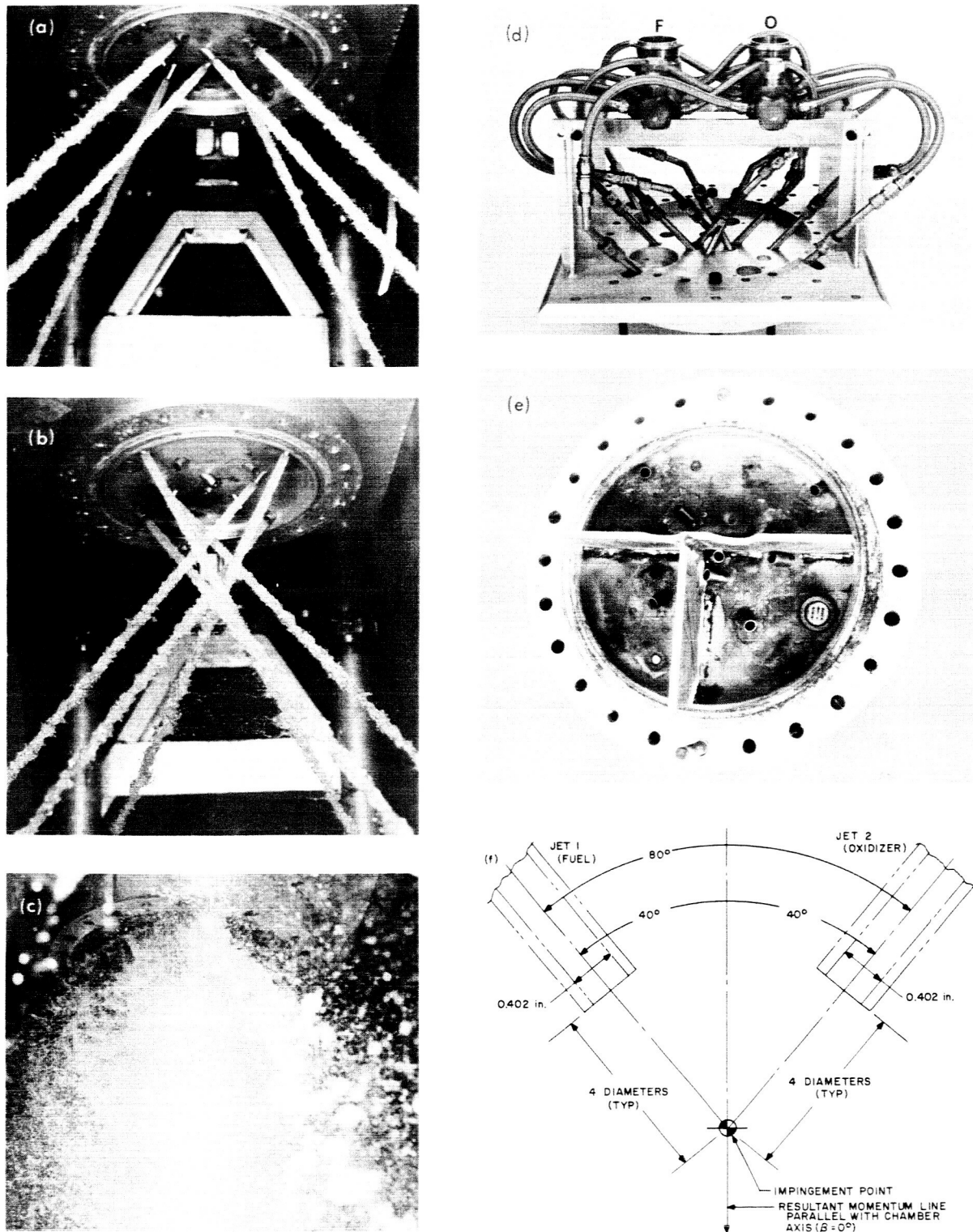(c) Combined flow. (d) Manifold configuration. (e) Injector face.
(f) Element geometry

Fig. 24. Hydraulic and geometric characteristics of RMIR Injector 7. (a) Fuel jets. (b) Oxidizer jets.
(c) Combined flow. (d) Manifold configuration. (e) Injector face, showing
baffles. (f) Element geometry

Fig. 25. Hydraulic and geometric characteristics of RMIR Injector 8. (a) Fuel jets. (b) Oxidizer jets.
(c) Combined flow. (d) Manifold configuration. (e) Injector face, showing
baffles. (f) Element geometry
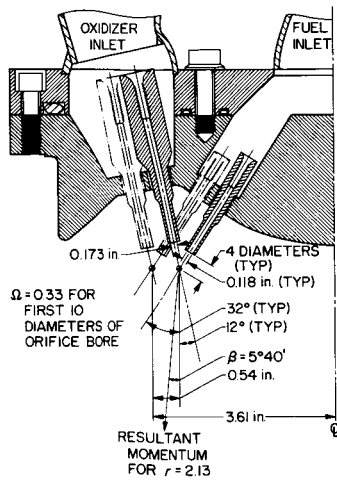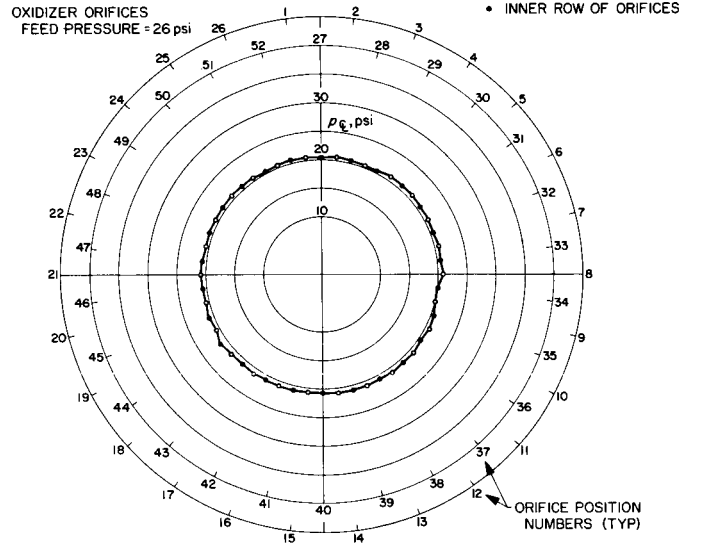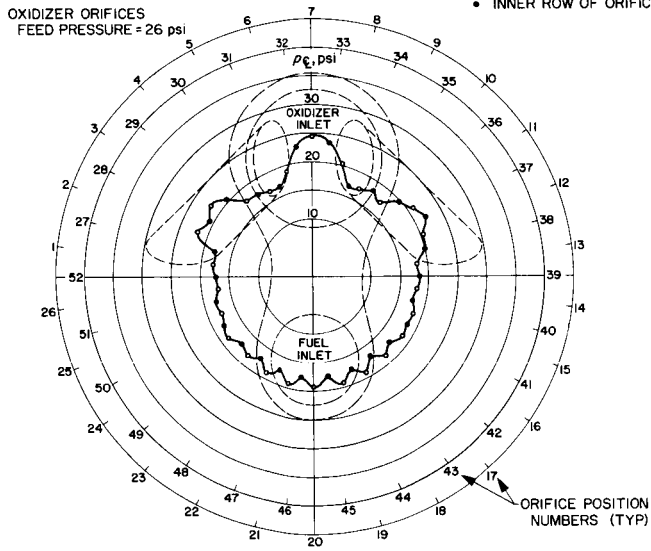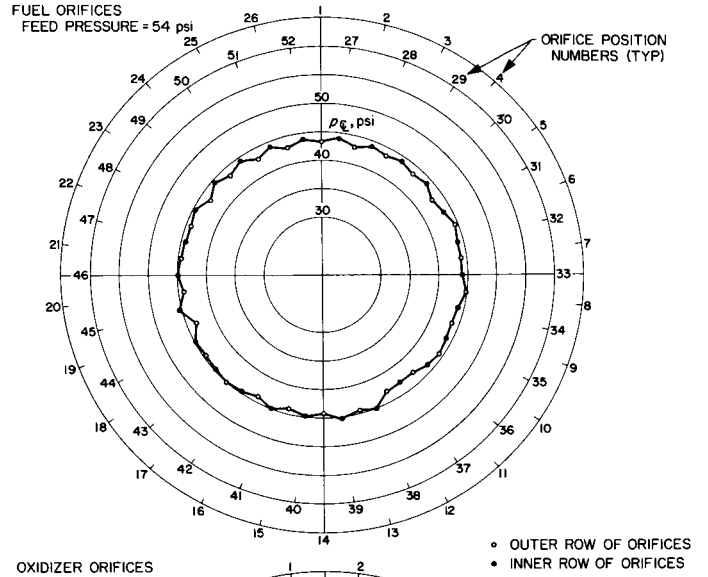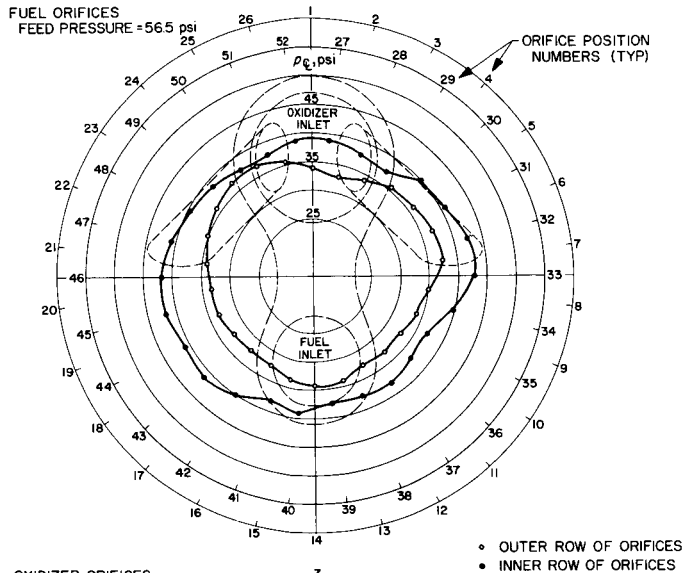
Fig. 26. Jet properties of RMIR Injector 1 with *Corporal* manifold
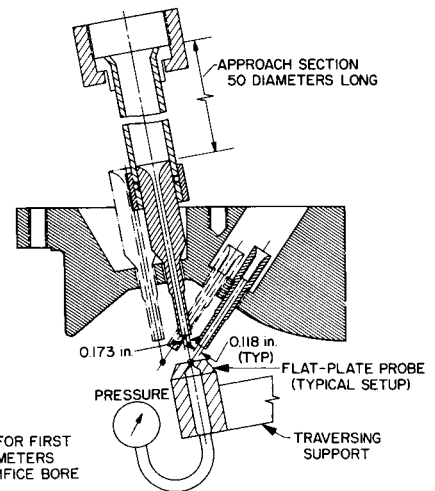
Fig. 27. Jet properties of individually fed orifices for RMIR Injector 1

of the manifold design have a marked influence on these same jet properties, even though no distinction is made in these data between velocity-profile effects and variations in individual flow rates. An attempt to illustrate the latter effect is represented by the phantom sketch of the manifold inlets superimposed on the graph in Fig. 26. It seems fairly obvious, at least with respect to the oxidizer manifold, that the centerline stagnation pressures are maximum in the manifold regions where one would expect a stagnation zone (specifically, immediately below the main entrance tube and at the exits of both side branches), and even the gradual increase that one might expect as the flow approaches the plane of symmetry on the side opposite the inlet is apparent. In the fuel manifold, a substantial nonsymmetry is apparent, but even more significant is the fact that, in general, the entire inner row of orifices is characterized by a relatively low centerline stagnation pressure: i.e., a nonsymmetrical, unstable (progressively changing) velocity profile. The nonsymmetry can probably be attributed to the curvature in the upstream piping, but there seems to be no rational explanation for the differences between the inner and outer rows, other than that they result from a very complex manifold flow; as will be seen, this characteristic

was never really eliminated in the subsequent modifications of the manifold.

In an effort to achieve the intended jet properties for the four *Corporal*-like injectors, a substantial development of the manifold was undertaken. This resulted finally in the compromise solution indicated in the sketch and exploded assembly photograph of Fig. 28. The properties of the *Corporal*-like injectors (identified as units 1 to 4) were evaluated with this manifold. It can be seen from the data presented in Figs. 29 to 32 that this final version of the manifold, together with the orifice design, produced a system in which flow rates for individual orifices, after installation in the injector, varied by as much as 5% (fuel orifices of Injector 2) and, in isolated instances, even exceeded that value. In no case was the maximum variation less than 3% (e.g., Injector 3), even though the flow rate variation prior to installation rarely exceeded 2% for the oxidizer orifices and 3% for the fuel orifices. In addition, the centerline-stagnation-pressure ratios showed variations exceeding 10% of the mean, which, in all instances, were decreased substantially when the injectors were fed by a quiescent upstream system. It is evident that this degradation of the velocity profile
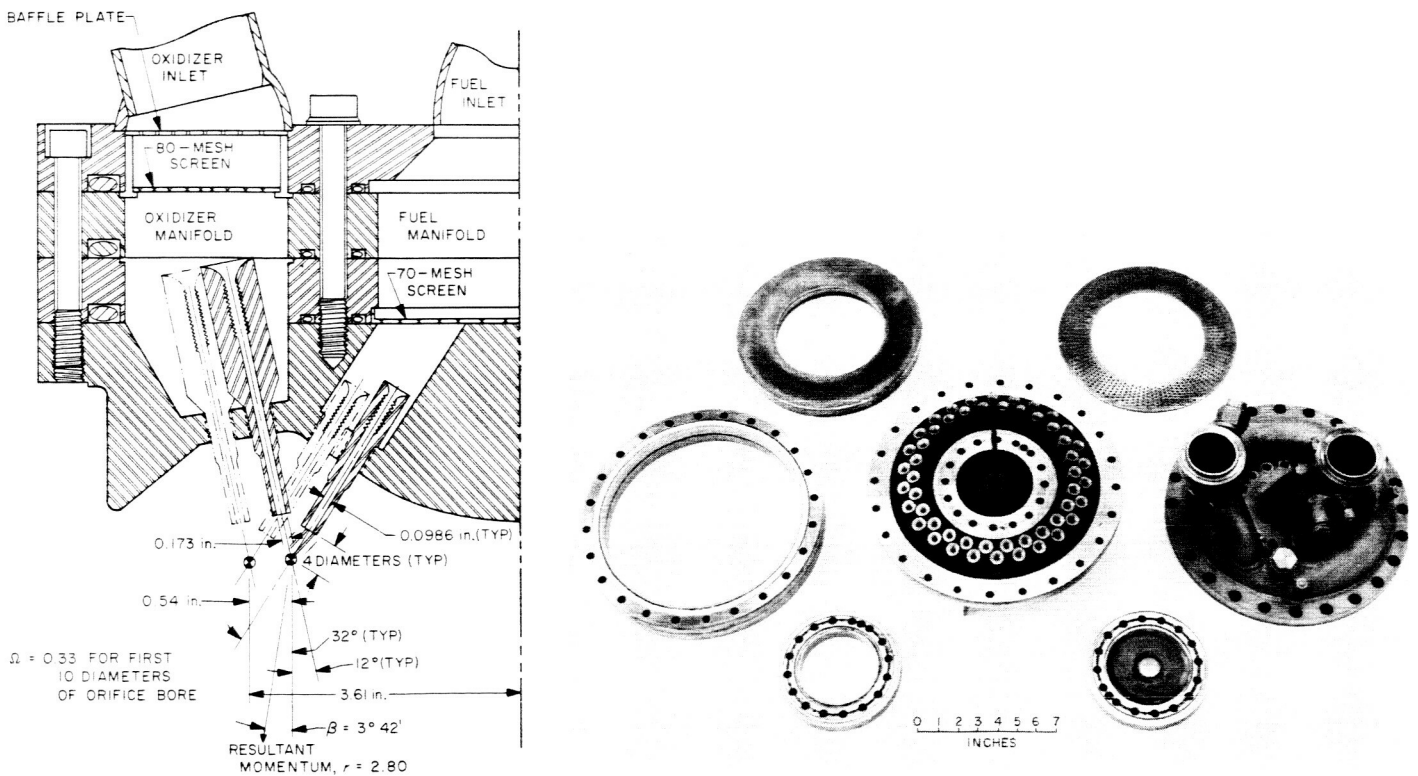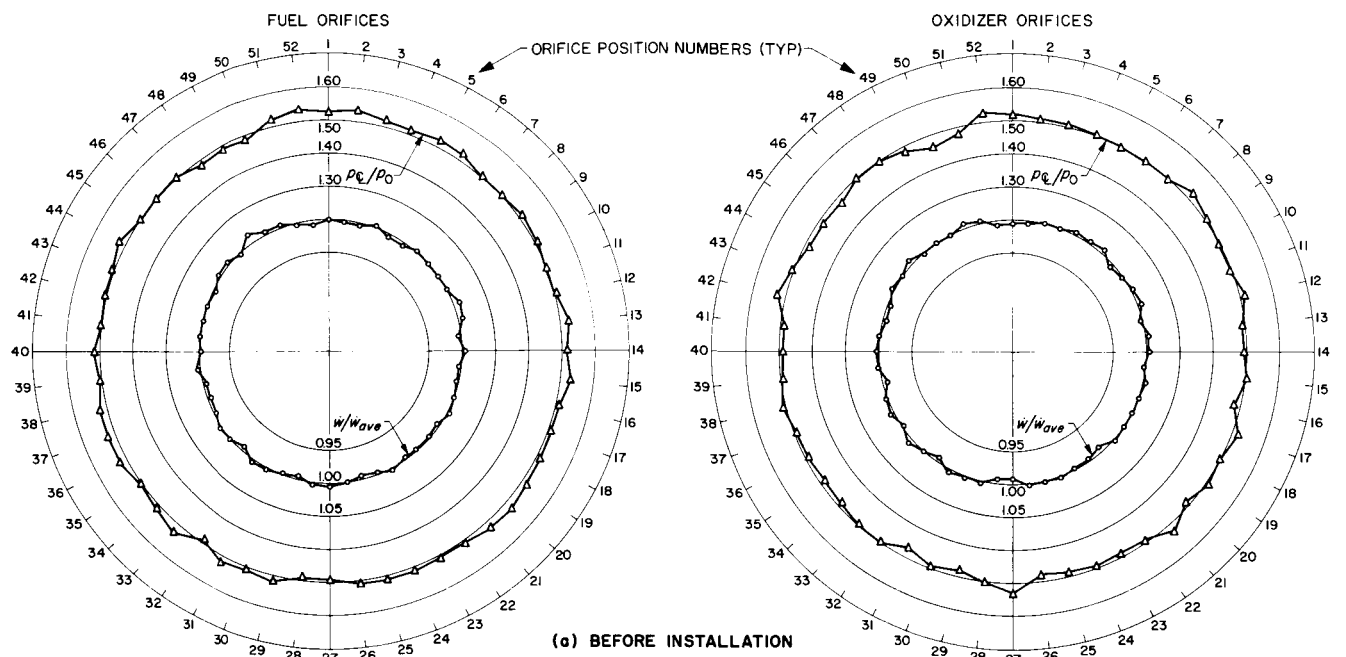

Fig. 28. Manifold and typical orifice geometry for RMIR *Corporal*-like injectors

FUEL ORIFICES

OXIDIZER ORIFICES

(a) BEFORE INSTALLATION

$\dot{w}_{ave}$ = 0.2485 lb/sec

$\dfrac{\dot{w}}{\dot{w}_{ave}}$ = 1.00 ± 1% (EXCEPT ONE DATA POINT)

$\dfrac{p_{\mathcal{C}}}{p_0}$ = 1.50 ± 2%

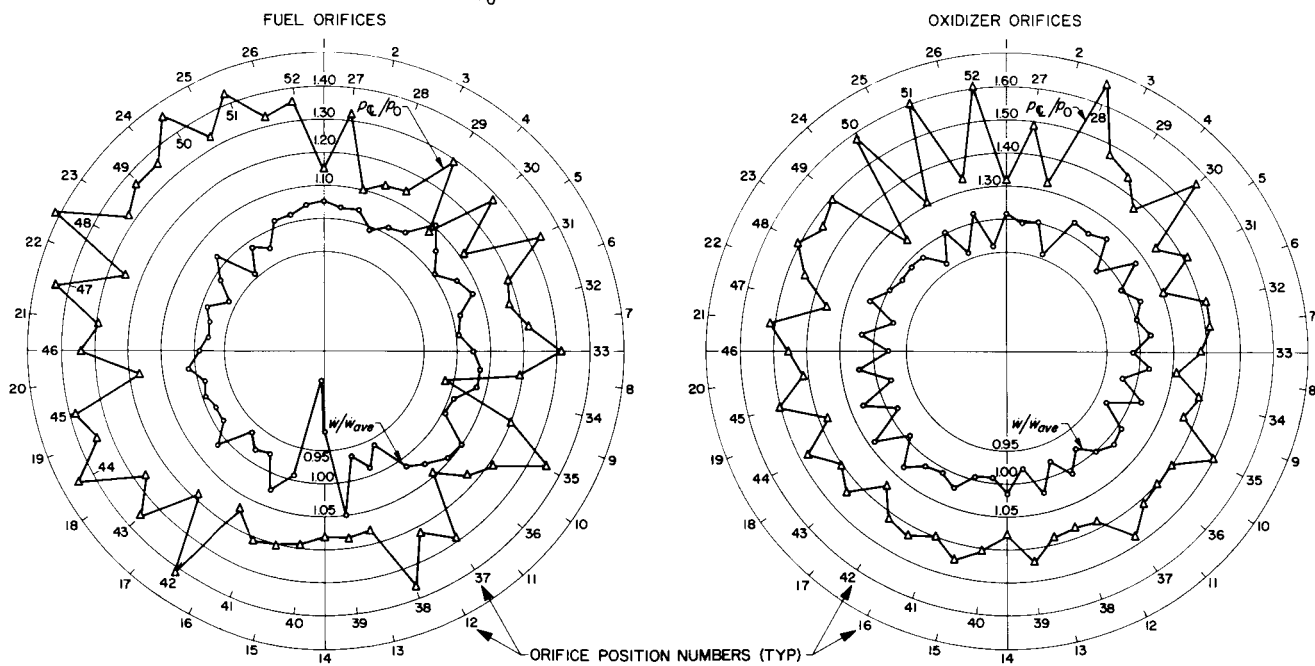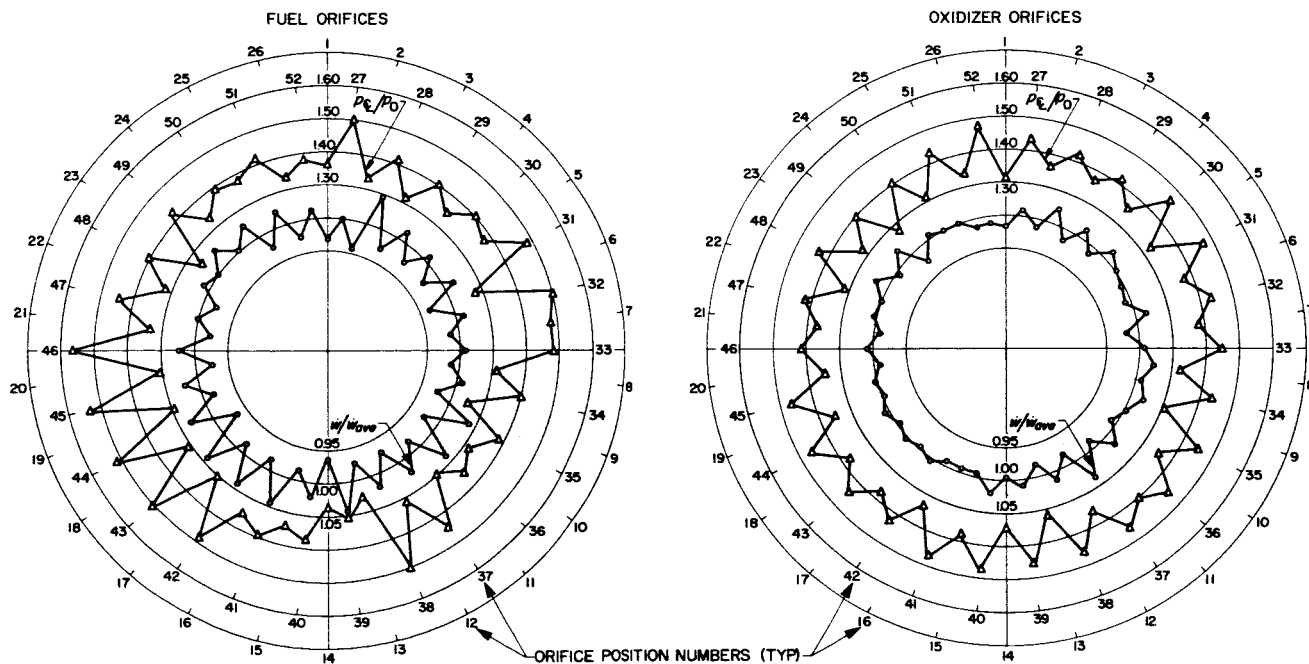ORIFICE POSITIONS AS VIEWED FROM CHAMBER

TEST FLUID: H_2O

$\dfrac{\dot{w}}{\dot{w}_{ave}} = \dfrac{\text{ORIFICE WEIGHT FLOW RATE}}{\text{AVERAGE WEIGHT FLOW RATE}}$

$\dfrac{p_{\mathcal{C}}}{p_0} = \dfrac{\text{CENTERLINE STAGNATION PRESSURE}}{p \text{ FOR UNIFORM VELOCITY PROFILE}}$

$\dot{w}_{ave}$ = 0.46897 lb/sec

$\dfrac{\dot{w}}{\dot{w}_{ave}}$ = 1.00 ± 1%

$\dfrac{p_{\mathcal{C}}}{p_0}$ = 1.49 ± 2.7%

FUEL ORIFICES

OXIDIZER ORIFICES

(b) AFTER INSTALLATION

$\dot{w}_{ave}$ = 0.3406 lb/sec

$\dfrac{\dot{w}}{\dot{w}_{ave}}$ = 1.00 ± 5% (EXCEPT ONE DATA POINT)

$\dfrac{p_{\mathcal{C}}}{p_0}$ = 1.30 ± 16.9%

$\dot{w}_{ave}$ = 0.4669 lb/sec

$\dfrac{\dot{w}}{\dot{w}_{ave}}$ = 1.00 ± 4.3%

$\dfrac{p_{\mathcal{C}}}{p_0}$ = 1.45 ± 10.3%

Fig. 29. Properties of jets for RMIR Injector 1 with modified manifold

Fig. 30. Properties of jets for RMIR Injector 2 with modified manifold

FUEL ORIFICES

OXIDIZER ORIFICES

(a) BEFORE INSTALLATION
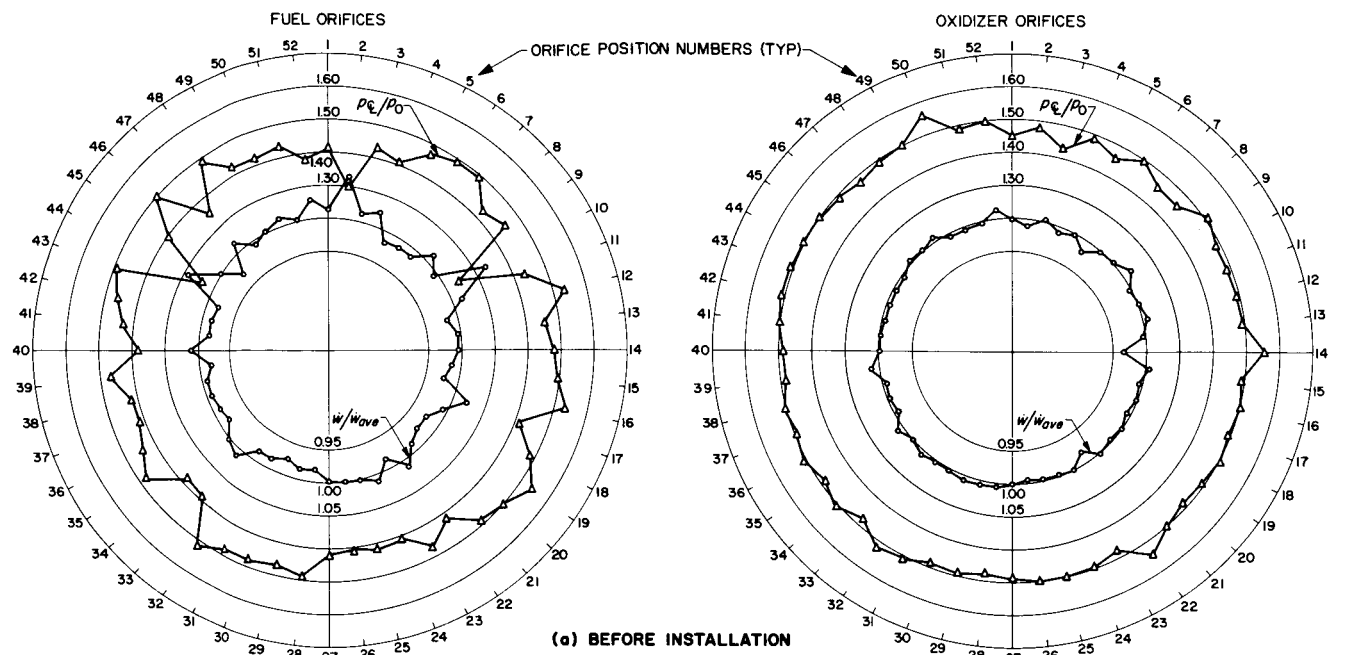
$\bar{w}_{ave}$ = 0.231 lb/sec

$\dfrac{w}{\bar{w}_{ave}}$ = 1.00 ± 3% (EXCEPT THREE DATA POINTS)

$\dfrac{p_{\xi}}{p_0}$ = 1.45 ± 6.9% (EXCEPT THREE DATA POINTS)

ORIFICE POSITIONS AS VIEWED FROM CHAMBER

TEST FLUID: H_2O

$\dfrac{w}{\bar{w}_{ave}}$ = $\dfrac{\text{ORIFICE WEIGHT FLOW RATE}}{\text{AVERAGE WEIGHT FLOW RATE}}$

$\dfrac{p_{\xi}}{p_0}$ = $\dfrac{\text{CENTERLINE STAGNATION PRESSURE}}{p \text{ FOR UNIFORM VELOCITY PROFILE}}$
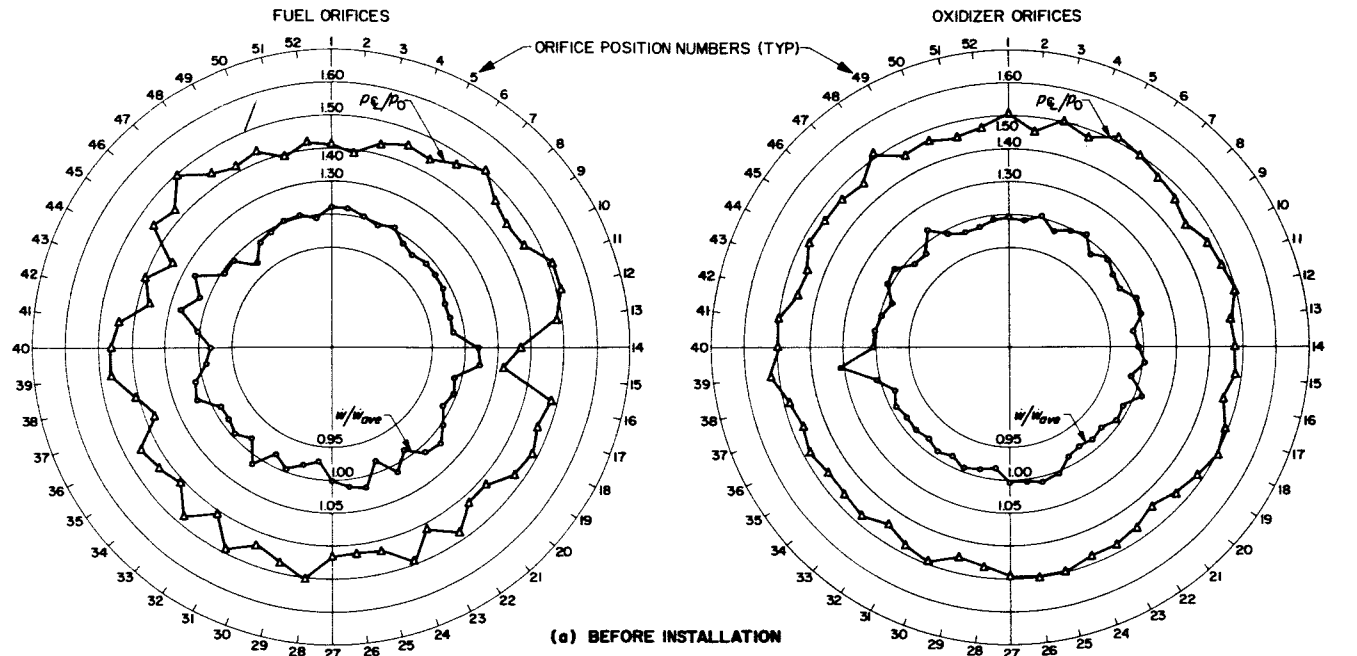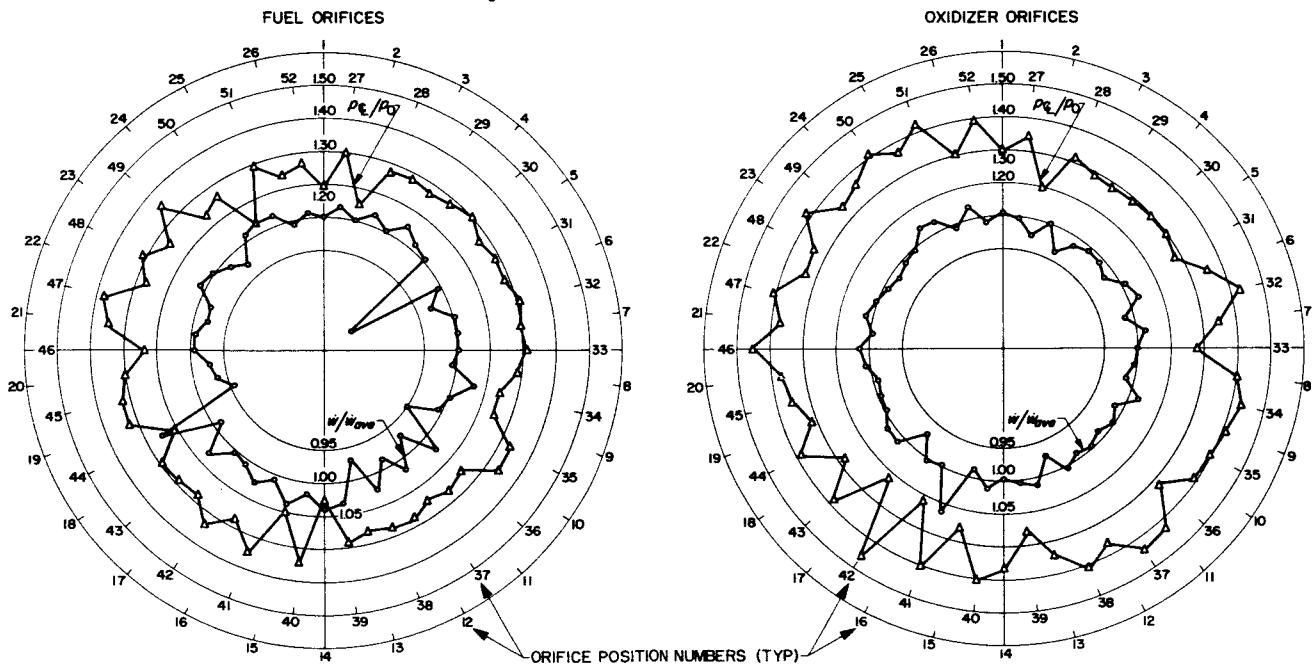
$\bar{w}_{ave}$ = 0.518 lb/sec

$\dfrac{w}{\bar{w}_{ave}}$ = 1.00 ± 2% (EXCEPT ONE DATA POINT)

$\dfrac{p_{\xi}}{p_0}$ = 1.48 ± 5.4%

FUEL ORIFICES

OXIDIZER ORIFICES

(b) AFTER INSTALLATION
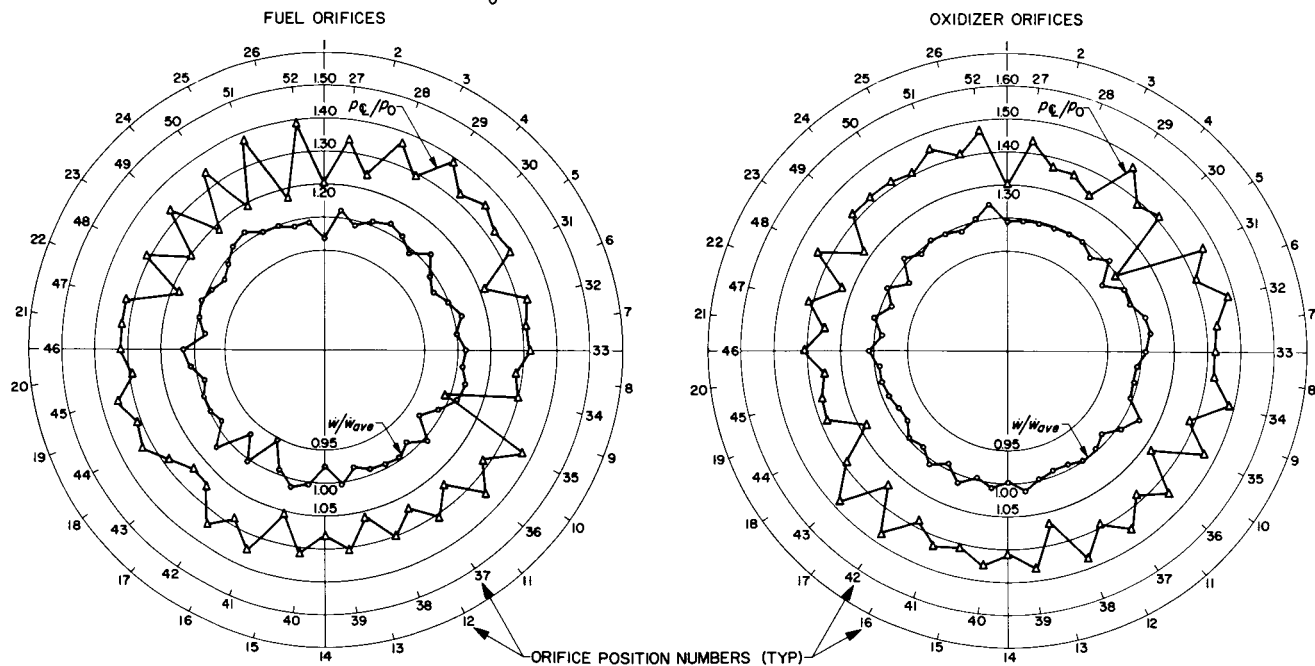
$\bar{w}_{ave}$ = 0.225 lb/sec

$\dfrac{w}{\bar{w}_{ave}}$ = 1.00 ± 3% (EXCEPT ONE DATA POINT)

$\dfrac{p_{\xi}}{p_0}$ = 1.28 ± 8.6% (EXCEPT ONE DATA POINT)

$\bar{w}_{ave}$ = 0.488 lb/sec

$\dfrac{w}{\bar{w}_{ave}}$ = 1.00 ± 3%

$\dfrac{p_{\xi}}{p_0}$ = 1.40 ± 5.7% (EXCEPT TWO DATA POINTS)

Fig. 31. Properties of jets for RMIR Injector 3 with modified manifold

Fig. 32. **Properties of jets for RMIR Injector 4 with modified manifold**

is less noticeable in the oxidizer manifold than in the fuel manifold, ranging from 5.4 to 10% in the former and from 11.2 to 16% in the latter.

The experimental data showing symmetry and similarity of the jet velocity profiles have not been reproduced here, since, in general, the nonconformance of p_{ℓ}/p_0 to the value expected, as taken from Ref. 14 or from data in the literature (for example, Ref. 34) for fully developed turbulent flow, indicated a nonsymmetrical velocity profile.

It was therefore concluded that, in general, the Corporal-like injector designs failed to produce the desired jet properties. Further, it was not possible to devise a scheme for quantitative evaluation of the effects of these variations on the mass and mixture-ratio distributions produced by these injectors. However, even though it was quite clear from the data of Ref. 1 that symmetry and similarity of velocity profiles are significant and are superimposed on variations due to discrepancies between predicted and actual flow rates, it was concluded that a meaningful combustion experiment could be performed with this design and that, in the event that improved injection control appeared warranted, then a complete redesign of this particular configuration would be justified.

In an effort to circumvent these problems, three of the subsequent designs (Injectors 5, 7, and 8 in its final version) utilized relatively long orifices connected to relatively simple manifolds by flexible tubes. For Injectors 5 and 7, the orifices were 100 diameters long; for Injector 8 they were 50 diameters long. As indicated in Figs. 22 and 24 (which include inset photographs of Injectors 5 and 7), this technique resulted in a Medusa-like appearance of the upstream plumbing system; however, the conditions achieved on the combustion-chamber side were uniformly predictable and, as nearly as could be determined, gave the required jet properties. As in the Corporal-like injectors, the data obtained included the centerline-stagnation-pressure ratios, flow rates, and flat-plate pressure distributions for individual orifices fed by the actual manifold. However, it was found in this case that the jet properties were, within experimental accuracies, those that would have been predicted for fully developed turbulent flow (Ref. 14). These experimental data are summarized in Table 2.

In the case of Injector 6 (Fig. 23), a rather ambitious attempt to produce the desired jet properties with a somewhat more sophisticated manifold was only partially successful. This effort was prompted by a desire to minimize the length of the large oxidizer orifices (approximately 0.50 in. in diameter), which, for $L/d = 100$, would have

Table 2. Hydraulic properties of orifices for RMIR Injectors 5, 7, and 8

Parameter	RMIR Injectors							
	Injector 5		Injector 7		Injector 8		Injector 8, Mod I[a]	
	Fuel	Oxidizer	Fuel	Oxidizer	Fuel	Oxidizer	Fuel	Oxidizer
Manifold pressure, psi Discharge pressure, psi	60 Ambient	30 Ambient	195 Ambient	195 Ambient	313 120	320 120	142 Ambient	
Nominal flow rate, lb/sec Maximum departure from nominal, %	0.1625 ±0.3	0.3550 ±0.9	0.925 +1.5 −4.6	0.923 +1.8 −4.4	5.01 +4.4 −3.0	4.97 +3.6 −5.6	5.00 ±0.5	
Discharge coefficient, overall Discharge coefficient for Reynolds number range	$0.50 < C_d < 0.55$ $4 \times 10^4 < Re < 1.5 \times 10^5$		$0.49 < C_d < 0.53$ $4 \times 10^4 < Re < 1.5 \times 10^5$		$0.50 < C_d < 0.54$ $10^5 < Re < 4 \times 10^5$		$C_d \simeq 0.62$ $Re \simeq 3 \times 10^5$	
Nominal p_{ℓ}/p_0 Maximum departure from nominal, %	1.505 ±1.0	1.450 ±0.7	1.375 +4.00 −1.81	1.376 +2.47 −2.00	1.441 +2.0 −2.1	1.431 +9.6 −6.9	1.33 ±1.0	
Symmetry criterion,[b] % p_{ℓ}	0.8	2.5	1.2	1.05	10.9	14.7	10	

Test conditions
1. Test fluid: H_2O
2. Stagnation pressures and pressure distributions taken with flat-plate probe at a point 4 diameters from orifice exit (Ref. 33).
3. Orifice geometry as shown in Table 1.

Overall test results
Manifold effects were determined to have a negligible influence on the jet properties of these injectors.

[a] Straight tubes for oxidizer orifices; $L/d = 55$.
[b] $(p_0 + p_{90} + p_{180} + p_{270})_{R=1.0}/4p_0$

been some 50 in. long. Another objective was to demonstrate the suitability of some of the manifolding concepts that had been evolved in the effort expended on the *Corporal*-like injectors. In particular, it was believed that many of the difficulties associated with the *Corporal*-like manifold could be eliminated if axial symmetry in a relatively quiescent inlet flow could be achieved. The suggestions presented in Ref. 14 for minimizing orifice lengths would then be applicable and, if all this could be achieved with reasonable manifold volumes, it might be possible to demonstrate a geometry that could be applied to flight design.

The final configuration intended to satisfy these several objectives, as well as the requirements for mass and mixture-ratio distribution outlined in Section III, is presented in Fig. 23. It is seen that, in both oxidizer and fuel systems, the so-called *vaned turn* has been utilized: in the oxidizer system as an integral part of the orifice, and in the fuel system as part of the upstream manifold. In addition, baffle plates and screens were incorporated in both diffusers, and hemispherical screens were mounted over the orifice inlets in an effort to approximate a truly quiescent flow at the orifice inlet. As suggested in Ref. 14, the orifices included contoured entries, turbulence-inducing sections in the initial 5 diameters, and a total length of at least 20 diameters. That this approach was only partially successful is indicated by the data in Table 3, which summarizes the properties of these jets.

With regard to the vaned turns incorporated here (and also in the initial configuration of Injector 8), it may be pertinent to note that a search of the literature failed to provide any design information for such a device. However, intuition suggested that the influence of the bend could be dissipated in a relatively short downstream length if (1) the velocity profile approaching the turn was uniform, (2) the pressure drop across each of several essentially rectangular passages (formed by inserting vanes along chordal planes parallel to the flow) was the same for a given velocity, and (3) the height dimension of the passage was perpendicular to the plane of the bend and small relative to the diameter of the tube. A subsequent evaluation of several different geometries showed that reasonable jet properties could be achieved with approximately 5 diameters of tube downstream from a mitered 45-deg bend containing five passageways characterized by the same hydraulic radius[a] and extending upstream a distance equivalent to 8 hydraulic radii and downstream a distance equivalent to 40 hydraulic radii.

---

[a]*Hydraulic radius* is defined as passage area/wetted perimeter; thus, in a circular pipe, $R_h = d/4$.

This is the geometry illustrated in Fig. 33, which also shows its embodiment in the actual oxidizer orifices for Injectors 6 and 8.

The influence of the bend on the velocity profile of the jet produced by such a device can be inferred from the flat-plate pressure distributions shown in Fig. 34. Here, data for a typical mitered elbow with and without vanes are compared with a similar distribution produced by a straight orifice of the same length. As might be expected, the velocity profile downstream of the bend without vanes is highly distorted, and the installation of the vanes produces a near-normal jet that is only slightly nonsymmetrical in the plane of the bend. As in the case of the *Corporal*-like injectors, this distortion was accepted for the initial evaluation, since it was found that variations introduced by the manifolds were of the same approximate magnitude as those produced by the bend.
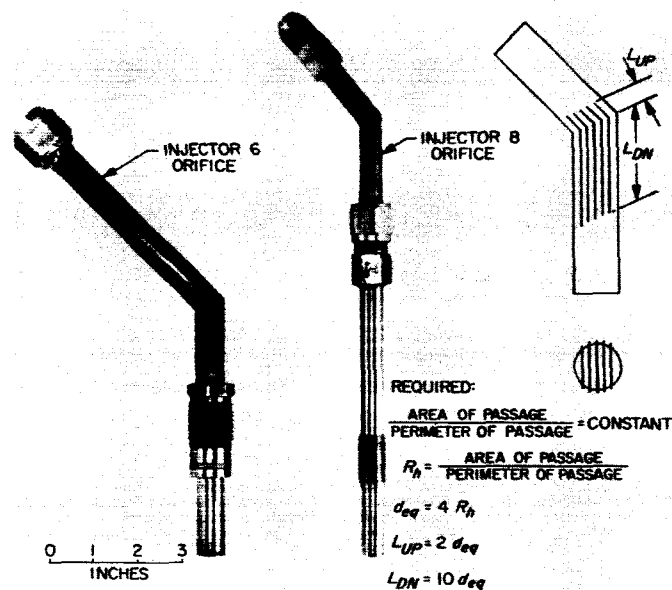

Fig. 33. Mitered and vaned turn (45 deg)

Unfortunately, these efforts served only to verify the experiences associated with the *Corporal*-like injectors, indicating that adequate control of jet characteristics is completely dependent on the elimination of manifold effects, and that the attainment of truly quiescent conditions at the entrance of the orifice is extremely difficult in the minimal manifold volumes desired for flight applications.

Table 3. Hydraulic properties of RMIR Injector 6

Parameter	Oxidizer orifices						Fuel orifices					
	1-O	2-O	3-O	4-O	5-O	6-O	1-F	2-F	3-F	4-F	5-F	6-F
Supply pressure, psi	70	70	70	70	70	70	120	120	120	120	120	120
Flow rate, lb/sec	3.50	3.50	3.48	3.45	3.50	3.44	2.66	2.72	2.56	2.69	2.52	2.73
$\dot{w}/\dot{w}_{ave}$	1.006	1.006	1.000	0.992	1.006	0.989	1.005	1.028	0.968	1.017	0.953	1.032
$p_{\mathcal{L}}/p_0$	1.34	1.40	1.44	1.33	1.48	1.30	1.38	1.33	1.30	1.38	1.31	1.36
Symmetry criterion[a], % $p_{\mathcal{L}}$	4.9	13.2	11.8	3.6	16.6	10.4	0.6	2.9	0.7	2.4	4.9	4.7

Test conditions and geometry	1. Oxidizer orifices separately fed from 85 diameters of ½-in.-ID tube. 2. After assembly in manifold, orifices calibrated with 25-psi back pressure to prevent cavitation; C_d (overall) $\simeq$ 0.59 for $10^5 <$ Re $< 3 \times 10^5$. 3. A 45-deg vaned and mitered turn incorporated in orifices.	1. Fuel orifices separately fed from 55 diameters of 1.1-in.-ID tube. 2. After assembly in manifold, orifices calibrated with ambient discharge pressure; 0.73 $< C_d$ (overall) $<$ 0.79 for $10^5 <$ Re $< 4 \times 10^5$.

Overall test conditions

1. Test fluid: H_2O.
2. Stagnation pressures and pressure distributions taken with flat-plate probe at a point 4 diameters from orifice exit (Ref. 33).
3. Orifice geometry as shown in Table 1 and Fig. 23.

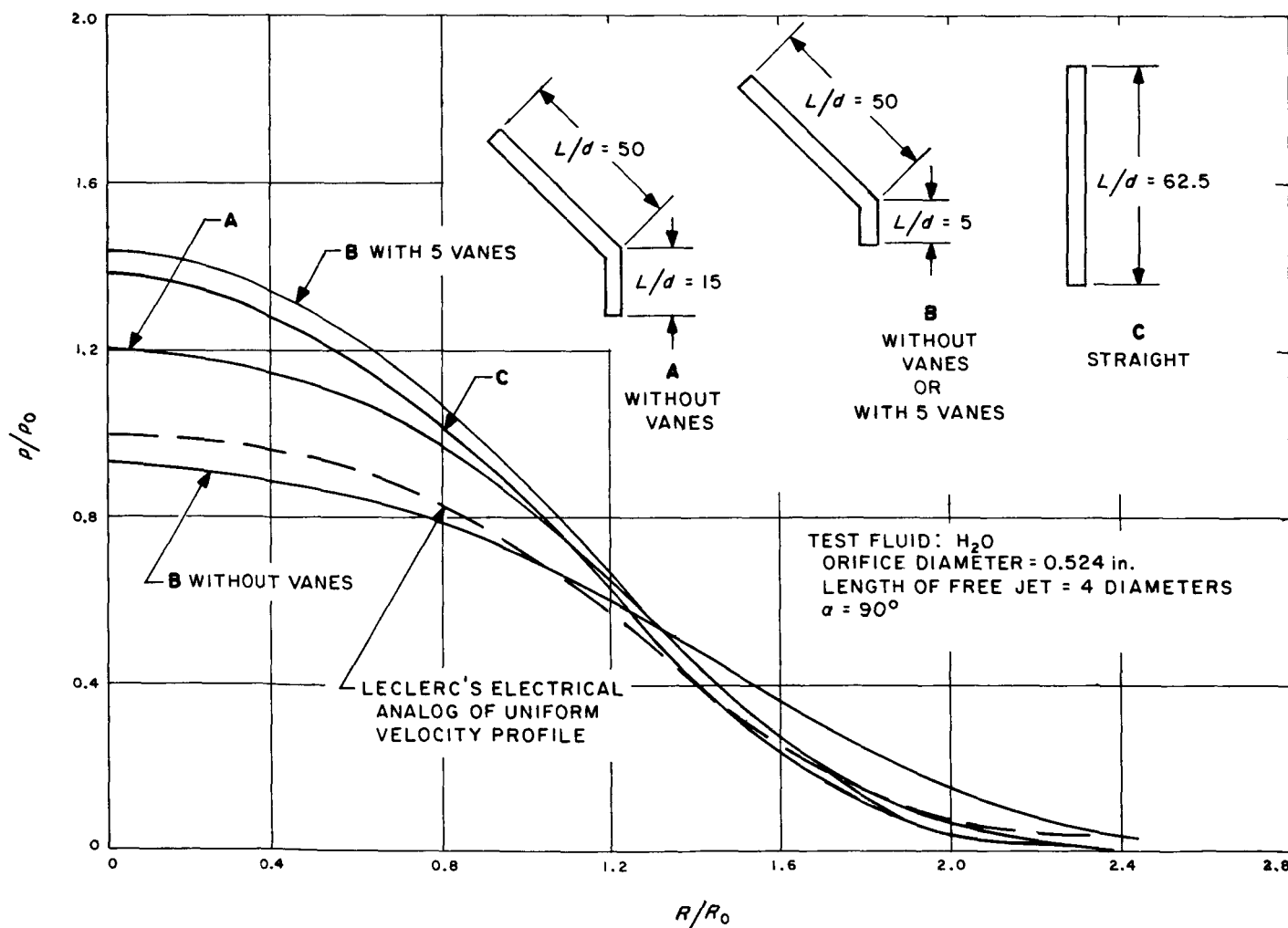[a] $(p_0 + p_{90} + p_{180} + p_{270})_{R=1.0}/4\overline{p_0}$

Fig. 34. Influence of 45-deg mitered and vaned turn on flat-plate pressure distribution produced by a free-liquid jet

In an effort to minimize orifice length, the vaned turn was also utilized for Injector 8 (Fig. 25). However, in the course of the combustion evaluation, it became necessary to replace the oxidizer orifices with 55-diameter-long tubes coupled to relatively long flex lines, in an attempt to eliminate certain spurious combustion effects (Ref. 8). As noted therein, for a part of the performance evaluation, the jets were formed from fully developed turbulent pipe flow without any apparent change in gross operating characteristics. The pertinent properties of the jets produced by these several configurations are included in Table 2.

C. Superficial Jet Properties

High-speed-flash photographs (exposed for approximately 2.0 μsec) were taken of water jets formed by Injectors 1 to 8, in order to ascertain their superficial characteristics and verify their directional stability. It was impossible, by this technique, to differentiate these jets from those produced by fully developed turbulent flow, as illustrated in Ref. 14 for comparable Reynolds numbers. Typical photographs of the injectors, with both separate and combined flows through each set of orifices, are presented in Figs. 21 to 25. In all cases, the flow rates were substantially reduced from design levels in order to improve the clarity of the photographs. Only in the case of the *Corporal* injector (Fig. 3) was there any clearcut evidence of the manifold effects that became apparent in the other measurements. Also, the excellent directional control achieved in the fully developed turbulent flow produced by Injectors 5 and 7 is clearly illustrated by the impingement of jets in conformance with centerline geometry at distances approaching 100 diameters from the orifice exit. (These are, of course, jets that simulate the same propellant, since impingement of a propellant with its "unlike" mate normally occurs much closer to the injector face.)

VI. SUMMARY AND CONCLUDING REMARKS

A logical injector design procedure based in part on the properties of nonreactive sprays produced by a pair of unlike impinging streams was utilized in the design of a series of eight different injectors. A technique for defining in a quantitative sense the mass distribution of sprays was developed and used in describing the mass distributions that characterized this series of multi-element injection schemes. The properties of the jets produced by each injector design were evaluated and are summarized herein.

This investigation resulted in the following conclusions:

1. The usual injector manifold can have an overwhelming influence on the properties of the jets produced by the usual injector orifice. Thus, if the injection scheme is to be controlled, predictable, or even reproducible on a local basis, it is essential that manifold effects be controlled or eliminated.

2. In application to item 1, above, the recommendations of Ref. 14 with regard to orifice geometry are inadequate to control jet properties unless the orifice is supplied with a relatively quiescent inlet flow.

NOMENCLATURE

A area, in.^{2}

A_0 tube area $= 0.0227$ in.^{2}

A_s area represented by sample, in.^{2}

c^* characteristic exhaust velocity, ft/sec $= (p_c A_t g)/\dot{w}$

c^*_{th} equilibrium c^* at indicated r, ft/sec

C_d discharge coefficient

C_F nozzle thrust coefficient

d diameter, in.

d_{eq} equivalent diameter, in.

D optical density of photographic emulsion $= \log(1/T)$

F thrust, lbf

g local gravitational acceleration, taken as 32.17 ft/sec^2

G local flow rate per unit area, lb/(sec in.^{2})

I_s specific impulse, sec

K area correction factor $= A_s/A_0$

L length, or distance from impingement point, in.

L^* characteristic length of combustion chamber, in.

n number of samples in which $\phi < \phi_0$

$\bar{n}$ number of samples in which $\phi > \phi_0$ (i.e., ϕ designated as $\bar{\phi}$)

N number of injector elements

p pressure, psi

P momentum per second $= (\dot{w}_{el} V)/g$

r mixture ratio $= \dot{w}_{2el}/\dot{w}_{1el}$

r_{unif} mixture ratio which satisfies uniformity criterion

R radius, in.

R_h hydraulic radius, in.

t time, sec

T transmission, or relative optical transmittance of photographic emulsion ($1/T =$ opacity)

V mean velocity, ft/sec

$\dot{w}_{el}$ total flow rate of spray $= (\dot{w}_{1el} + \dot{w}_{2el})$, lb/sec

$\dot{w}_s$ total local flow rate of spray $= (\dot{w}_{1s} + \dot{w}_{2s})_{\theta,R}$, lb/sec

α impingement angle: total angle included between stream centerlines, deg

β complement of true angle between resultant momentum line and a plane perpendicular to chamber axis, deg

γ specific heat ratio

δ density of fluid, lb/cu ft

ε_c nozzle-contraction area ratio

ε_e nozzle-expansion area ratio

η_m mixing factor (from Ref. 2)

$$\eta_m \equiv 100 \left\{ 1 - \left[\sum_0^n \frac{K\dot{w}_s(\phi_0 - \phi)}{(\Sigma K\dot{w}_s)\phi_0} + \sum_0^{\bar{n}} \frac{K\dot{w}_s(\phi_0 - \bar{\phi})}{(\Sigma K\dot{w}_s)(\phi_0 - 1)} \right] \right\}$$

θ angle of rotation about resultant momentum line, taken from arbitrary reference position usually designated as 0 when aligned with the fuel orifice, deg

λ nozzle-divergence loss factor

σ true angle between resultant momentum line and path of particle, deg

ζ true angle between resultant momentum line and bisector of jet centerlines (taken as positive when bisector is rotated clockwise in relation to resultant momentum line), deg

ϕ local mass-fraction ratio of spray $= [\dot{w}_{2s}/(\dot{w}_{1s} + \dot{w}_{2s})]_{\theta,R}$

ϕ_0 nominal mass-fraction ratio of spray $= \dot{w}_{2el}/(\dot{w}_{1el} + \dot{w}_{2el})$

ψ solid angle of spherical segment of sample, deg

Ω roughness factor of surface, defined as height of projection divided by radius

Subscripts

0   reference value or ambient pressure

1   first component of spray (simulated fuel)

2   second component of spray (simulated oxidizer)

NOMENCLATURE (Cont'd)

ave	average	mp	model plane
B	boundary	p	plane
c	chamber	pD	value proportional to D_{max} (on a plane)
DN	downstream	R	radial distance
eff	effective	s	sample
el	element	t	throat
exp	experimental	th	theoretical
i, j, k	ith, jth, kth values in a series	UP	upstream
m	mixing		
max	maximum	z	along resultant momentum line
min	minimum	w	water

REFERENCES

1. Rupe, J. H., *The Liquid Phase Mixing of a Pair of Impinging Streams*, Progress Report No. 20-195, Jet Propulsion Laboratory, Pasadena, California, August 6, 1953.

2. Rupe, J. H., *A Correlation Between the Dynamic Properties of a Pair of Impinging Streams and the Uniformity of Mixture-Ratio Distribution in the Resulting Spray*, Progress Report No. 20-209, Jet Propulsion Laboratory, Pasadena, California, March 28, 1956.

3. Rupe, J. H., "A Technique for the Investigation of Spray Characteristics of Constant Flow Nozzles," *Third Symposium (International) on Combustion, Flame and Explosion Phenomena*, Madison, Wisconsin, 1948. The Williams & Wilkins Co., Baltimore, Maryland, 1949, pp. 680–694.

4. Rupe, J. H., "Bridging the Gap Between Injector Hydraulics and Combustion Phenomena in Liquid Propellant Rocket Engines," *Bulletin of the First Meeting of the Joint Army-Navy-Air Force Liquid Propellant Group* (New Orleans, Louisiana, November 3–5, 1959): Vol. III. Rocket Engine Research and Development. Liquid Propellant Information Agency, Johns Hopkins University, Silver Springs, Maryland.

5. Clayton, R. M., et al., *An Experimental Correlation of the Nonreactive Properties of Injection Schemes and Combustion Effects in a Liquid-Propellant Rocket Engine: Part II. On Instrumentation, Experimental Apparatus, and Experimental Techniques*, Technical Report No. 32-255, Jet Propulsion Laboratory, Pasadena, California (to be published).

6. Rupe, J. H., et al., *An Experimental Correlation of the Nonreactive Properties of Injection Schemes and Combustion Effects in a Liquid-Propellant Rocket Engine: Part III. On the Relation Between Gross Performance Level and Injection Schemes*, Technical Report No. 32-255, Jet Propulsion Laboratory, Pasadena, California (to be published).

REFERENCES (Cont'd)

7. Jaivin, G. I., et al., *An Experimental Correlation of the Nonreactive Properties of Injection Schemes and Combustion Effects in a Liquid-Propellant Rocket Engine: Part IV. Relating the Injection Pattern to Heat Transfer to the Chamber Wall,* Technical Report No. 32-255, Jet Propulsion Laboratory, Pasadena, California (to be published).

8. Rupe, J. H., *An Experimental Correlation of the Nonreactive Properties of Injection Schemes and Combustion Effects in a Liquid-Propellant Rocket Engine: Part V. On the Influence of Vanes on Combustion and Combustion Stability,* Technical Report No. 32-255, Jet Propulsion Laboratory, Pasadena, California (to be published).

9. Clayton, R. M., et al., *An Experimental Correlation of the Nonreactive Properties of Injection Schemes and Combustion Effects in a Liquid-Propellant Rocket Engine: Part VI. The Relation Between the Starting Transient and Injection Hydraulics,* Technical Report No. 32-255, Jet Propulsion Laboratory, Pasadena, California (to be published).

10. Rupe, J. H., *An Experimental Correlation of the Nonreactive Properties of Injection Schemes and Combustion Effects in a Liquid-Propellant Rocket Engine: Part VII. The Performance Characteristics of Injection Schemes Utilizing High-Flow-Rate Elements,* Technical Report No. 32-255, Jet Propulsion Laboratory, Pasadena, California (to be published).

11. Nerheim, N. M., *An Experimental Correlation of the Nonreactive Properties of Injection Schemes and Combustion Effects in a Liquid-Propellant Rocket Engine: Part VIII. On the Experimental Performance of the Pentaborane–Hydrazine Propellant Combination,* Technical Report No. 32-255, Jet Propulsion Laboratory, Pasadena, California, April 30, 1962 (Confidential).

12. Datner, R. P., and Dawson, E. F., "Testing of Repetitive Pattern Injectors," in *1000-lb Thrust Chambers with Chamber-to-Throat Area Ratios of 4.5 Using WFNA and JP-3,* Report No. 255 (Spec), Aerojet-General Corporation, El Monte, California, July 25, 1952.

13. Rupe, J. H., *Experimental Studies of the Hydrodynamics of Liquid Propellant Injection,* External Publication No. 388, Jet Propulsion Laboratory, Pasadena, California, June 7, 1957.

14. Rupe, J. H., *On the Dynamic Characteristics of Free-Liquid Jets and a Partial Correlation with Orifice Geometry,* Technical Report No. 32-207, Jet Propulsion Laboratory, Pasadena, California, January 15, 1962.

15. Northup, R. P., "Flow Stability in Small Orifices," paper presented at *1951 ARS Annual Convention,* Atlantic City, New Jersey, November 28–30, 1951.

16. Wright, B., *Liquid Flow Characteristics of Small Diameter Unsubmerged Short Tube Orifices Discharging to Atmospheric Pressure,* Report 610-801, Bendix Aircraft Corporation, Eclipse-Pioneer Division, Teterboro, New Jersey, August 15, 1962 (Confidential).

17. Heidmann, M. F., and Humphrey, J. C., *Fluctuations in a Stream Formed by Two Impinging Streams,* NACA TN 2349, National Advisory Committee for Aeronautics, Washington, D. C., April 1951.

REFERENCES (Cont'd)

18. Heidmann, M. F., and Foster, H. H., *Effect of Impingement Angle on Drop Size Distribution and Spray Pattern of Two Impinging Water Jets,* NASA TN D-872, National Aeronautics and Space Administration, Washington, D. C., July 1961.

19. Foster, H. H., and Heidmann, M. F., *Spatial Characteristics of Water Spray Formed by Two Impinging Jets at Several Jet Velocities in Quiescent Air,* NASA TN D-301, National Aeronautics and Space Administration, Washington, D. C., July 1960.

20. Ryan, N. W., *Mixing and Atomization by Impingement of Unconfined Liquid Jets,* Ph.D. Thesis, Massachusetts Institute of Technology, Cambridge, Massachusetts, December 30, 1948.

21. Ingebo, R. D., *Drop-Size Distributions for Impinging-Jet Breakup in Air-Streams Simulating the Velocity Conditions in Rocket Combustors,* NACA TN 4222, National Advisory Committee for Aeronautics, Washington, D. C., December 19, 1957.

22. Ingebo, R. D., *Vaporization Rates and Drag Coefficients for Iso-Octane Sprays in Turbulent Air Streams,* NACA TN 3265, National Advisory Committee for Aeronautics, Washington, D. C., October 1954.

23. Ingebo, R. D., "Heat Transfer and Drag Coefficients for Ethanol Drops in a Rocket Chamber Burning Ethanol and Liquid Oxygen," *Eighth Symposium (International) on Combustion,* Pasadena, California, August 28–September 3, 1960. The Williams & Wilkins Co., Baltimore, Maryland, 1962.

24. Ingebo, R. D., *Photomicrographic Tracking of Ethanol Drops in a Rocket Chamber Burning Ethanol and Liquid Oxygen,* NASA TN D-290, National Aeronautics and Space Administration, Washington, D. C., June 1960.

25. DeJuhasz, K. J., and Meyer, W. E., *Bibliography on Sprays,* The Texas Company, Refining Department, Technical and Research Division, New York, 1948. (Revised, May 1949.)

26. Marshall, W. R., Jr., "Atomization and Spray Drying," *Chemical Engineering Progress Monograph Series* (American Institute of Chemical Engineers), Vol. 50, No. 2, 1954.

27. Elverum, G. W., Jr., and Morey, T. F., *Criteria for Optimum Mixture-Ratio Distributions Using Several Types of Impinging-Stream Injector Elements,* Memorandum No. 30-5, Jet Propulsion Laboratory, Pasadena, California, February 25, 1959.

28. *Combined Bimonthly Summary No. 59,* April 1–June 1, 1957, pp. 48–50, Jet Propulsion Laboratory, Pasadena, California, June 15, 1957 (Confidential).

29. Farber, M., *The Performance of Aniline–Furfuryl Alcohol Mixtures with Nitric Acid,* Memorandum No. 20-92, Jet Propulsion Laboratory, Pasadena, California, May 26, 1954 (Confidential).

30. LeClerc, A., *Deflection of a Liquid Jet by a Perpendicular Boundary,* M.S. Thesis, State University of Iowa, Iowa City, Iowa, 1948.

31. Mason, D. M., Petker, I., and Vango, S. P., *Viscosity and Density of the Nitric Acid–Nitrogen Dioxide–Water System,* Progress Report No. 20-214, Jet Propulsion Laboratory, Pasadena, California, January 29, 1954.

REFERENCES (Cont'd)

32. Rupe, J. H., and Jaivin, G. I., "Experimental Measurements of Local Heat Transfer in a Liquid Propellant Rocket Engine," paper presented at *Sixth Liquid Propulsion Symposium*, Los Angeles, California, September 23–25, 1964.

33. Rupe, J. H., *A Dynamic-Head Probe for Evaluating the Properties of Free Liquid Jets*, Progress Report No. 20-299, Jet Propulsion Laboratory, Pasadena, California, May 23, 1956.

34. Tietjens, O. K. G., *Applied Hydro- and Aeromechanics*, based on the lectures of L. Prandtl; J. P. Den Hartog, Translator. McGraw-Hill Book Co., Inc., New York, 1934.

ACKNOWLEDGMENT